

ornl

**OAK RIDGE
NATIONAL
LABORATORY**

MARTIN MARIETTA

OPERATED BY
MARTIN MARIETTA ENERGY SYSTEMS, INC.
FOR THE UNITED STATES
DEPARTMENT OF ENERGY

MARTIN MARIETTA ENERGY SYSTEMS LIBRARIES

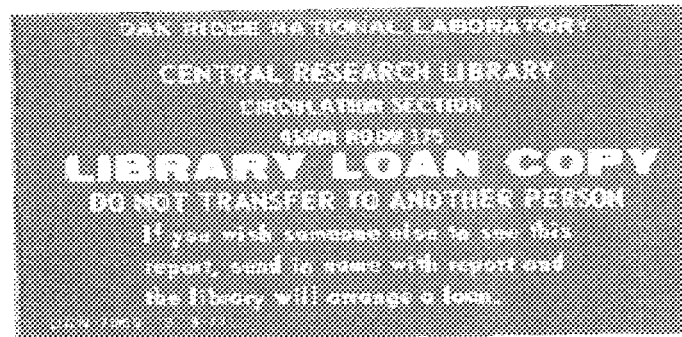


3 4456 0280495 4

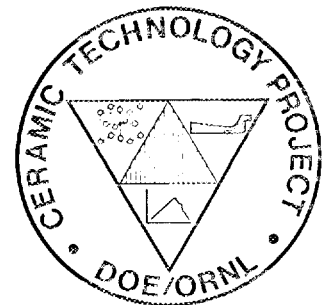
ORNL/TM-10468

Analysis of Adhesion Test Methods and the Evaluation of Their Use for Ion-beam-mixed Metal/Ceramic Systems

J. E. Pawel



CERAMIC TECHNOLOGY FOR
ADVANCED HEAT ENGINES



Printed in the United States of America. Available from
National Technical Information Service
U.S. Department of Commerce
5285 Port Royal Road, Springfield, Virginia 22161
NTIS price codes - Printed Copy A06 Microfiche A01

This report was prepared as an account of work sponsored by an agency of the United States Government. Neither the United States Government nor any agency thereof, nor any of their employees, makes any warranty, express or implied, or assumes any legal liability or responsibility for the accuracy, completeness, or usefulness of any information, apparatus, product, or process disclosed, or represents that its use would not infringe privately owned rights. Reference herein to any specific commercial product, process, or service by trade name, trademark, manufacturer, or otherwise, does not necessarily constitute or imply its endorsement, recommendation, or favoring by the United States Government or any agency thereof. The views and opinions of authors expressed herein do not necessarily state or reflect those of the United States Government or any agency thereof.

Metals and Ceramics Division

ANALYSIS OF ADHESION TEST METHODS AND THE
EVALUATION OF THEIR USE FOR ION-BEAM-MIXED
METAL/CERAMIC SYSTEMS

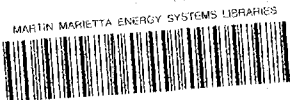
J. E. Pawel

Date Published: July 1988

NOTICE: This document contains information of
preliminary nature. It is subject to revision
or correction and therefore does not represent
a final report.

Prepared for the
Assistant Secretary for Conservation and Renewable Energy,
Office of Transportation Systems,
Advanced Materials Development Program
EE 04 00 00 0

Prepared by the
OAK RIDGE NATIONAL LABORATORY
Oak Ridge, Tennessee 37831
operated by
MARTIN MARIETTA ENERGY SYSTEMS, INC.
for the
U.S. DEPARTMENT OF ENERGY
under contract DE-AC05-84OR21400



3 4456 0280495 4

CONTENTS

LIST OF FIGURES	v
LIST OF TABLES	ix
ACKNOWLEDGMENTS	xi
ABSTRACT	1
CHAPTER I, INTRODUCTION	3
CHAPTER II, LITERATURE REVIEW	5
TESTING METHODS	5
The Scratch Test	5
The Acoustic Emission Test	17
The Pull Test	21
ION-BEAM MIXING	23
Introduction	23
Effect on Adhesion	23
CHAPTER III, EXPERIMENTAL PROCEDURE	25
SUBSTRATE MATERIALS	25
SUBSTRATE CLEANING PROCEDURE	25
FILM DEPOSITION	26
SPECIMEN CHARACTERIZATION	28
SCRATCH TEST	28
ACOUSTIC EMISSION TEST	30
PULL TEST	30
ION-BEAM MIXING	31
CHAPTER IV, RESULTS AND DISCUSSIONS	33
THE SCRATCH TEST	33
Systems Analyzed	33
Scratch Characteristics	34
Analyses	43
THE PULL TEST	56
EFFECTS OF ION-BEAM MIXING	60
Adhesion to Sapphire Substrates	60
Adhesion to Silicon Carbide and Silicon Nitride Substrates	64

CHAPTER V, CONCLUSIONS	77
THE SCRATCH TEST	77
THE PULL TEST	79
EFFECTS OF ION-BEAM MIXING	79
REFERENCES	81

LIST OF FIGURES

Fig. 1. Forces at the lip of the stylus indentation as assumed by Benjamin and Weaver. *Source*: Benjamin, P., and Weaver, C., "Measurement of Adhesion of Thin Films," *Proc. Royal Soc. London A* 254 (1960) 163 10

Fig. 2. Schematic view of the stylus on the surface. The radius of the circle of contact is a , and the stylus travels in the positive x -direction. *Source*: Hamilton, G. M., and Goodman, L. E., "The Stress Field Created by a Circular Sliding Contact," *J. Appl. Mech.* 88 (1966) 71 12

Fig. 3. Points of maximum yield parameter below the stylus for various coefficients of friction. The stylus travels in the positive x -direction, and the x -axis lies in the plane of the surface. *Source*: Hamilton, G. M., and Goodman, L. E., "The Stress Field Created by a Circular Sliding Contact," *J. Appl. Mech.* 88 (1966) 71 12

Fig. 4. Stretching of the film during indentation. This stretching results in tensile stresses in the film under the stylus 14

Fig. 5. Typical scratch profile made with a 0.2-mm-radius stylus tip. *Source*: Laeng, P., and Steinmann, P. A., "Adhesion Testing of Hard CVD Coatings Using the Scratch Test," p. 723 in *Proc. 8th Intern. Conf. on Chemical Vapor Deposition*, John M. Blocher, Jr., Guy E. Vuillard, and Georg Wahl, eds., The Electrochemical Society, Inc., Pennington, NJ, 1981 15

Fig. 6. Schematic representation of the crack formed ahead of the stylus moving from left to right. Other cracks have been passed over by the stylus. *Source*: Je, J. H., Gyarmati, E., and Naoumidis, A., "Scratch Adhesion Test of Reactively Sputtered TiN Coatings on a Soft Substrate," *Thin Solid Films* 136 (1986) 57 16

Fig. 7. Height profile across the end of the channel showing the crack formed ahead of the stylus. Scratching is from left to right. *Source*: Je, J. H., Gyarmati, E., and Naoumidis, A., "Scratch Adhesion Test of Reactively Sputtered TiN Coatings on a Soft Substrate," *Thin Solid Films* 136 (1986) 57 16

Fig. 8. Model of failure by the scratch test. Elastic energy stored just ahead of the stylus causes de-adhesion, which propagates ahead of the stylus and is stopped by cohesive cracking of the film. Movement of the stylus on the detached film causes microcracking in the scratch path. Source: Je, J. H., Gyarmati, E., and Naoumidis, A., "Scratch Adhesion Test of Reactively Sputtered TiN Coatings on a Soft Substrate," *Thin Solid Films* 136 (1986) 57 18

Fig. 9. Electron beam power as a function of time for the depositions of the zirconium film 27

Fig. 10. The scratch tester. The following parts are labeled: (a) drive shaft, (b) movable stage, (c) load platform, (d) strain gage, (e) axis of lever arm rotation, (f) carpenter's level, (g) balance weight, (h) motor, (i) horizontal plane adjusters for stage, (j) stylus. Actual length: 50 cm 29

Fig. 11. Stylus skipping caused by system vibrations. Scratch made on aluminum/glass system under a normal load of 0.45 g. The speed of the stylus travel was increased to exaggerate the skipping effect. Scratch direction is from left to right 35

Fig. 12. Scratch made on aluminum/glass system under a normal load of 2.0 g. Scratch direction is from left to right 35

Fig. 13. Typical scratch profiles. 37

Fig. 14. Scratch made on zirconium/sapphire specimen under a normal load of 30 g. Scratch direction is from left to right. Scanning electron micrograph, 1600X 38

Fig. 15. Scratch made on zirconium/sapphire specimen under a normal load of 40 g. Scratch direction is from left to right. Scanning electron micrograph, 1650X 38

Fig. 16. Scratch made on nickel/sapphire specimen under a normal load of 150 g. The white streaks signify film removal. Scratch direction is from left to right. Scanning electron micrograph, 1430X 39

Fig. 17. Scratches made on aluminum/glass specimen under a normal load of 0.45 g. Scratch direction is from left to right 39

Fig. 18. Scratches made on aluminum/glass specimen under a normal load of 1.0 g. Scratch direction is from left to right 40

Fig. 19. Full-length view of scratches in Figs. 17 and 18 before ultrasonic cleaning. Scratch direction is from left to right. 42X	40
Fig. 20. Thinning of zirconium film under normal stylus loads of (a) 10 g and (b) 200 g. 128X	41
Fig. 21. Effect of surface flaw on scratching of zirconium/sapphire system. Scratch direction is from left to right. Scanning electron micrograph, 1600X	41
Fig. 22. Transverse profile of a scratch showing ductile extrusion of nickel film on a sapphire substrate	42
Fig. 23. Transverse profile of a scratch showing absence of ductile extrusion of a chromium film on a sapphire substrate.	42
Fig. 24. Scanning electron micrograph of a 250-g normal load scratch on a chromium/sapphire specimen. Scratch direction is from left to right. 1000X	43
Fig. 25. Two regions of compressive failure caused by a 450-g normal load scratch on a zirconium/sapphire specimen. Scratch direction is from left to right	45
Fig. 26. Tensile failure behind the meaning stylus caused by a 400-g normal load on a zirconium/sapphire specimen. Scratch direction is from left to right	46
Fig. 27. Theoretical line of constant maximum tensile stress acting in the plane of the surface for a friction coefficient of 0.25. The stylus moves in the positive x-direction, and a is the radius of the circle of contact. Source: Hamilton, G. M., and Goodman, L. E., "The Stress Field Created by a Circular Sliding Contact," <i>J. Appl. Mech.</i> 88 (1966) 371	47
Fig. 28. Theoretical and experimental values of the radius of the circle of contact for scratches on aluminum/glass specimens	53
Fig. 29. Original 30-nm zirconium film on silicon carbide. The bright spots are electron discharges from the substrate, revealing the pores in the film. Scanning electron micrograph, 300X	65

LIST OF TABLES

Table 1.	Shear stresses calculated using the plastic model analysis for scratches on zirconium/sapphire	49
Table 2.	Shear stresses calculated using the plastic model analysis for scratches on chromium/sapphire	50
Table 3.	Shear stresses calculated using the plastic model analysis for scratches on nickel/sapphire	50
Table 4.	Shear stresses calculated using the plastic model analysis for scratches on aluminum/glass	52
Table 5.	Shear stresses calculated using the elastic model analysis for scratches on zirconium/sapphire comparing the results obtained for different values of Young's Modulus, E	54
Table 6.	Radial and shear stresses calculated using the elastic model analysis for scratches on chromium/sapphire	55
Table 7.	Radial and shear stresses calculated using the elastic model analysis for scratches on nickel/sapphire	55
Table 8.	Pull test results for specimens with gold release layer	58
Table 9.	Stresses recalculated assuming reduced area under the pin by omitting area over the gold release layer	59
Table 10.	Comparison of critical shear stresses calculated using the plastic model analysis for scratches on chromium/sapphire	61
Table 11.	Comparison of critical shear stresses calculated using the elastic model analysis for scratches on chromium/sapphire	62
Table 12.	Pull test results for ion-beam-mixed specimens	64
Table 13.	Pull test strength of aluminum film on silicon carbide substrate	67
Table 14.	Pull test strength of zirconium film on silicon carbide substrate	70

Table 15.	Pull test strength of 515-nm zirconium film on silicon nitride substrate	74
Table 16.	Pull test strength of 530-nm zirconium film on silicon nitride substrate	76
Table 17.	Analysis methods useful in the determination of critical values for film de-adhesion for the systems investigated	78

ACKNOWLEDGMENTS

This report is a thesis presented for the Master of Science Degree, The University of Tennessee, Knoxville, in June, 1987.

The author would like to express her gratitude to her major professor, Dr. C. J. McHargue, for his support and guidance throughout the course of this research. Appreciation is also extended to Dr. J. F. Wasserman for his technical and professional guidance and to Dr. R. A. Buchanan for his many worthwhile suggestions.

This material is based upon work supported under a National Science Foundation Graduate Fellowship. Financial support provided under the Ceramic Technology for Advanced Heat Engines Project, Metals and Ceramics Division, Oak Ridge National Laboratory (ORNL), administered by Dr. D. R. Johnson, is gratefully acknowledged.

The author is grateful to Mr. D. S. Easton and Mr. C. K. H. DuBose for technical assistance needed for thin-film evaporation; to Dr. S. P. Withrow, Dr. T. P. Sjoreen, Dr. M. B. Lewis, and Mr. S. W. Cook for assistance with the ion-beam mixing procedure; and to Dr. C. S. Yust for his advice on scratch testing. Technical assistance with scanning electron microscopy provided by Dr. T. F. Page and additional microscopy and photography by the Metallography Group of the Metals and Ceramics Division, Mr. R. S. Crouse, Mr. T. J. Henson, Mr. B. C. Leslie, Mr. J. W. Nave, and Ms. C. L. Angel, are gratefully acknowledged.

Thanks are also extended to Mr. A. V. Blalock and Mr. J. S. Kinsley for their assistance in operating and maintaining electronic equipment. The author would also like to acknowledge Mr. Blalock's contributions to equipment design and experimental procedure.

Special thanks go to Mr. J. J. Campbell and Mr. D. S. Easton for their help with laboratory equipment and procedures.

The reliable and patient efforts of the departmental secretaries, Ms. Eunice Hinkle and Ms. Berdie Parsons, and particularly the author's ORNL secretary and typist, Ms. Lou Pyatt, are most gratefully acknowledged.

ANALYSIS OF ADHESION TEST METHODS AND THE
EVALUATION OF THEIR USE FOR ION-BEAM-MIXED
METAL/CERAMIC SYSTEMS*

J. E. Pawel

ABSTRACT

Several thin film adhesion tests have been examined to determine which provides the most reliable method for the measurement of the adhesion of thin metallic films to ceramic substrates. An attempt was made to use the testing techniques described to measure adhesion changes caused by ion beam mixing for a variety of metal/ceramic systems. The techniques analyzed were the scratch test, the acoustic-emission test, and the pull test. The major variables of the scratch test include film thickness, substrate hardness, and stylus radius, but it is not known precisely what effects changes in these have on the measurement of adhesion. The scratch analyses methods discussed in the literature, each describing a load or stress on the system that is presumed to cause de-adhesion, do not always hold because none of the analyses account for both plastic and elastic deformation or incorporate many of the important parameters. The scratch test was much more likely to reveal a critical value for de-adhesion for relatively brittle films such as chromium than for ductile films such as nickel.

The acoustic-emission test did not work for the scratch testing equipment used in this research. Whatever specimen emissions might have occurred were overshadowed by those of the drive motor, which could not be adequately isolated from the system.

An adaptation of the pull test, utilizing a thin gold layer under a portion of the test film, was developed because the adhesion of the test films was greater than the strength of the epoxy used in the standard test. Because this nonadherent layer served as a reproducible crack, the analysis was analogous to that used in fracture toughness testing. Comparison of film adherence was based on the calculation of the stress intensity factor necessary to cause film de-adhesion. The results of this modified pull test were very promising and involved fewer parameters than the scratch test.

Scratch test data for most of the systems exhibiting critical values for de-adhesion revealed that ion-beam mixing significantly improved the adhesion of the films to their substrates. Ion-beam-mixed films also withstood a greater applied tensile stress and a greater stress-intensity factor without de-adhesion than unmixed films with similar flaws.

*Research sponsored by the U.S. Department of Energy, Assistant Secretary for Conservation and Renewable Energy, Office of Transportation Systems, as part of the Ceramic Technology for Advanced Heat Engines Project of the Advanced Materials Development Program, under contract DE-AC05-84OR21400 with Martin Marietta Energy Systems, Inc.

CHAPTER I

INTRODUCTION

Thin films can be used to make a monolithic material suitable for special requirements in a variety of applications. Such films can be used to provide resistance to wear, corrosion, abrasion, erosion, galling, tarnish, radiation damage, or high-temperature oxidation, as well as to reduce electrical resistance and friction. They also can provide lubrication, prevent sticking, and provide special magnetic or dielectric properties.¹ The use of thin metallic films on ceramic substrates represents an important area. Specifically, the films in this research are used as electrical contacts for semiconductors and as intermediate layers to enhance the adherence of thermal barrier coatings. The effectiveness, durability, longevity, and strength of a film all depend intimately on the degree of adhesion between the film and its substrate. One of the goals of this research is the determination of a reliable method for the measurement of the adhesion of thin metallic films to ceramic substrates. Measurement of adhesion of ductile metallic films on brittle ceramic substrates poses a problem, however, because the "cotton-bud" test (removal of a film by rubbing with a cotton swab) and the "3M" test (removal of a film by plastic tape) are highly qualitative; the widely used quantitative tests, though, have found the most success with brittle films on ductile substrates. Also, adhesion tests often yield no clear separation between the film and its substrate, and different testing methods give different values of adhesion.

One method of improving the interfacial bonding between a film and its substrate is by a form of ion implantation called ion beam mixing in which the film is bombarded with heavy ions of sufficient energy to penetrate the film and enter the interfacial region. A second goal of this research is to investigate the adhesion change as a function of ion beam mixing for several systems.

The testing methods analyzed and discussed in this paper are the scratch test, the acoustic emission test, and the pull test. The various aspects and parameters of each test must be recognized and understood before any significance can be given to the data. A brief introduction to ion-beam mixing and its effects on thin film adhesion is included in the literature review, and an attempt is made to use the testing techniques described to measure adhesion changes caused by ion-beam mixing for a variety of systems.

CHAPTER II

LITERATURE REVIEW

TESTING METHODS

The Scratch Test

Introduction. The scratch test was developed by Benjamin and Weaver² from a technique originally described, but not analyzed, by O. S. Heavens in 1950. In this method, a smoothly rounded stylus point is drawn across the film surface. The vertical load on the stylus is increased until the film is stripped from the substrate. The critical load is defined as that load on the stylus at which the coating is stripped cleanly from the substrate.

By varying substrate materials for the same film material, Benjamin and Weaver found that the critical load did depend on the nature of the substrate but saw no direct relationship between the critical load and the substrate hardness or elasticity. The critical load also varied with film material (on the same substrate) but did not correlate with a specific film property such as hardness. Furthermore, for films exceeding a certain thickness, the critical load became constant; a continuous variation with thickness would be expected if the load depended on some mechanical property of the film. From these results, they concluded that the critical load is determined by the interfacial properties of the system.

Analysis of the horizontal forces led Benjamin and Weaver to the following proposal. When a rounded point is drawn across a coated surface and the adhesion of the point to the coating is good, shearing must occur at the weakest point, either at the coating/substrate interface or within the substrate. Assuming that the cohesive forces within the substrate are greater than the adhesive forces of the interface, the shearing should occur at the interface, and, thus, the force should be less than the shearing found when the stylus is passed over the uncoated substrate material and only cohesive shearing is possible. When the adhesion of the point to the coating is poor, the stylus slides over the film for

increasing normal loads until the deformation of the substrate is sufficient to loosen the film. Because the substrate is plastically deformed, the metal film is also deformed to the indentation shape. This causes the film to stretch and a shearing force to develop between the film and the substrate. This shearing force increases with increasing load until the adhesive bonds between the substrate and film are broken at the lip of the indentation, where the shearing forces are maximum. Once the de-adhesion occurs at the lip of the indent, the shearing extends over the whole indentation. The stylus continues to deform the substrate as it travels, shearing adhesive bonds over the advancing profile and pushing the sheared material aside. The authors found, experimentally, that the former is not the case but that the latter analysis involving the deformation of the substrate is in close agreement with the experimental evidence, especially because plastic deformation of the substrate was observed in every case.

Benjamin and Weaver developed an equation relating the shearing force per unit area to the stylus load, stylus radius, and substrate hardness. Comparison of this equation using experimental data with calculations of the force required to overcome van der Waals forces at the interface shows that the former gives numbers of the same order of magnitude as the latter. Further experiments revealed that the critical load increased with stylus radius but that the shearing force, as calculated from their equation, remained reasonably constant.

Complexities of the Scratch Test. Since Benjamin and Weaver's work in 1960, many other researchers have investigated the scratch test and have concluded that it is much more complex than the original analysis implied.³⁻¹² Even Benjamin and Weaver² admitted that their theory was based on an idealized indentation shape and that they had neglected elastic deformation.

Butler, Stoddart, and Stuart³ found that detached film could be pressed back into the path by the stylus or that a film could be thinned to transparency without detachment, and, thus, the critical load could not be determined on the basis of a clear stylus track. They also indicated that a much larger number of film parameters, such as yield stress, surface condition, density, and grain size, also are factors in apparent adhesion differences. In addition, they pointed out that the sequence of

yield in the film, interfacial region, and substrate may be controlled by many factors. These remarks have been verified by others.^{8,9}

In 1975 Charles Weaver⁵ concluded, using scanning electron micrographs of the scratch path that showed hillocks ahead, and to the side, of the stylus, that the original theory of detachment by shearing could not be valid.

Laeng and Steinmann⁶ pointed out the importance of the failure mode: not only that it affects the value of the critical load, but also that some modes do not show a straightforward track clearing and do involve local flaking. They advised careful examination of the scratches. Je, Gyarmati, and Naoumidis¹¹ also reported that the mode of coating failure varies with the substrate material, film material, film thickness, and film production method.

Laugier⁷ showed friction to play a critical and complex role in the film stripping process. This is discussed in more detail in a later section.

Partial elastic recovery of the substrate was noted by Perry,⁸ and Perry, Laeng, and Hintermann⁹ pointed out that substrate surface roughness may be a factor. Perry¹³ later reported a dependence on shear moduli and concluded that the relationship between the critical load and the actual adhesion strength is not yet understood.

In 1986 Valli, Makela, and Matthews¹² noted that adhesion may seem to be improved in an inferior film because a film that is porous can more readily accommodate deformations. They also reported a dependence of the data on indenter material, film surface finish and geometry, coating surface condition and geometry, and air humidity during testing.

In spite of all of the ambiguities and complexities of the scratch test, many researchers consider it to be the best of the many adhesion tests^{2,10,12} and realize that it has great value as a comparative test, particularly for films on the same substrate^{6,14} or the same film/substrate systems.^{3,4,12,13,15,16} Weaver and Parkinson¹⁷ used the scratch test to study the diffusion of gold and aluminum layers on a substrate and obtained such consistent results that this experiment is considered convincing evidence that the critical load is determined primarily by the adhesion between film and substrate.⁵ Mehrotra and

Quinto¹⁸ pointed out that for their work the critical load values from duplicate scratches were almost identical.

However, critical loads determined from the scratch test are often reported as being within some scatterband or using histograms because they can vary significantly for identical systems.^{10,13,19} Weaver⁵ noted that low measurements of adhesion can be easily explained as weak spots and suggested that the highest values are closest to the true adhesion. Perry,¹³ on the other hand, used the criterion that the onset of loss is decisive because this is soon followed by general failure in practice. He also reported that the criterion of taking the first local loss of film as the critical load or the regular loss along the scratch path makes little difference within the scatterband.

Variations in Film Thickness. There has been some controversy over the effect of film thickness on the critical load. Benjamin and Weaver² reported that the critical load became constant for films exceeding a certain thickness. The initial sloping part of the load vs film thickness curve, Benjamin and Weaver stated, is not due to a defect of the method, but, rather, due to film structure, which may not be continuous at small thicknesses.

Chopra,²⁰ after reviewing the work of Benjamin and Weaver, noted that their conclusion is only valid for peeling of the film under the critical load. Because in practice the stylus scratches the film, the critical load is determined by the mechanical properties of the film, as well as by adhesion. Chopra's experimental results do indeed show a strong dependence on film thickness for film thicknesses greater than about 200 nm. From his data, Chopra concluded that for film thicknesses less than 200 nm the critical load is a reasonable measure of adhesion.

The work of Butler, Stoddart, and Stuart³ also showed that a greater load was required to thin a thick, soft film to transparency than for a thin, soft film. In addition, different detachment modes were observed for the thick and very thin films. The authors explained their results by using the analysis of Hamilton and Goodman²¹ for a sphere impressed on a semi-infinite flat surface. For this case, plastic deformation can first occur within the body rather than at the surface and at a distance on the order of the film thicknesses studied here. Thus, a very thick film may contain the initial yield point, but plastic deformation may occur first in the substrate under a thin film.

Perry,^{13,22} like Chopra, found that the critical load increased with coating thickness. In his analysis, the scratch test involves the inducement of a shear stress at the interface as a result of deformation of the system; therefore, a thicker layer may require a greater surface load to attain the same shear stress at the interface. Je, Gyarmati, and Naoumidis¹¹ concurred with Perry's results and conclusion. Perry and Pulker²³ noted the same phenomenon and also the fact that the behavior of large film thicknesses was less reproducible because of the effect of mechanical stress in the film on the adhesion. Laeng and Steinmann⁶ and Hammer et al.¹⁰ also reported the increase of the critical load with increasing film thickness.

In contrast, Kikuchi, Baba, and Kinbara¹⁹ found that for the systems studied in their work, the mean value of adhesion was almost independent of film thickness.

Variations in Substrate Hardness, Stylus Hardness, and Stylus Radius. The critical load has been found to increase with substrate hardness^{10,13} and stylus hardness¹⁹ although Hamersky²⁴ found it to be indirectly dependent on stylus hardness. Also, Hamersky obtained reproducible results only while using a stylus radius larger than 0.2 mm; Laeng and Steinmann⁶ verified Hamersky's conclusion of critical load dependence on stylus radius.

Analyses of the Scratch Test. Benjamin and Weaver² found the shearing force per unit area F based primarily on the classical equations of Hertz describing the deformation of a flat surface under a hard sphere. For purely elastic deformation, the radius of the circle of contact is given by

$$a = 1.1 \left\{ (1/2)Wgr \left[(1/E_1) + (1/E_2) \right] \right\}^{1/3} ,$$

where r is the radius of the sphere, E_1 and E_2 are the moduli of elasticity of the sphere and the surface, and W is the load.

Benjamin and Weaver assumed the forces on the tip are as shown in Fig. 1, where F is the shearing force per unit area, W is the stylus load, r is the radius of the tip, P is analogous to a hydrostatic mean pressure, and a is the radius of the circle of contact, given as

$$a = (Wg/\pi P)^{1/2} .$$

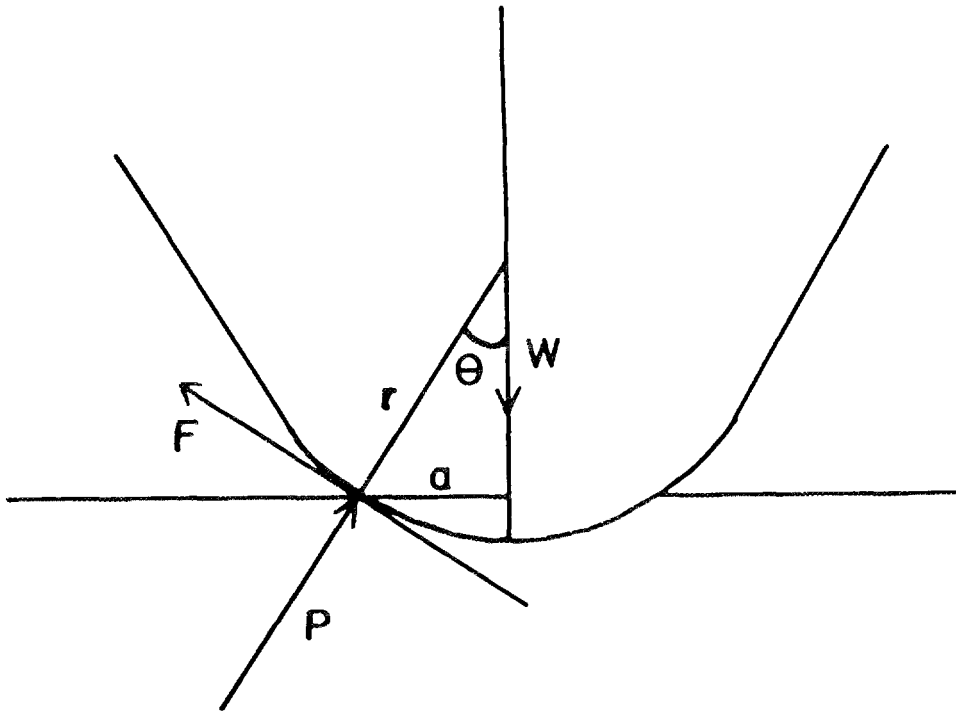


Fig. 1. Forces at the lip of the stylus indentation as assumed by Benjamin and Weaver. *Source*: Benjamin, P., and Weaver, C., "Measurement of Adhesion of Thin Films," *Proc. Royal Soc. London A* 254 (1960) 163.

Once full plasticity around the sphere is reached, the mean pressure over the contact area remains constant and equal to the indentation hardness. From this,

$$F = P \tan\theta = [a/(r^2 - a^2)^{1/2}] P .$$

This shear force is a direct measure of adhesion because it is assumed that it moves an atom of one layer from one equilibrium position to the next. If x is the distance between symmetrical equilibrium positions, then the height of the potential barrier is $(1/2) F x$, which is considered to be the energy of adhesion.

Butler, Stoddart, and Stuart,³ like Benjamin and Weaver, found that the scratch path involved deformation of both the film and the substrate. Load, film thickness, and relative physical properties of the film and substrate all affected the results. The scratch was usually a groove with a smooth center and raised sides. Often, a layer of the film remained in the center.

Two modes of film detachment were noted by these authors. The film could be cracked and partially detached after the stylus passed, perhaps because of failure of the film and interface to support the stresses resulting from high substrate deformations. Alternately, the film became detached in an annulus around the stylus. Movement of the stylus left folds at the track edges although the film sometimes did not tear or become carried away. In some cases, even when high loads distorted the system, no detachment was observed.

In this study, it was shown that separation of the film and substrate usually did not take place directly under the stylus but, rather, ahead of the stylus. This is in agreement with the theoretical results of Hamilton and Goodman²¹ who in 1966 obtained equations for the stress field caused by a loaded spherical tip moving over a flat surface. Their yield parameter was defined using the von Mises criterion, which is the square root of the second invariant of the stress deviator, which in Cartesian form is

$$J_2 = p_{xy}^2 + p_{xz}^2 + p_{yz}^2 + (1/6)[(p_{yy} - p_{zz})^2 + (p_{zz} - p_{xx})^2 + (p_{xx} - p_{yy})^2] .$$

Yield occurs when the square root of J_2 is equal to the material yield point in simple shear. The Cartesian stress components p_{ij} are derived in the paper. Evaluation of the above equation in the xz -plane (Figs. 2 and 3) for a coefficient of friction equal to zero reveals that the maximum yield parameter occurs on the centerline of the tip (z -axis) at a distance below the surface equal to one-half of the circle of contact radius. As the coefficient of friction is increased, the maximum yield parameter moves toward the surface and in the positive x -direction; however, a second maximum develops on the surface at a point behind the stylus, and this second maximum supersedes the first for a coefficient of friction of 0.5.

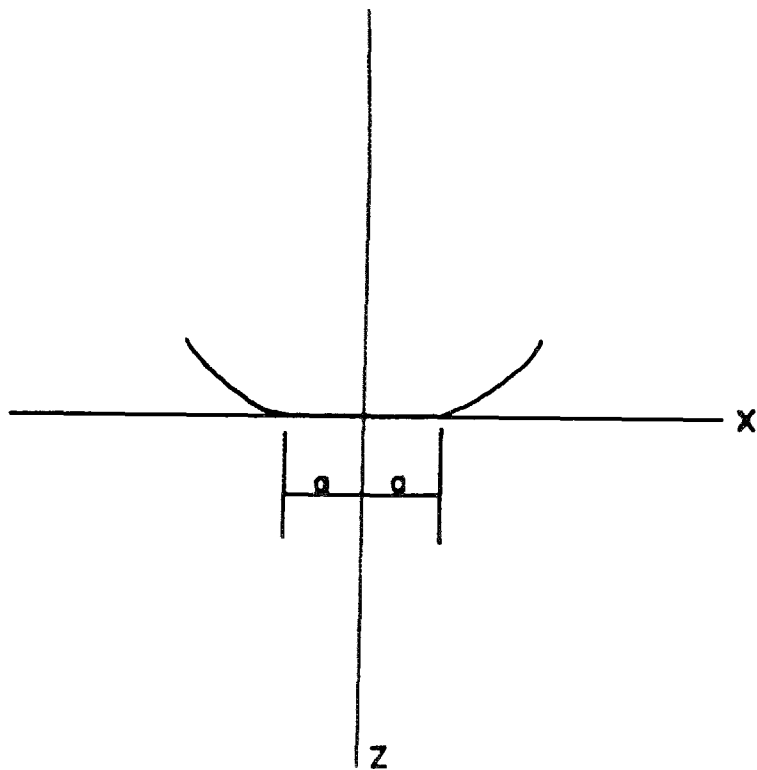


Fig. 2. Schematic view of the stylus on the surface. The radius of the circle of contact is a , and the stylus travels in the positive x -direction. Source: Hamilton, G. M., and Goodman, L. E., "The Stress Field Created by a Circular Sliding Contact," *J. Appl. Mech.* 88 (1966) 71.

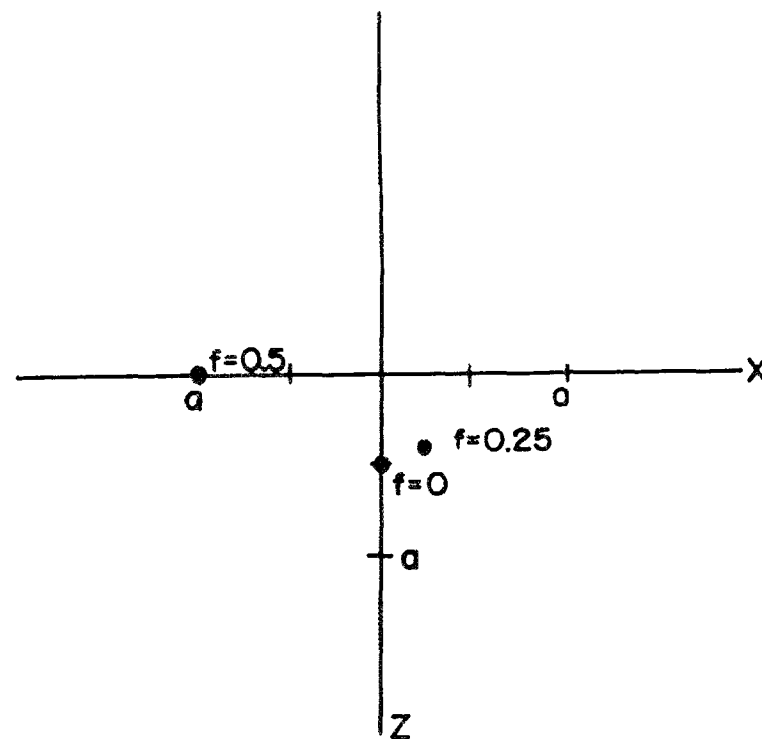


Fig. 3. Points of maximum yield parameter below the stylus for various coefficients of friction. The stylus travels in the positive x -direction, and the x -axis lies in the plane of the surface. Source: Hamilton, G. M., and Goodman, L. E., "The Stress Field Created by a Circular Sliding Contact," *J. Appl. Mech.* 88 (1966) 71.

Laugier⁷ suggested a model of the scratch test that included the coefficient of friction as a parameter. From stress equations of a hard sphere pressed against a flat surface developed by Hertz, Timoshenko, and Goodier,²⁵ and Hamilton and Goodman,²¹ he derived an expression for the total radial compressive stress acting at the leading edge of the moving indenter:

$$\sigma = (P/2\pi a^2) \{ (4 + \nu_1)(3\pi f/8) - (1 - 2\nu_1) \} ,$$

where ν_1 is Poisson's ratio for the flat surface, W is the normal load, a is the radius of contact, and f is the coefficient of friction. This total compressive stress is a combination of the radial tensile stress present at the lip of the indentation caused by stretching of the film during deformation (Fig. 4) and the radial compressive stress generated by the movement of the stylus. From this expression for the radial stress - and assuming that the radius of the indenter r is much greater than the radius of the circle of contact - Laugier found the shear stress to be approximately

$$\tau \approx \sigma(a/r) .$$

Letting $\nu_1 = 0.3$, the expression for the compressive stress becomes

$$\sigma \approx (Wg/2\pi a^2)(0.5f - 0.4) .$$

The coefficient of friction f is seen to be very important: for a low coefficient of friction, the stress at the leading edge is tensile, and the film will not "lift" from the substrate even if sufficient force to cause detachment has occurred. This would account for thinning of the film in the scratch path without material removal.

Laugier contended that his equations for conditions ahead of the stylus remain valid in spite of their dependence on elastic parameters because the onset of plasticity occurs at the trailing edge of the stylus for higher friction coefficients (from the analysis of Hamilton and Goodman, Fig. 3).

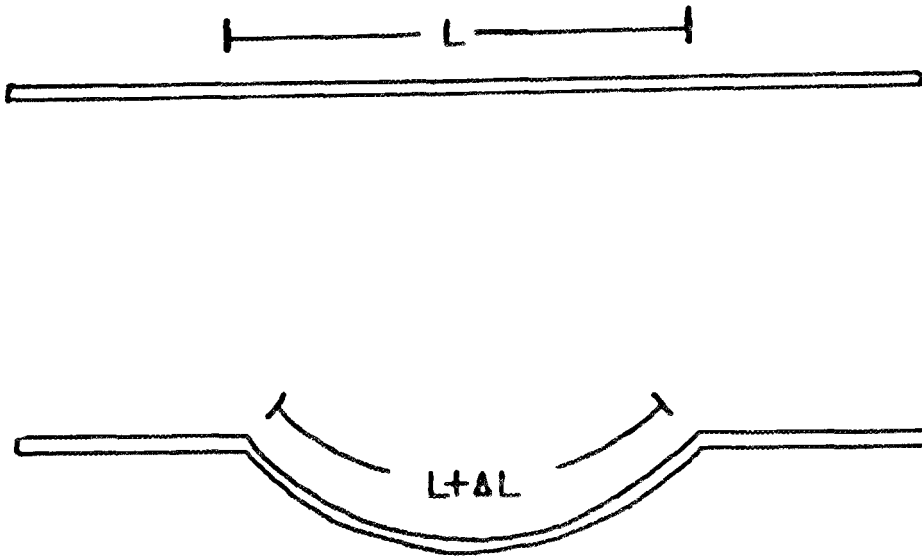


Fig. 4. Stretching of the film during indentation. This stretching results in tensile stresses in the film under the stylus.

In 1975 Weaver⁵ admitted the scratching process was more complex than originally thought and tried to reconcile the observations with the previous successful use of the test. Because vacuum-deposited films are almost always in a state of tensile stress, he postulated that once the perimeter of the contact area is detached, the loosened edge of the film would tend to lift and peel away from the substrate, creating cracks. As the stylus advanced, it would push down the loosened edge, creating a hillock ahead of the stylus. If the stress is insufficient to produce crack extension, the loosened film would fold up in front of the stylus or be pushed aside until the stylus reached the end of the crack, at which point the process would be repeated. Evidence of this mechanism was found in electron micrographs that showed a periodic folding along the edges of the track, the spacing of which corresponded to the distance at which film was detached ahead of the stylus. Weaver attributed translucency without detachment to insufficient friction between the stylus and the film to transfer the force to the interface.

Other researchers^{6,8} also found that the edges of the channel were subjected to gross plastic deformation and that high walls developed. Extensive elastic recovery followed the passage of the stylus, and this may explain why the scratches were wider and shallower than the stylus geometry would indicate.⁸ A typical scratch profile is shown in Fig. 5. Cracking of the coating at the lip of the channel,^{8,13} as well as flaking of the coating ahead of the stylus,¹⁰ has been noted. Detached fragments were pressed back onto the substrate in several cases.^{10,11} Micrographs from the work of Je, Gyarmati, and Naoumidis¹¹ clearly show cracking ahead of the moving stylus (Fig. 6); a profile of the end revealed that the crack was not formed by bending (Fig. 7).

Takadoun et al.²⁶ studied the topography of scratches on films and observed continuous ridges along the edges of the channel and sometimes inside the channel; these ridges were attributed to substantial plastic deformation of the surface. Perry and Pulker²³ also noted that the substrate used in their work was highly damaged during film removal.

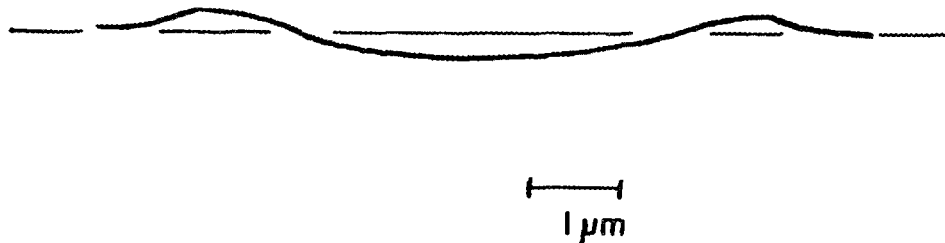


Fig. 5. Typical scratch profile made with a 0.2-mm-radius stylus tip. Source: Laeng, P., and Steinmann, P. A., "Adhesion Testing of Hard CVD Coatings Using the Scratch Test," p. 723 in *Proc. 8th Intern. Conf. on Chemical Vapor Deposition*, John M. Blocher, Jr., Guy E. Vuillard, and Georg Wahl, eds., The Electrochemical Society, Inc., Pennington, NJ, 1981.

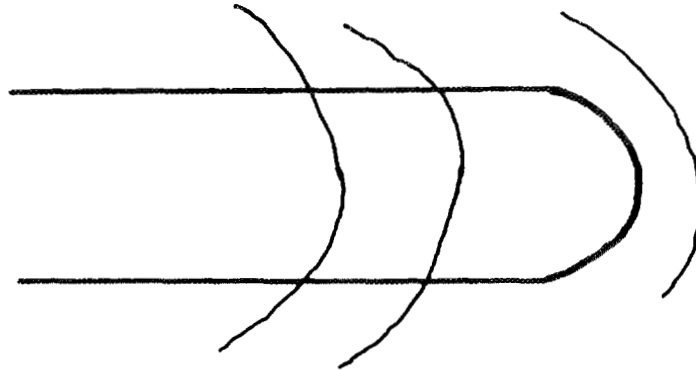


Fig. 6. Schematic representation of the crack formed ahead of the stylus moving from left to right. Other cracks have been passed over by the stylus. *Source:* Je, J. H., Gyarmati, E., and Naoumidis, A., "Scratch Adhesion Test of Reactively Sputtered TiN Coatings on a Soft Substrate," *Thin Solid Films* 136 (1986) 57.



Fig. 7. Height profile across the end of the channel showing the crack formed ahead of the stylus. Scratching is from left to right. *Source:* Je, J. H., Gyarmati, E., and Naoumidis, A., "Scratch Adhesion Test of Reactively Sputtered TiN Coatings on a Soft Substrate," *Thin Solid Films* 136 (1986) 57.

Laeng and Steinmann⁶ found Benjamin and Weaver's model to be invalid for the hard coatings used in their work. They included in their analysis a dimensionless parameter

$$X = L/(r^2 H) ,$$

where L is the critical load, r is the tip radius, and H is the substrate hardness, but found this to be, itself, dependent on the coating thickness and tip radius and, thus, failed to obtain quantitative values of the adhesion strength.

In 1984 Laugier²⁷ proposed the following analysis of the scratch test by using an energy description of the film removal. This method was suggested by the unsatisfactory fact that interfacial shearing, assumed by many to be responsible for de-adhesion when a critical load was reached, did not always result in film removal. Also, a necessary condition for coating removal ahead of the stylus is that the film must be under compression. Laugier concluded that for ductile films the material expands and lifts from the substrate to relieve the elastic energy stored in the compressively stressed region ahead of the stylus when this energy is sufficient to provide the work of adhesion and the work to deform the coating. This building up and relieving of stress produces folds along the edges of the scratch path. In the case of brittle materials, fragmentation or spalling of the coating occurs ahead of the stylus when the elastic energy is sufficient to provide the work of adhesion for detachment and work of fragmentation. It is assumed that for both types of films, the work of adhesion is much more significant. Figure 8 shows the de-adhesion caused by energy stored ahead of the stylus. When this de-adhesion propagation was stopped, a cohesive crack formed between the detached and undetached material. Microcracking may occur as the stylus passes over the detached film.

The Acoustic Emission Test

Introduction and Analysis. A scratch testing system can be equipped with an accelerometer, usually mounted just above the scratching stylus, that acts as an acoustic detector. Many researchers have reported good correlation between the acoustic-emission signal and loss of film adhesion.^{6, 8, 10, 11, 13, 18, 22, 28, 29}

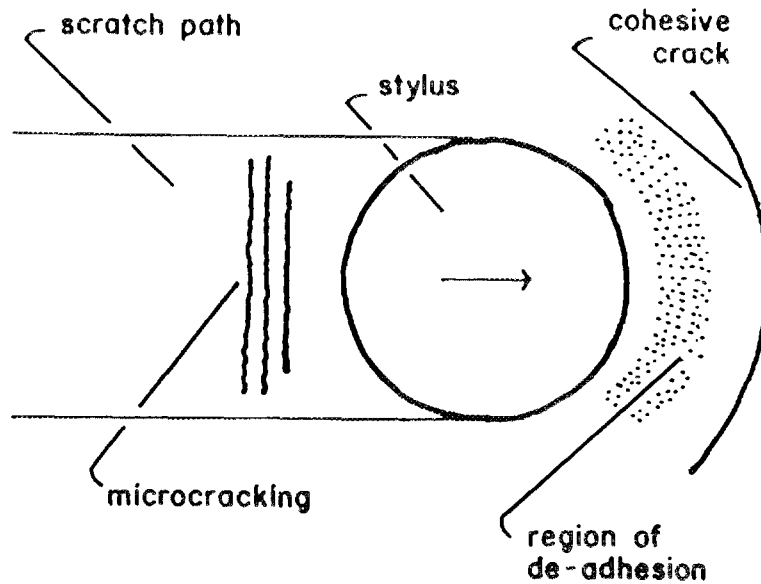


Fig. 8. Model of failure by the scratch test. Elastic energy stored just ahead of the stylus causes de-adhesion, which propagates ahead of the stylus and is stopped by cohesive cracking of the film. Movement of the stylus on the detached film causes microcracking in the scratch path. Source: Je, J. H., Gyarmati, E., and Naoumidis, A., "Scratch Adhesion Test of Reactively Sputtered TiN Coatings on a Soft Substrate," *Thin Solid Films* 136 (1986) 57.

When a material undergoes deformation or fracture, some of the elastic energy induced by the local stresses can be released in the form of stress waves,³⁰⁻³³ which produce small displacements that can be detected on the surface by a sensor. One theory for metals is that stress waves are generated from expanding plastic zones--the small area at the tip of a crack that undergoes plastic deformation as a result of stress concentration.³⁰ Change in the amplitude distribution of the acoustic signal has been observed as a precursor to failure, and it is believed that this is due to the beginning of local cleavage at the crack tip as instability begins.³¹ It has been observed for metals that acoustic emission only occurs when the previous maximum stress level is exceeded, indicating that the acoustic emission is dependent on plastic strain.³⁰

Acoustic emission signals are very dependent on the type of material, specimen size and geometry, previous stress in the specimen, and type of deformation processes.³⁰ The data must have statistical strength to lead to correct conclusions.³¹

A. A. Pollock³¹ proposed a relationship between released energy and the amplitude of the acoustic emission. Referring to a model of a mechanical instability for which the change in stored energy is proportional to the incremental deformation,

$$\Delta E \propto \Delta x ;$$

the kinetic energy released is proportional to the instability,

$$\Delta E \propto I ;$$

and, therefore, the instability is proportional to the incremental deformation,

$$I \propto \Delta x ,$$

he devised an analogous description of an acoustic emission event. In the first stage, the crack tip disrupts the equilibrium of the local material stresses as it moves forward rapidly. In the second stage, propagation of a stress wave restores the mechanical equilibrium. Using this analogy, the amplitude of an emission would be expected to be proportional to the incremental specimen deformation:

$$A \propto \Delta x, \text{ or } A = k_1 \Delta x .$$

According to classical wave theory, the energy should be proportional to the square of the amplitude:

$$\Delta E \propto A^2, \text{ or } \Delta E = k_2 (k_1 \Delta x)^2 = k_3 \Delta x^2 .$$

From this, the author concluded (and verified with experimental evidence) that the energy released as acoustic emission rises in proportion with the magnitude of the deformation event rather than remaining a constant proportion of the total elastic strain energy:

$$\Delta E \propto \Delta x^2 .$$

Thus, larger yields of acoustic emission result from larger deformation events.

Use in Scratch Testing. In 1971 Wilshaw and Rothwell³⁴ described an instrument, which they called an amycometer (from the Greek word for "scratch"), that measured both the normal force on a stylus and the acoustic emissions generated by microcracking of a glass surface as the stylus passed. They found an exact correspondence between the acoustic emissions and direct observation of the microcracks in an optical microscope.

Perry et al.^{8,22} have investigated the relationship between acoustic emissions and loss of coating adhesion for several systems. From these data, it was concluded that acoustic emissions are associated with lateral crack propagation under a shear stress. No emissions were generated when the coating cracked perpendicular to the surface. Perry used his results as a measure of the load-bearing capacity of the coating, which could be due to cohesive and/or adhesive failure. Like Perry, Laeng and Steinmann⁶ concluded from their work that there was no acoustic emission when the coating cracked perpendicular to the surface.

Perry⁸ recorded acoustic emission as a function of stylus load and found more than a hundredfold increase in the emission at the same load where microscopic examination revealed a change in surface morphology and some local loss. In spite of his good correlation between film damage and emissions, Perry cautioned that experience is needed to attribute an increased acoustic signal to adhesive or cohesive loss or to film cracking.

Je, Gyarmati, and Naoumidis¹¹ compared an optical micrograph of a scratch track with the associated acoustic emissions. These data indicated that each crack formation results in an acoustic signal peak.

Use in Other Tests. Acoustic emission has also been used in adhesion tests other than scratch tests. In 1975 Curtis³² used acoustic emissions derived from stressing adhesively bonded lap joints to conclude that (for the adhesives tested) more emissions will be released during failure for a weaker bond. Room and Rawlings³⁵ investigated layered automobile finishes and found that loss of adhesion, macrocracking, and microcracking all resulted in acoustic emission for which there was good correlation between the emission and the degree of damage. Different failure mechanisms were characterized by emissions centered on specific

amplitudes. For scale cracking during high-temperature oxidation, Perkins and Meier³³ believed the source of the emissions to be cracks running parallel to the specimen surface, revealed by scanning electron microscopy. Bunnell, Crowe, and Hart³⁶ found the monitoring of acoustic emission events to be extremely sensitive to surface damage effects in ceramics.

The Pull Test

Introduction. The pull test is a direct measure of the tensile force required to pull the film off normal to the substrate surface. Pins or studs of some kind are attached to the film surface and then pulled off by a calibrated instrument such that the force of removal is known. The major difficulties of this method are in applying to the film a truly normal force rather than a peeling force caused by misalignment and in the attachment of the pin to the film without grossly affecting the film under investigation or the interface between the film and the substrate.³⁷ The limit of the test is the strength of the adhesive used to secure the pin to the film.^{9,12,38,39} Another difficulty is that failure can occur in a complex manner involving several of the interfaces in the system (pin/epoxy/film/substrate) rather than being confined to a single interface.^{36,40}

Consistent results by a number of researchers,^{38,41} as well as the straightforwardness of this method, imply that it is a viable means of investigation. Varchenya and Upit⁴² reported a mean spread of less than 20% for their data.

Variations in Cement Thickness and Bond Strength. In 1976 Jacobsson³⁸ analyzed the pull test in great detail and found the test to be dependent also on variations in cement thickness and homogeneity and on bonding strength variations. The stress will be higher than the average stress at a region where the cement is thinner. Because this higher stress is transmitted to the film, first failure will occur at the locations of minimum cement. In practical cases, no new equilibrium is reached after this first failure, and, thus, total failure occurs. Using a simplified model with a uniform cement thickness distribution, Jacobsson and Kruse⁴³ showed that the force of adhesion measured for a nonuniform cement thickness F_B' is lower than the force of adhesion measured for a

perfectly uniform cement thickness F_B and is approximately given by

$$F_B' = F_B [1 - (1/2)(h_{max} - h_{min})/h_{min}] ,$$

where h_{max} and h_{min} are the maximum and minimum cement thicknesses.

In cases where the film adhesion strength varies, first failure may or may not lead to total failure, depending on the relative values of the maximum and minimum adhesive strengths.³⁸

Fracture Energy Analysis. Cannon, Fisher, and Evans⁴⁴ proposed a fracture mechanics analysis to describe the de-adhesion of a film under a normal tensile force. Cracks tend to extend normal to the maximum tensile stress, and crack extension is driven by the strain energy release rate G :

$$G = (-dW/dA + dU/dA) ,$$

where W and U are the external free energy and internal strain energy, respectively, and A is the crack area. One criterion is that extension of the crack occurs at a critical strain energy release rate G_C . The crack extension path is modified by variations in growth resistance, including those as a result of prior crack extensions and external atmospheres. Variations in film thickness may also influence G_C because the plastic zone size at the crack tip may be limited by the dimensions of the film. Experimentally, measurements and substrate cracking showed that maximum values of the fracture energies, obtained for clean, well-bonded systems, are similar to those of the substrate.

The work of adhesion W_{ad} is the difference in equilibrium energies of the metal and ceramic surfaces created and the metal/ceramic interface destroyed and would be G_C if interfacial fracture were a reversible process. G_C exceeds W_{ad} because the irreversible behavior of crack growth and any plasticity in the system. Fracture energies can be much lower than the maximum values, however, as a result poor bonding between the film and the substrate.

ION-BEAM MIXING

Introduction

Ion implantation originated in the early 1960s when semiconductor researchers began using beams of energetic ions to control the number and depth of the dopant atoms.⁴⁵ The technique had previously been used by physicists and nuclear chemists in their fundamental research into the nature of crystals and the changes caused by atomic collisions. The high-energy dopant ions originate at one end of an accelerator and are driven and focused by an electric field until they enter the target chamber and collide with the target material.⁴⁵ In ion beam mixing, the ion energies are adjusted such that most of the damage is done at the interface. Atoms from the film may be forward-sputtered into the substrate, and atoms from the substrate may be back-sputtered into the film. This transfer creates a transition layer at the interface,³⁹ eliminating the narrow interface through which a fracture may more easily propagate. Basta⁴⁶ referred to this process as "stitching" the coating to the substrate. In some cases, however, an abrupt interface remains.⁴⁷

Effect on Adhesion

Hondros⁴⁸ attempted to explain the increase in adhesion strength after ion beam mixing with a discussion of the thermodynamic work of adhesion and the surface free energy of materials. He asserted that a process, such as ion beam mixing, that reduces the interfacial energy increases the work of adhesion.

Many researchers^{16,19,47,49-53} have reported an improvement in film adhesion as the result of ion beam mixing. However, the apparent increase in adhesion may not be due solely to better adhesion. Ion beam modification can increase the hardness of the surface⁵⁴⁻⁵⁶ and decrease the frictional forces,^{16,57} which may be important parameters, depending on the testing mode.

CHAPTER III

EXPERIMENTAL PROCEDURE

SUBSTRATE MATERIALS

Four different substrate materials were used in this study.

Sapphire (Al_2O_3) single crystals, 25.4 mm in diameter and 1.0 mm thick, were supplied by Crystal Systems, Inc., Salem, Massachusetts. These crystals had been cut to within 2° of the basal plane and polished by the supplier. The crystals were annealed for 120 h at 1450 to 1500°C in air to remove any residual defects. Each crystal was cut into quarters such that the pieces could fit into the ion beam accelerator chamber.

Glass plates 25.4 by 12.7 mm were cut from standard glass microscope slides that had been precleaned and displayed few scratches when viewed optically.

Bars ($3 \times 6 \times 52$ mm) of reaction-bonded silicon nitride (RBN) and sintered alpha silicon carbide (SASC) were supplied by Garrett Gas Turbine Company, Phoenix, Arizona. After being polished to a metallographic finish, the bars were coated with either 15 or 30 nm of aluminum or zirconium and ion beam mixed to various doses by personnel of the Solid State Division of Oak Ridge National Laboratory. These specimens were then used for adhesion testing.

SUBSTRATE CLEANING PROCEDURE

The following cleaning procedure was used for the sapphire and glass substrates preceding film deposition:

1. ultrasonically cleaned in Micro laboratory cleaning solution (15 min for each side),
2. rinsed thoroughly in distilled water,
3. ultrasonically cleaned in acetone (10 min for each side),
4. rinsed thoroughly in distilled water,
5. ultrasonically cleaned in ethyl or isopropyl alcohol (5 min for each side),

6. rinsed with alcohol, and
7. oven dried at 100°C.

This technique, however, removed the 30-nm aluminum film on the RBN and SASC and was, therefore, not used on any of the other specimens that already had a film. Details are provided in a following section.

FILM DEPOSITION

Two apparatus were used for the film deposition.

The first system was an NRC Vacuum Coater consisting of a 10.16-cm-diam diffusion pump and 35-cm-diam, 60-cm-high bell jar and using electrical resistance to heat either a tungsten basket filled with the deposition metal or a tungsten wire coated with the material to be deposited. Lowest vacuum pressures were approximately 1.1×10^{-3} Pa; most depositions took place at a base pressure of about 2.7×10^{-2} Pa. Film thickness was judged optically through the bell jar.

The second system was an Airco Temescal tri-gun electron beam evaporation system with three separate and independent electron beam sources and a 15.2-cm-diam diffusion pump. In this system, bulk material was heated by an electron beam in a water-cooled copper crucible while the substrate specimen remained shielded by a movable shutter. Deposition rate and film thickness were monitored by a quartz crystal in the chamber. This crystal provided a feedback system to adjust the power to maintain the deposition rate and to shut the power off when the correct thickness had been attained. After the deposition rate reached a preset value of 1 nm/s, the substrate was exposed, and the deposition proceeded under electronic control. Base pressures were approximately 1.3×10^{-4} Pa, but pressures during deposition ranged up to 1.3×10^{-3} Pa. Although the substrates were not intentionally heated, radiant heating of the chamber raised the substrate temperatures to approximately 50°C.

The diagram in Fig. 9 shows the electron beam power as a function of time. During the rise and soak times, the bulk deposition material and the chamber were heated to the deposition temperatures to degas the

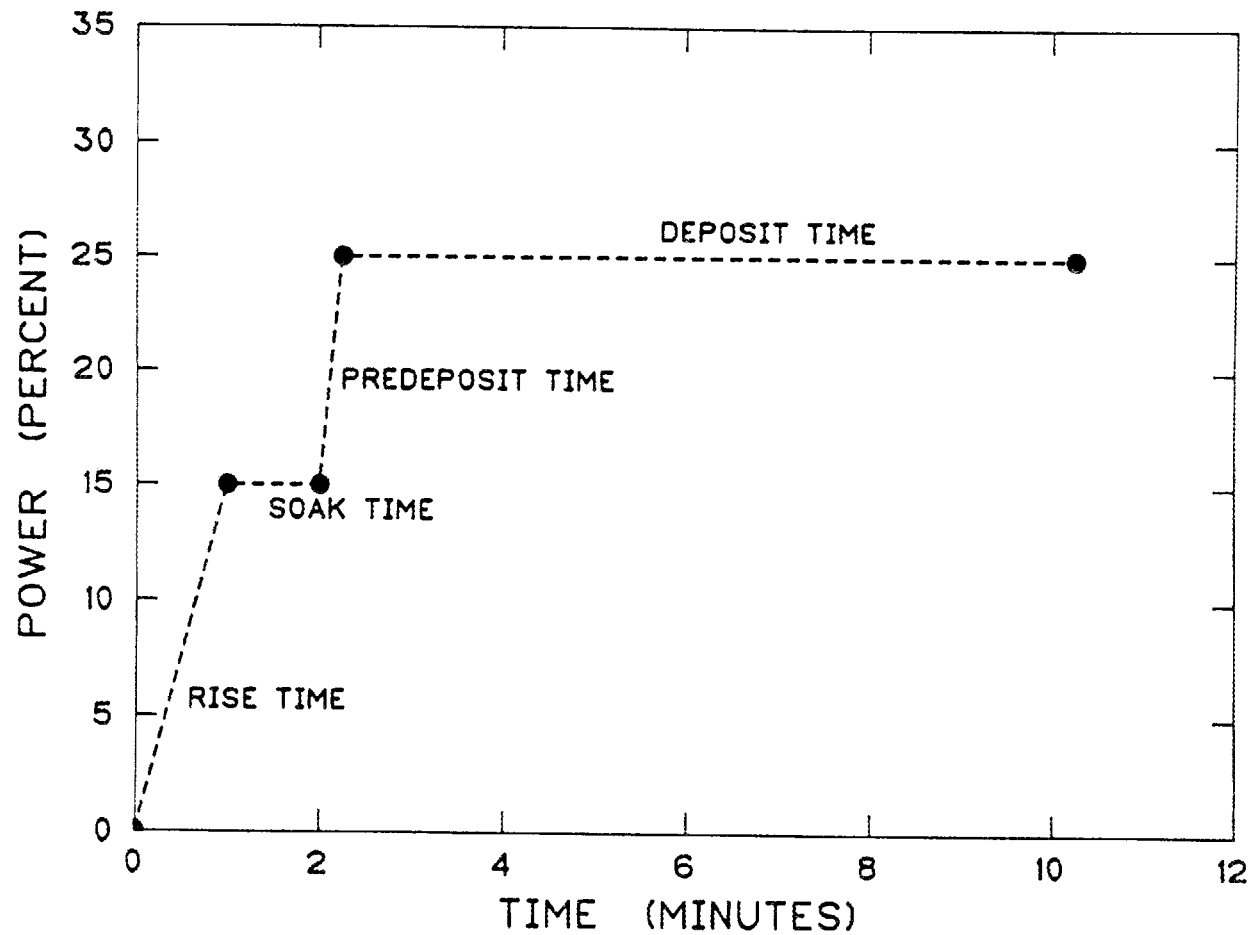


Fig. 9. Electron beam power as a function of time for the depositions of the zirconium film.

melt and drive off any surface oxides. The predeposit time allowed the deposition rate to reach the preset value before the specimen substrate was exposed.

Films of chromium, zirconium, nickel, and aluminum were deposited by one of these methods. Thicknesses of 100, 200, and 500 nm were deposited.

SPECIMEN CHARACTERIZATION

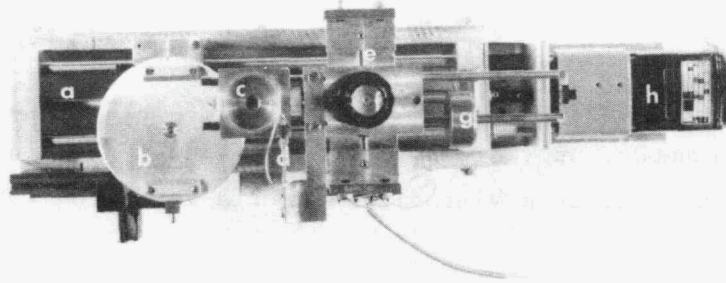
Hardness tests were performed using a Leitz Miniload Hardness Tester to determine the Vickers hardness. Substrate hardnesses were found by using a 100-g load for 30 s. Film/substrate hardnesses were found by using both a 100-g load for 30 s and a load such that the indentation depths were of the order of the scratches made during scratch testing.

Substrate and film surface characterizations were made by using a Tencor Alpha Step 200 profilometer fitted with a 0.22- μm -radius diamond stylus under a load of 2 to 4 mg. Scan lengths of 400 and 2000 μm were made. Arithmetic average surface roughness values, calculated by the instrument (ANSI Standard B46.1-1978, graphically determined), were taken as a measure of the surface roughness of both the substrate and film, and the step height at the edge of the film was used as a measure of the film thickness.

SCRATCH TEST

The scratch tester used for this project (Fig. 10) consisted primarily of a balanced lever arm with a diamond stylus and a load platform directly above the stylus. The stylus, a spherical diamond or steel penetrator for Rockwell Hardness testing, was a separate piece with adjustable extension below the load platform. To begin testing, the lever arm was exactly balanced in the horizontal position with the tip of the stylus just touching the specimen surface when the specimen was mounted on the movable stage below. The stylus and load platform mounted on the lever arm were rigidly attached to a strain gage such that all tangential (horizontal) forces on the stylus were measured.

YP4798



YP4799

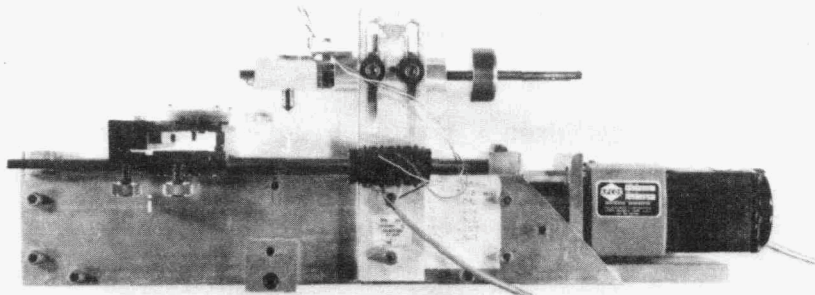


Fig. 10. The scratch tester. The following parts are labeled: (a) drive shaft, (b) movable stage, (c) load platform, (d) strain gage, (e) axis of lever arm rotation, (f) carpenter's level, (g) balance weight, (h) motor, (i) horizontal plane adjusters for stage, (j) stylus. Actual length: 50 cm.

The strain gage was adjusted to read zero in the no-load configuration. A load was then placed on the load platform. The stage with the specimen rigidly mounted was moved under the stylus at a constant speed of 1.6 mm/min by a gear ratio motor. The signal from the strain gage was output to an analog recorder that plotted tangential force on the stylus

vs time (which corresponded to length of the scratch). In each case, the specimen was aligned so that the scratch began at least 0.5 mm before the edge of the film and continued approximately 1 mm across the film.

Although there existed some vibrations of the system caused by the gear ratio drive motor, unpredictable vibrations were eliminated by operating the equipment on a Vibraplane inertia isolation table.

ACOUSTIC EMISSION TEST

In the current investigation, an accelerometer was mounted to the side of the stylus on the load platform. This was then connected to a shock amplifier and the amplifier connected to a strip chart recorder. More than fifty scratches were made with varying film materials, normal loads, chart sensitivities and speeds, amplifier sensitivities, and frequency filters. However, no patterns that signified loss of adhesion emerged; in fact, no difference could be detected between when the stylus was running on the bare substrate and when it crossed onto the film. It is suspected that whatever specimen emissions might have occurred were overshadowed by those of the drive motor, which could not be adequately isolated from the system.

PULL TEST

The pull testing was done using a Sebastian I Adherence Tester manufactured by the Quad Group. In this test, pre-epoxied bonding pins supplied by the Quad Group were attached to the film surface by clips and then oven cured. Much experimentation was done to determine the cure cycle that would deliver the maximum epoxy strength and adherence to both the film and the pin. This was found to be a 0.5-h temperature ramp to 150°C, 1.5 h at 150°C, and then oven cooled to room temperature. The specimens were then allowed to sit at room temperature for at least 24 h before testing. The tensile stress required to remove the pin was indicated on a digital display, and the accuracy was specified as being $\pm 10\%$. An analog recorder was also attached to the equipment so that a force vs time plot was also generated, thus allowing the calculation of the energy to failure.

Other commercial epoxies were also used in conjunction with the Sebastian Adherence Tester studs that did not have a precoat of epoxy. None of these had a greater bonding strength than the pre-epoxied pins, and, thus, no data are reported for these trials.

ION-BEAM MIXING

The ion beam mixing was performed on all of the sapphire and glass specimens by using the Oak Ridge National Laboratory 5-MeV Van de Graaff accelerator supplying Fe^+ ions at 1 MeV to a fluence of 1×10^{17} ions/cm². A portion of each specimen was masked to preserve a virgin region.

The computer code E-DEP-1 (version 5) supplied by the Naval Research Laboratory^{5,8} was used to calculate the distribution of energy deposited into elastic collisions as a function of heavy-ion penetration depth into an amorphous material. These data gave assurance that the ion beam was penetrating the film and mixing was occurring in the interfacial region.

•

•

•

•

•

CHAPTER IV

RESULTS AND DISCUSSIONS

THE SCRATCH TEST

The scratching of a thin, ductile film on a brittle substrate is a very complex phenomenon.

The final judgment of the film's integrity in this study was based on the transmission of light through the specimen: because the substrate was transparent and the film opaque, transmitted light signified film absence. There are drawbacks to this method, as noted in the literature review, because ductile films may be thinned to transparency by sideways extrusion and some films, although nonadherent, may be pressed back into the scratch path under the passing stylus. An attempt was made to distinguish between film loss and film thinning. Also, the total stress state of the film, including inherent stresses developed during growth and thermal cycling, and applied stresses caused by normal loading and friction, may be sufficient in preventing the film from pulling away from the substrate, and, thus, de-adhesion will not be detected. Some judgment must be used in defining film loss. Small portions of film removed may be due to flaws (either inherent or created during handling) and may or may not be considered important, depending on the purpose of the experiment. In this work, only regular or continuous, easily detected stripping was considered significant.

Systems Analyzed

Aluminum Films on Glass. Difficulty in the analysis of very adherent films led to the use of aluminum films on glass substrates because this system proved to have very low adherence. The films did not pass the tape test (were removed by plastic tape), and optical microscopy using a light source below the transparent substrate revealed the critical load (defined as that normal load at which the film is stripped from the substrate) as being less than 1 g (0.0098 N). The aluminum films were 120 nm thick and had an average arithmetic surface roughness of 5 nm. Although no noticeable differences in the film

surfaces were found from surface profilometry, large differences in the coefficients of friction under the stylus, at the same normal load, were recorded.

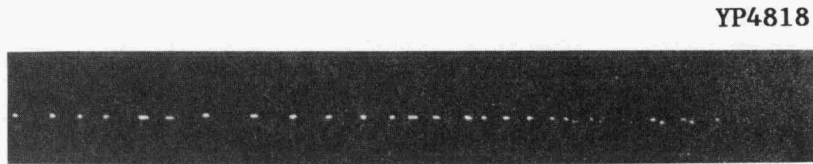
Nickel and Chromium Films on Sapphire. Based on some earlier promising results, chromium was chosen as a film material. Hondros⁴⁸ observed that nickel had relatively poor adhesion to sapphire, and it was felt that this system had good promise for measurable improvement by ion-beam mixing. Nickel films and chromium films on sapphire substrates proved to be much more adherent than the aluminum films to glass. Typical critical loads, although inconsistent, were of the order of 50 g. These films were approximately 200 nm thick.

Zirconium Films on Sapphire. Two of the zirconium films were extremely adherent to their sapphire substrates. Even scratches made under a 300-g load did not cause de-adhesion of the film. Scratches made using normal loads less than 150 g were not visible in an optical microscope at a magnification of 40X. Other scratches were barely visible even under a magnification of 700X. However, another of these specimens had relatively poor adherence: the critical load for it was approximately 10 g.

Scratch Characteristics

System Vibrations and Noise. System vibrations as a result of the gear ratio drive motor were apparent for the very low normal loads used to investigate the aluminum/glass systems. Figure 11 shows a scratch made under a 0.45-g normal load but at a speed 50 times faster than used for actual testing to exaggerate the skipping effect. Figure 12 shows a similar pattern obtained during an actual test under a normal load of 2 g. This skipping was not apparent at higher loads because the change in loading caused by this vibration is such a small percentage of the total loading for the more heavily loaded scratches.

Noise generated by the strain gage, strain gage analyzer, analog recorder, and connecting cables lowered the resolution of the tangential force measurement. The lack of sensitivity to very subtle changes in the tangential force may have prevented a more accurate description of the stress state of the film.

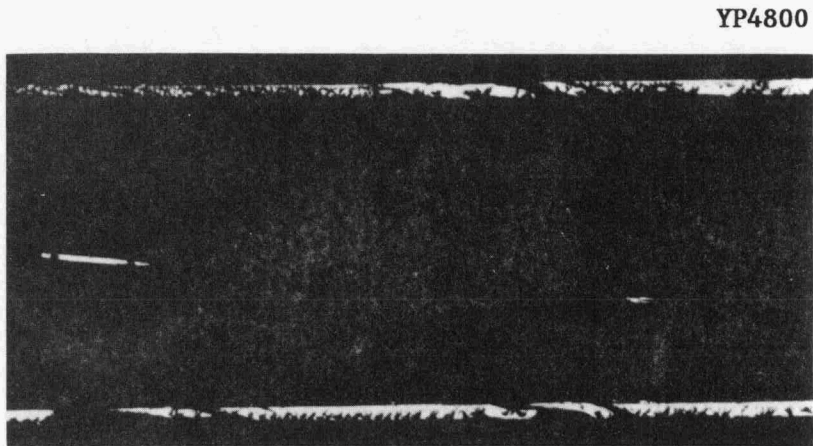


(a) Transmitted light. 42X.

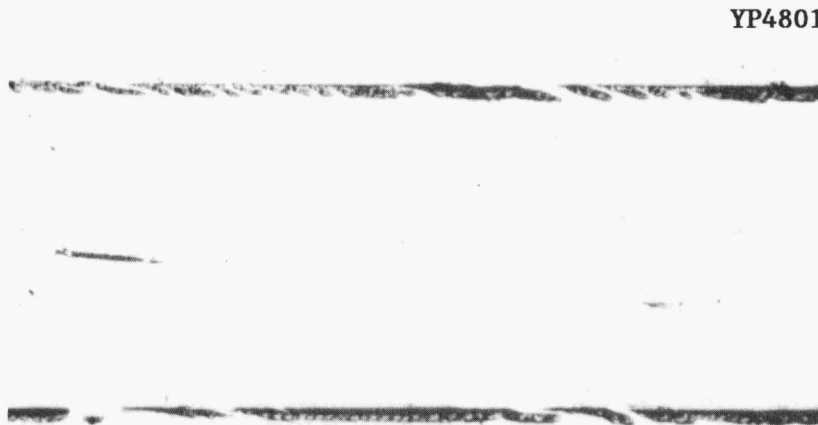


(b) Reflected light. 450X.

Fig. 11. Stylus skipping caused by system vibrations. Scratch made on aluminum/glass system under a normal load of 0.45 g. The speed of the stylus travel was increased to exaggerate the skipping effect. Scratch direction is from left to right.



(a) Transmitted light. 68X.



(b) Reflected light. 68X.

Fig. 12. Scratch made on aluminum/glass system under a normal load of 2.0 g. Scratch direction is from left to right.

Because of the combined effects of system vibrations and noise, the scratch test can be considered to have a lower limit. Adhesion levels below this limit cannot be adequately measured.

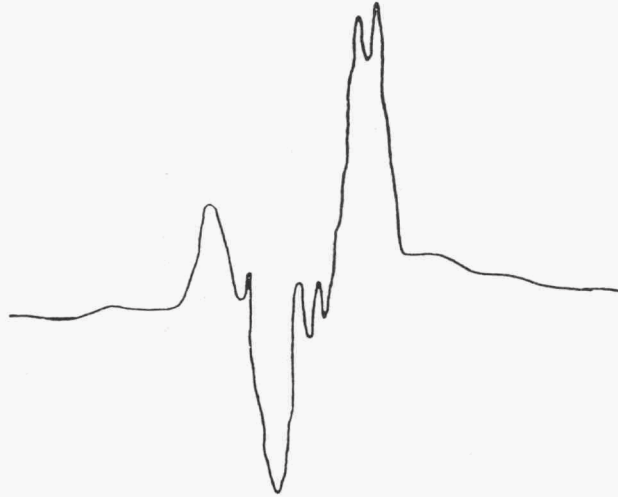
Characteristics of the Scratch Path. Typical scratch profiles are shown in Fig. 13. The ridges beside the path may or may not be present, depending on the deformation mode. Ridges in the center of the track are quite common.

The scratch path is, in general, neither uniform nor symmetrical, even at loads higher than the critical loads. This is evident from both the profiles of Fig. 13 and the micrographs of Figs. 14-16. For the aluminum/glass systems, some of the film material pushed out of the path of the stylus remained attached to the side of the channel. These pile-ups often immediately preceded a section of narrow track or a skipped region, indicating that material had piled up ahead of the stylus, sufficiently increasing the resistance to motion to cause the stylus to rise onto the film surface to keep on moving. Many of these flakes were not removed in an ultrasonic bath, denoting that the film was not broken from the side of the channel. Figures 17 and 18 show two such regions, before and after ultrasonic cleaning. It is not known what contribution the system vibrations made to this skipping. The irregularity, however, implied that the vibrations were not the most significant aspect. Figure 19 shows the full length of the scratches in Figs. 17 and 18, and it can be seen that the skipping is not regular.

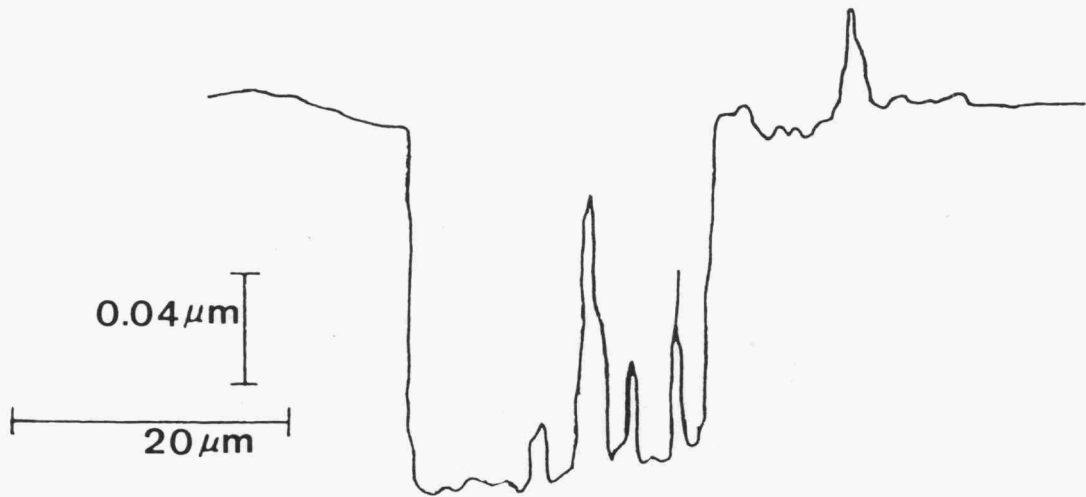
Thinning of the film under the stylus was particularly apparent for the zirconium films on sapphire, possibly because of a stress state unfavorable to film removal, even if de-adhesion has occurred.⁷ Film thinning under both 10- and 200-g normal loads can be seen Fig. 20.

Occasionally, significant scratching was initiated by the presence of a surface flaw. This is illustrated clearly in Fig. 21.

Deformation Modes. Comparison of the scratches made by the diamond stylus on the chromium and nickel films on sapphire substrates revealed a significant difference in the deformation modes. Transverse profiles of the scratches made on nickel/sapphire systems showed hillocks all along



(a) Nickel film on sapphire.



(b) Aluminum film on glass.

Fig. 13. Typical scratch profiles.

YP4796

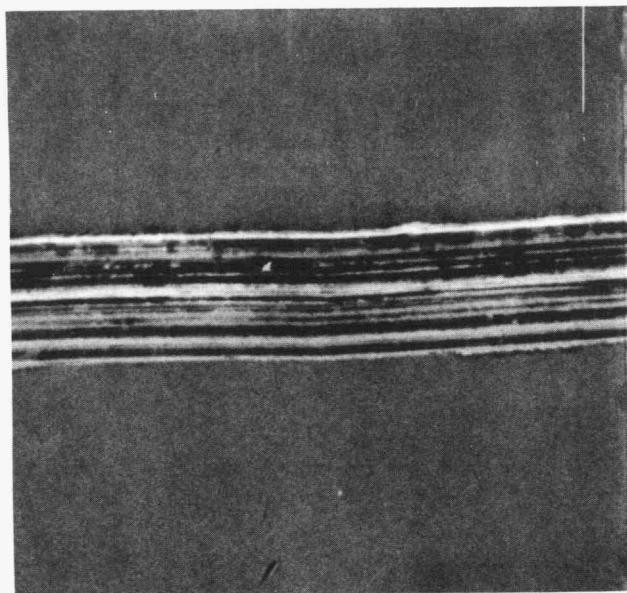


Fig. 14. Scratch made on zirconium/sapphire specimen under a normal load of 30 g. Scratch direction is from left to right. Scanning electron micrograph, 1600X.

YP4797

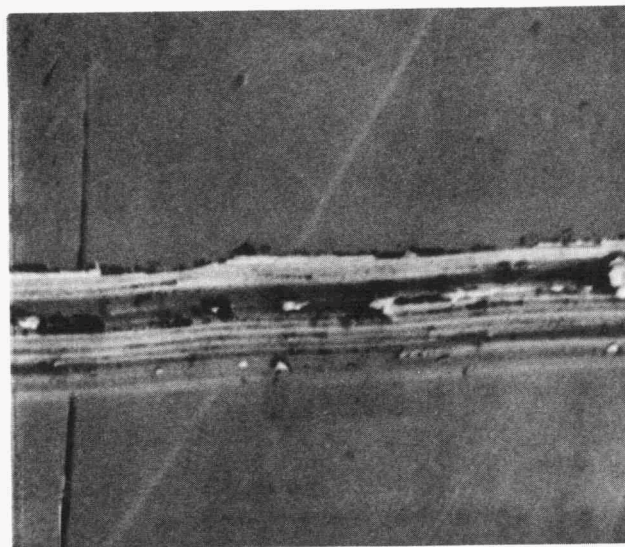


Fig. 15. Scratch made on zirconium/sapphire specimen under a normal load of 40 g. Scratch direction is from left to right. Scanning electron micrograph, 1650X.

YP4793

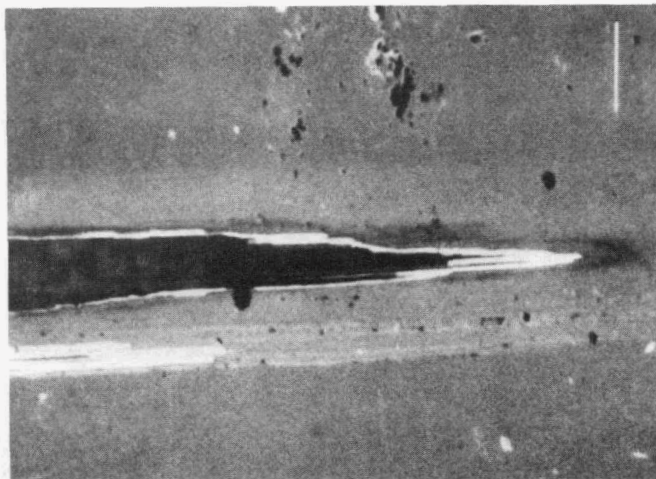
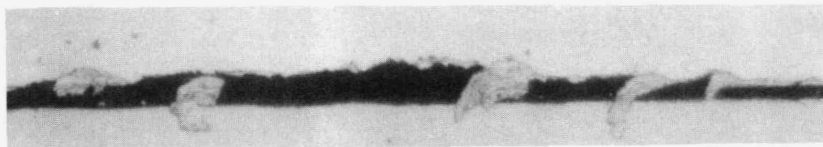


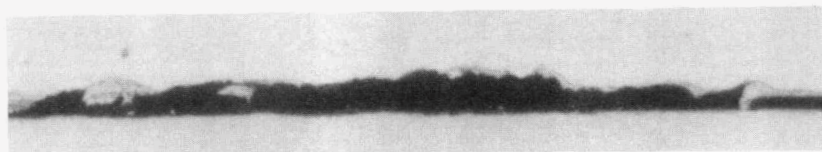
Fig. 16. Scratch made on nickel/sapphire specimen under a normal load of 150 g. The white steaks signify film removal. Scratch direction is from left to right. Scanning electron micrograph, 1430X.

YP4795



(a) Before ultrasonic cleaning. 450X.

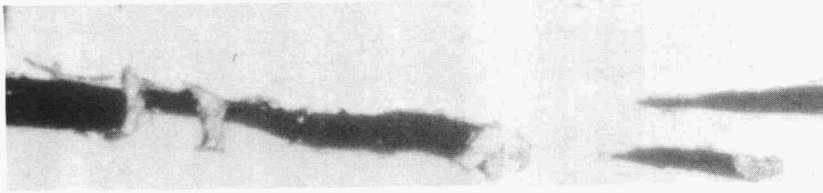
YP4790



(b) After ultrasonic cleaning. 450X.

Fig. 17. Scratches made on aluminum/glass specimen under a normal load of 0.45 g. Scratch direction is from left to right.

YP4794



(a) Before ultrasonic cleaning. 450X.

YP4789



(b) After ultrasonic cleaning. 450X.

Fig. 18. Scratches made on aluminum/glass specimen under a normal load of 1.0 g. Scratch direction is from left to right.

YP4788



YP4787



Fig. 19. Full-length view of scratches in Figs. 17 and 18 before ultrasonic cleaning. Scratch direction is from left to right. 42X.

YP4811

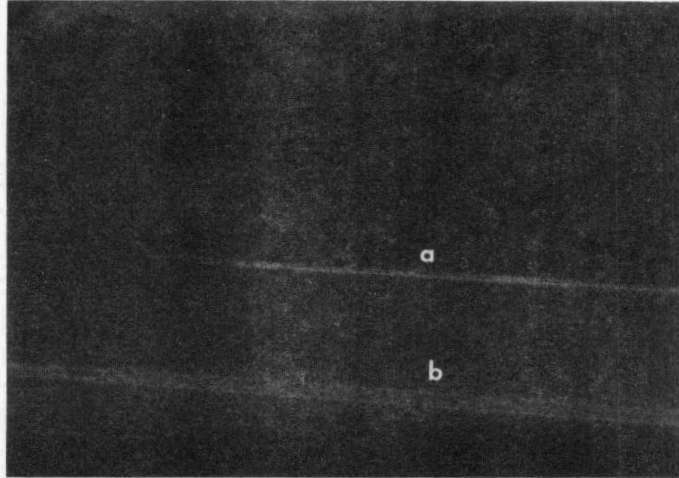


Fig. 20. Thinning of zirconium film under normal stylus loads of (a) 10 g and (b) 200 g. 128X.

YP4804

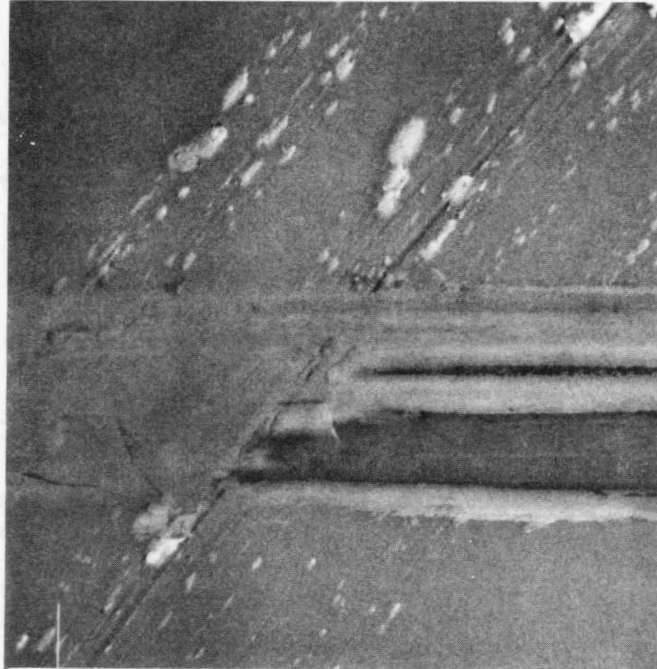


Fig. 21. Effect of surface flaw on scratching of zirconium/sapphire system. Scratch direction is from left to right. Scanning electron metallograph. 1600X.

ORNL-DWG 88-2204

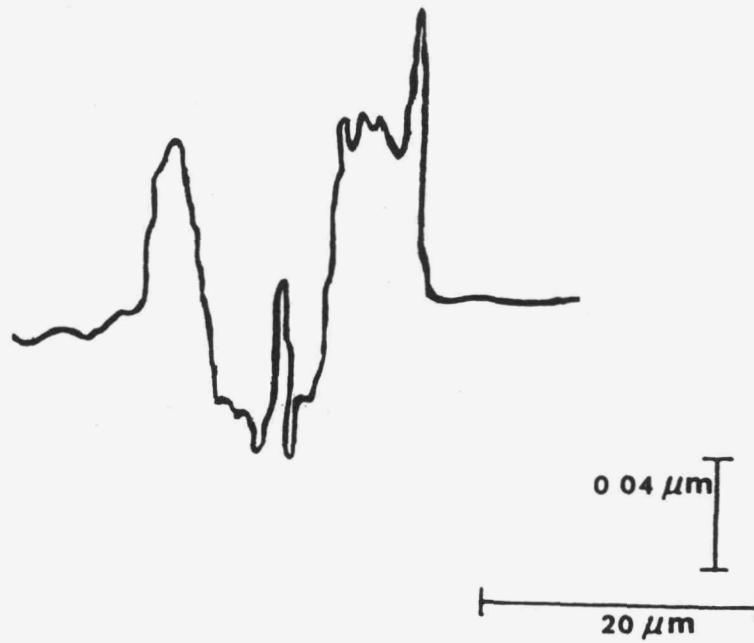


Fig. 22. Transverse profile of a scratch showing ductile extrusion of nickel film on a sapphire substrate.

ORNL-DWG 88-2205

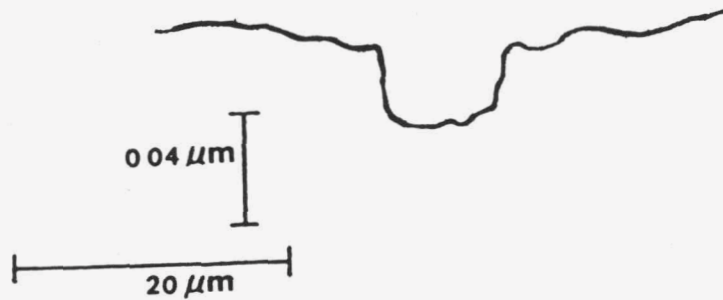


Fig. 23. Transverse profile of a scratch showing absence of ductile extrusion of chromium film on a sapphire substrate.

YP4805

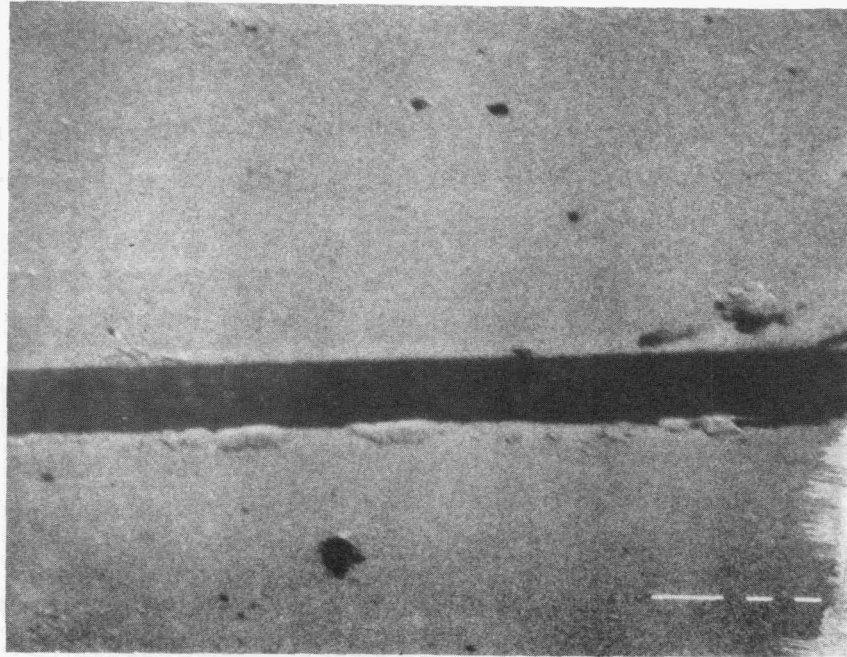


Fig. 24. Scanning electron micrograph of a 250-g normal load scratch on a chromium/sapphire specimen. Scratch direction is from left to right. 1000X.

quantitatively compared unless the failure mode differences are accounted for by determining the actual stress states of the film at the location of failure. This example points out the necessity of microscopic examination to determine the failure mode because testing parameters may have a great effect.

Analyses

Variations in Styli and Film Thickness. The scratch test was used only to compare the adhesion of similar systems. Theoretically, it is evident that variations in styli and film thickness are both very important variables.

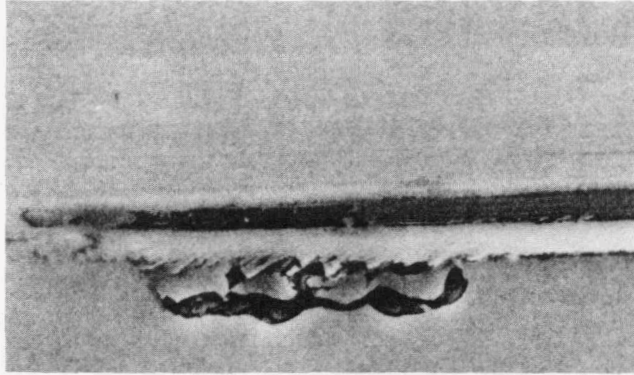
the edge of the scratch channel (Fig. 22). This is indicative of ductile extrusion under the stylus. Scratches made on chromium/sapphire systems, however, showed no evidence of extrusion in either profiles or micrographs (Figs. 23 and 24). Figure 24 does show some material along the side of the channel, but the irregularity of its occurrence indicates that the film was broken and then pushed aside by the passing stylus rather than extruded from underneath the stylus.

The scratches in Fig. 25 were made on an ion-beam-mixed zirconium/sapphire system. These show a compressive failure in the form of "bubbles" to the side of the scratch path, which has only been thinned: film removal occurred only in the "popped out" regions to the side of the channel. Because evaporated films are almost always in a state of tension, the compressive stresses were most likely generated ahead of the moving stylus in both the film and the substrate. Also, if it were the film alone that failed, de-adhesion would have initiated immediately next to the path where the film was weakened rather than away from the track as it appears to have done.

The analysis of Hamilton and Goodman²¹ describing the tensile stresses behind the moving stylus is supported by Fig. 26. Theoretical lines of constant tensile stress acting in the plane of the surface are shown in Fig. 27 for a coefficient of friction of 0.25. The line of constant maximum tensile stress lies in almost an identical location for a friction coefficient of 0.50. Comparison of Figs. 26 and 27 reveals that the cracks of Fig. 26 almost exactly propagate along the theoretical lines of maximum tensile stress. The dark lanes in the scratch paths of the micrographs are regions stripped of the film. It is interesting to note the lack of symmetry in the scratch path and the fact that the cleared portion actually changes sides (both micrographs of Fig. 26 are from the same track).

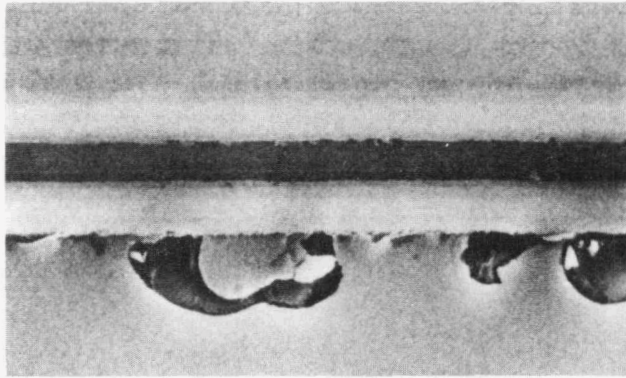
The systems illustrated in Fig. 25 and 26 were both from the same zirconium/sapphire specimen but the failure modes were very different: the first, in the ion-based-mixed region, was a compressive failure ahead of the moving stylus; the second, however, in the unmixed region, was a tensile failure behind the stylus. The results of these tests cannot be

YP4791



(a) Scanning electron micrograph. 1600X.

YP4816

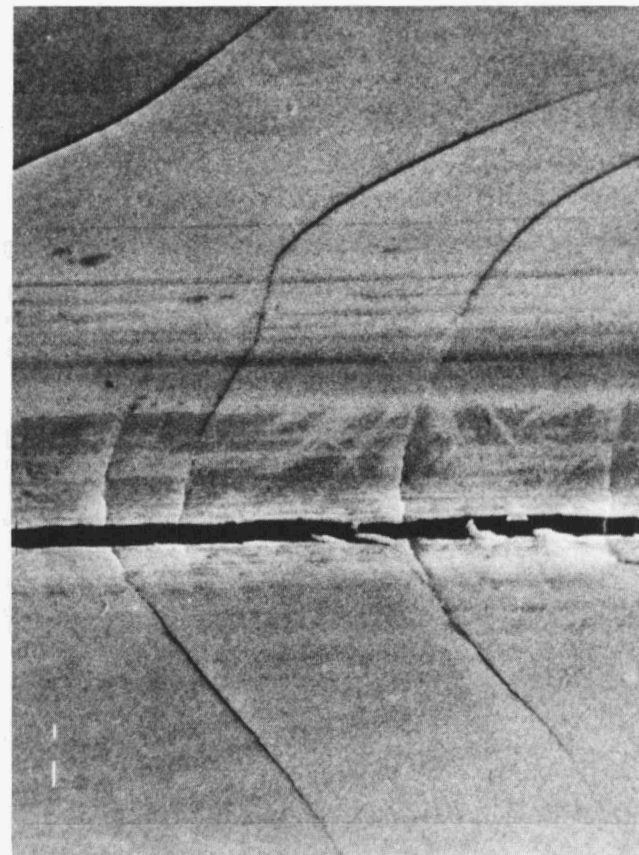
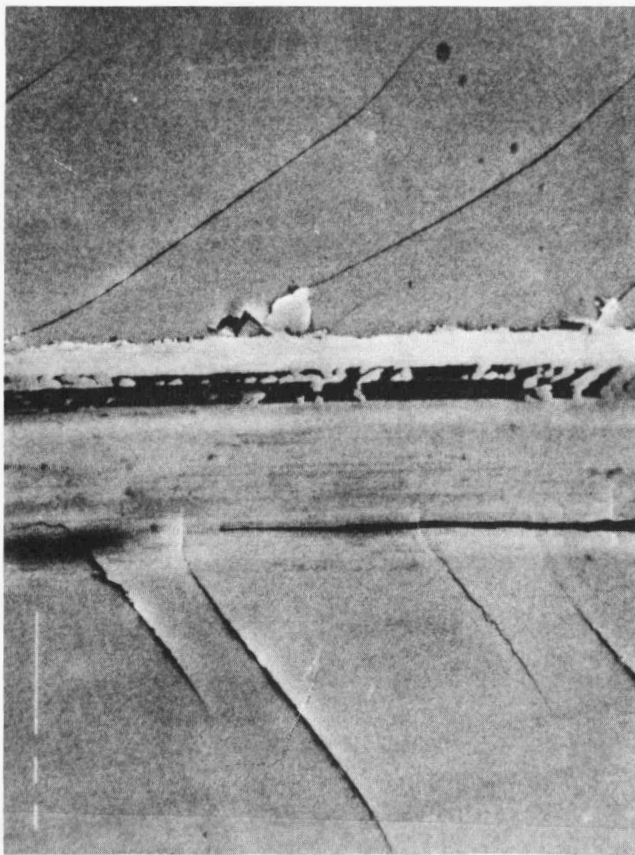


(b) Scanning electron micrograph. 1700X.

Fig. 25. Two regions of compressive failure caused by a 450-g normal load scratch on a zirconium/sapphire specimen. Scratch direction is from left to right.

YP4812

YP4813



(a) Scanning electron micrograph. 1600X.

(b) Scanning electron micrograph. 199X.

Fig. 26. Tensile failure behind the meaning stylus caused by a 400-g normal zirconium/sapphire specimen. Scratch direction is from left to right.

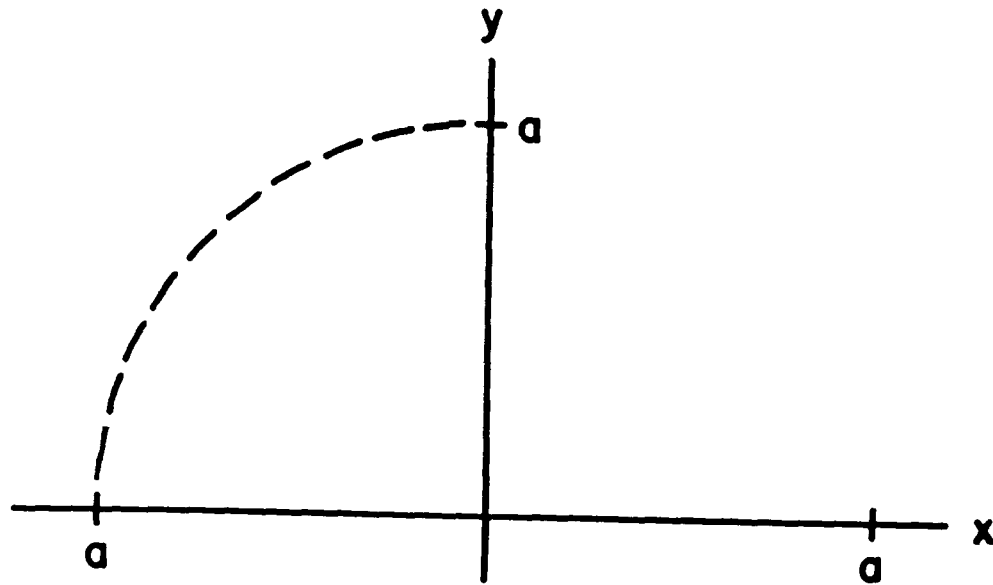


Fig. 27. Theoretical line of constant maximum tensile stress acting in the plane of the surface for a friction coefficient of 0.25. The stylus moves in the positive x -direction, and a is the radius of the circle of contact.

Source: Hamilton, G. M., and Goodman, L. E., "The Stress Field Created by a Circular Sliding Contact," *J. Appl. Mech.* 88 (1966) 371.

Stylus radius and hardness affect the penetration depth of the stylus into the specimen and, thus, are important factors in the stress distribution under the stylus. Frictional forces, which play a very important role in adhesion failure, are controlled partially by the stylus material and geometry. The point of maximum yield is often below the surface of the specimen. If all other factors are the same, the thickness of the film defines whether this point lies in the film or in the substrate. Because the material properties of the film and substrate differ, this is a critical consideration.

Analysis Based on Normal Load Criterion. The definition of film adhesive strength based on a critical normal load W to cause de-adhesion was not very consistent. This was not unexpected, however, because it has already been noted that there are a large number of significant parameters involved, including coefficient of friction, which can even vary along the same scratch. For some sets of data, a critical normal load could be defined, but because this was not the case for even a

majority of the data, the correlation probably was due to the dependence of other factors on the normal load. For example, an increase in the majority of the data, the correlation probably was due to the dependence of other factors on the normal load. For example, an increase in the normal load also increased the film and substrate deformations, the radial and shear stresses under the stylus, the mean pressure, the contact area of the stylus, and usually the tangential force.

Analysis Assuming Full Plasticity. Benjamin and Weaver² based their analysis of the scratch test on the assumption of full plasticity under the stylus. The shear stress at the lip of the indentation under a load W was defined as

$$F = \{a/(r^2 - a^2)^{1/2}\} P ,$$

where P is the indentation hardness of the substrate, r is the stylus radius, and a is the contact radius, defined, at full plasticity, as

$$a = (Wg/\pi P)^{1/2} .$$

The shear stresses generated from these equations were also often inconsistent with the loss of film material as defined by light transmission in a microscope. This shear stress increased with the normal load as predicted from the dependence of the shear force on the normal load. Table 1 shows the shear stresses generated from data for scratches on one of the zirconium/sapphire systems. Although higher shear stresses were more likely to result in film loss, there was no clearly defined critical shear stress above which the film was stripped.

The normal force shown in the tables is the effective normal force applied to the surface after the moment caused by the tangential force is accounted for. This moment occurs because the tangential force is not in a horizontal line with the center of rotation of the scratch tester lever arm, and because of the direction of motion, the moment serves to lessen the applied normal force on the surface.

Table 1. Shear stresses calculated using the plastic model analysis for scratches on zirconium/sapphire

Normal force (Newtons)	Tangential force (Newtons)	Shear stress (GPa)	Coefficient of friction	Film de-adhesion
0.0938	0.0128	0.1378	0.136	Yes
0.0948	0.0098	0.1385	0.104	No
0.1410	0.0181	0.1689	0.129	Yes
0.1426	0.0132	0.1699	0.093	Yes
0.1438	0.0098	0.1706	0.068	No
0.1849	0.0332	0.1935	0.179	Yes
0.1906	0.0164	0.1964	0.086	Yes
0.1909	0.0157	0.1966	0.082	Yes
0.2785	0.0464	0.2374	0.167	Yes
0.2844	0.0290	0.2400	0.102	Yes
0.2853	0.0265	0.2403	0.093	Yes
0.2856	0.0255	0.2405	0.089	Yes
0.3717	0.0607	0.2743	0.163	Yes
0.3777	0.0432	0.2765	0.114	Yes
0.3797	0.0373	0.2773	0.098	Yes
0.4664	0.0708	0.3073	0.152	Yes
0.4667	0.0699	0.3074	0.150	Yes
0.4718	0.0549	0.3091	0.116	Yes
0.9126	0.2009	0.4299	0.220	Yes
0.9209	0.1766	0.4318	0.192	Yes

Table 2 shows the good correlation between shear stress and film de-adhesion for a chromium/sapphire specimen. In contrast, the only shear stress that did not result in nickel film de-adhesion from sapphire was an intermediate value (Table 3). This latter may have been due to insufficient data to generate a statistically accurate result. Another possible explanation may lie in the difference in the deformation modes, as already discussed: the nickel/sapphire systems exhibited ductile extrusion of the film along the scratch path, but the chromium films showed no evidence of extrusion. Data taken for nickel/sapphire systems, then, would most likely be very dependent on the mechanical properties of the film and the friction between the film and the stylus and would not lend themselves to description by an equation neglecting these factors.

Table 2. Shear stresses calculated using the plastic model analysis for scratches on chromium/sapphire

Normal force (Newtons)	Tangential force (Newtons)	Shear stress (GPa)	Coefficient of friction	Film de-adhesion
0.0962	0.0057	0.1395	0.059	No
0.1400	0.0210	0.1683	0.150	No
0.1876	0.0251	0.1949	0.134	No
0.1904	0.0172	0.1963	0.090	No
0.1962	0.0000	0.1993	0.000	No
0.2828	0.0337	0.2393	0.119	No
0.2830	0.0332	0.2394	0.117	No
0.4669	0.0695	0.3074	0.149	No
0.4760	0.0426	0.3104	0.089	No
0.4769	0.0400	0.3107	0.084	No
0.4805	0.0293	0.3119	0.061	No
0.9334	0.1399	0.4347	0.150	No
0.9452	0.1052	0.4375	0.111	No
0.9528	0.0829	0.4392	0.087	No
0.9583	0.0666	0.4405	0.070	No
1.4051	0.1951	0.5334	0.139	No
1.8622	0.2931	0.6141	0.157	Yes
2.3540	0.2893	0.6905	0.123	Yes

Table 3. Shear stresses calculated using the plastic model analysis for scratches on nickel/sapphire

Normal force (Newtons)	Tangential force (Newtons)	Shear stress (GPa)	Coefficient of friction	Film de-adhesion
0.9376	0.1274	0.4357	0.136	Yes
1.3840	0.2570	0.5294	0.186	Yes
1.3874	0.2470	0.5301	0.178	Yes
1.3988	0.2135	0.5322	0.153	No
1.8653	0.2839	0.6147	0.152	Yes
1.8660	0.2818	0.6148	0.151	Yes

Data from scratches made with a steel stylus on aluminum/glass systems are shown in Table 4. The shear stress in this case correlated well with loss of adhesion. The theoretical and experimental values of the radius of the circle of contact a are plotted as a function of normal force in Fig. 28. The experimental values were an order of magnitude larger than the theoretical values, possibly because of the failure of the theory to account for the elastic deformation of the system.²

Analysis Assuming Elastic Conditions. Laugier⁷ assumed that adhesive failure of the film can occur under elastic conditions ahead of the stylus. The radial compressive stress ahead of the stylus is given by

$$\sigma = (Wg/2\pi a^2) \{ (4 + \nu_1)(3\pi f/8) - (1 - 2\nu_1) \} ,$$

and the shear stress is approximated by

$$\tau \approx \sigma(a/r) .$$

This analysis is examined more thoroughly in the literature review.

The equations of Laugier were used to generate values for the coefficients of friction, radial compressive stresses, shear stresses, and mean pressures for several systems. In each case, the elastic moduli were estimated at bulk substrate material values, and Poisson's ratio was taken as 0.3 for all materials. Errors resulting from not using a composite modulus occurred consistently; the effect was merely to adjust the numbers by a linear factor. Table 5 shows the values of the shear and radial stresses calculated for one set of zirconium/sapphire data. This specimen was chosen because the modulus of zirconium (94.5 GPa) varies by the largest amount from that of its substrate (410 GPa) for the four systems investigated. In some instances, the coefficient of friction was low enough to result in a tensile radial stress (denoted by a negative sign in the tables).

Data for the aluminum/glass and the zirconium/sapphire systems show no correlation between the calculated stress values and film de-adhesion. Even some of the tensile stresses generated, which theoretically should not result in film loss, did cause film de-adhesion, possibly because of

Table 4. Shear stresses calculated using the plastic model analysis for scratches on aluminum/glass

Normal force (Newtons)	Tangential force (Newtons)	Contact radius (mm)	Shear stress (GPa)	Coefficient of friction	Film de-adhesion
0.0013	0.0004	0.0002	0.0023	0.293	No
0.0015	0.0000	0.0002	0.0024	0.000	No
0.0025	0.0013	0.0003	0.0031	0.508	Yes
0.0029	0.0002	0.0003	0.0033	0.068	No
0.0029	0.0000	0.0003	0.0034	0.000	No
0.0035	0.0026	0.0004	0.0037	0.719	Yes
0.0040	0.0013	0.0004	0.0039	0.320	Yes
0.0044	0.0000	0.0004	0.0041	0.000	Yes
0.0044	0.0000	0.0004	0.0041	0.000	Yes
0.0044	0.0000	0.0004	0.0041	0.000	Yes
0.0085	0.0038	0.0006	0.0058	0.450	Yes
0.0085	0.0038	0.0006	0.0058	0.450	Yes
0.0087	0.0032	0.0006	0.0058	0.372	Yes
0.0088	0.0028	0.0006	0.0059	0.322	Yes
0.0092	0.0017	0.0006	0.0060	0.180	Yes
0.0094	0.0011	0.0006	0.0061	0.114	Yes
0.0095	0.0010	0.0006	0.0061	0.104	Yes
0.0175	0.0062	0.0008	0.0083	0.353	Yes
0.0180	0.0048	0.0009	0.0084	0.267	Yes
0.0180	0.0048	0.0009	0.0084	0.267	Yes
0.0180	0.0048	0.0009	0.0084	0.267	Yes
0.0183	0.0038	0.0009	0.0085	0.209	Yes
0.0183	0.0038	0.0009	0.0085	0.209	Yes
0.0184	0.0037	0.0009	0.0085	0.203	Yes
0.0441	0.0144	0.0013	0.0131	0.327	Yes
0.0450	0.0120	0.0014	0.0132	0.266	Yes
0.0451	0.0116	0.0014	0.0133	0.257	Yes

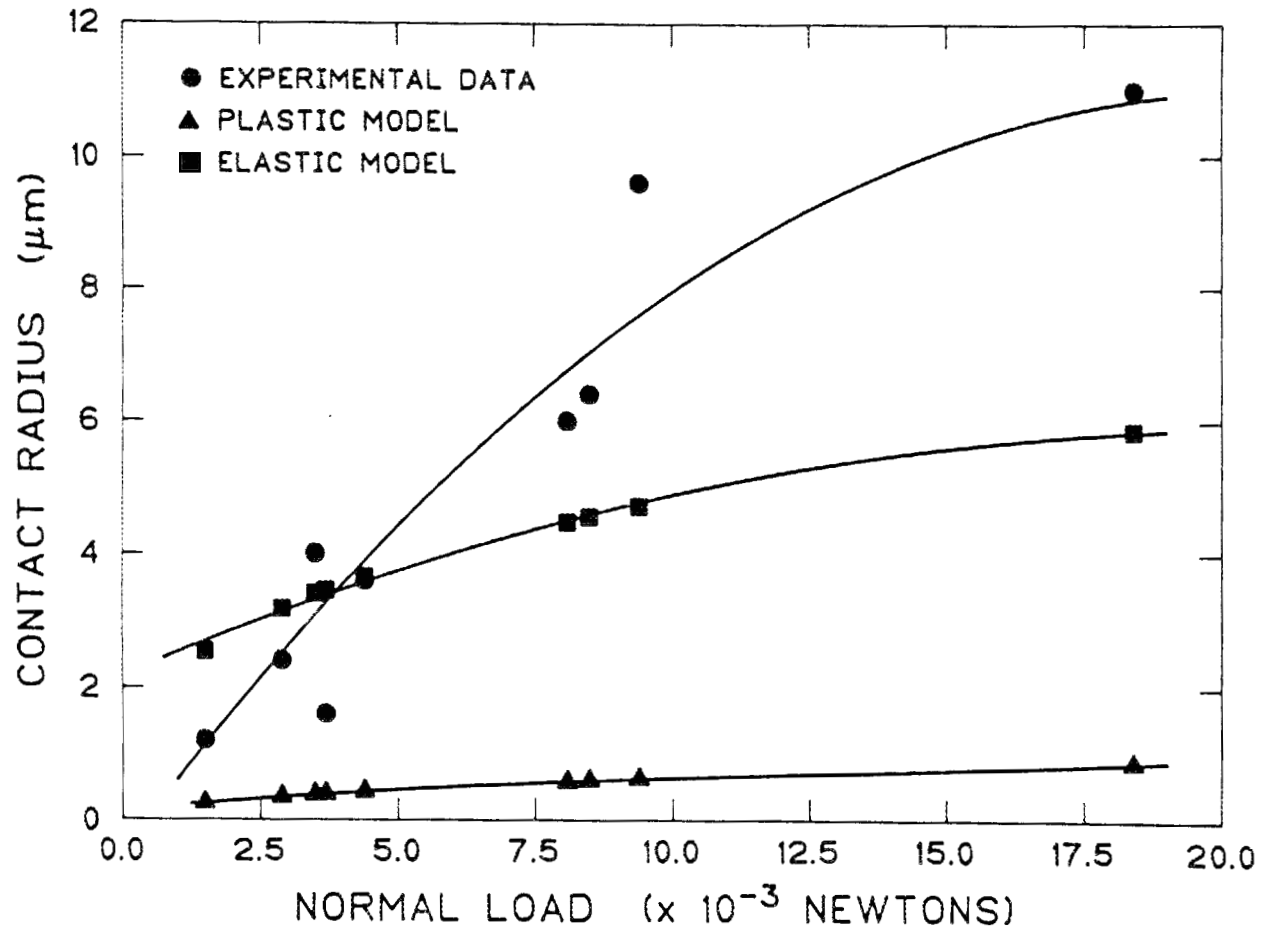


Fig. 28. Theoretical and experimental values of the radius of the circle of contact for scratches on aluminum/glass specimens.

Table 5. Shear stresses calculated using the elastic model analysis for scratches on zirconium/sapphire comparing the results obtained for different values of Young's Modulus, E

Normal force (Newtons)	Tangential force (Newtons)	Shear stress (MPa) using		Ratio of shear stresses
		E of Al ₂ O ₃	E of Zr	
0.0938	0.0128	6.11	4.07	1.5
0.0948	0.0098	2.65	1.77	1.5
0.1410	0.0181	6.99	4.67	1.5
0.1426	0.0132	1.97	1.31	1.5
0.1438	0.0098	-1.53	-1.02	1.5
0.1849	0.0332	16.9	11.3	1.5
0.1906	0.0164	1.20	0.80	1.5
0.1909	0.0157	0.56	0.38	1.5
0.2785	0.0464	19.4	12.9	1.5
0.2844	0.0290	5.19	3.46	1.5
0.2853	0.0265	3.12	2.08	1.5
0.2856	0.0255	2.33	1.55	1.5
0.3717	0.0607	22.6	15.1	1.5
0.3777	0.0432	9.57	6.39	1.5
0.3797	0.0373	5.23	3.49	1.5
0.4664	0.0708	22.7	15.2	1.5
0.4667	0.0699	22.1	14.8	1.5
0.4718	0.0549	11.8	7.86	1.5
0.9126	0.2009	68.9	46.0	1.5
0.9209	0.1766	55.4	3.69	1.5

an inaccurate estimate of Poisson's ratio that could result in this sign change. Figure 28 also shows the radii of the circles of contact for some of the scratches made on aluminum/glass specimens and analyzed by this model. For the most part, the theoretical values are less than the experimental values: this is probably because the theory does not account for any plastic deformation, even during stylus passase.

As when analyzed by the technique of Benjamin and Weaver, loss of adhesion of chromium from sapphire correlated well with maximum compressive radial stresses, maximum shear stresses, and maximum mean pressures (Table 6), but these values for the nickel/sapphire systems were intermediate for the only scratch not resulting in film loss (Table 7). This is probably due to the different deformation modes.

Table 6. Radial and shear stresses calculated using the elastic model analysis for scratches on chromium/sapphire

Normal force (Newtons)	Tangential force (Newtons)	Radial stress (GPa)	Shear stress (MPa)	Film de-adhesion
0.4805	0.0293	-0.187	-5.70	No
0.9584	0.0665	-0.126	-4.82	No
0.0962	0.0057	-0.121	-2.15	No
0.4769	0.0400	0.052	1.57	No
0.1904	0.0172	0.086	1.93	No
0.4760	0.0426	0.109	3.31	No
0.9528	0.0829	0.106	4.04	No
0.2830	0.0332	0.335	8.54	No
0.2828	0.0337	0.354	9.02	No
0.1876	0.0251	0.419	9.33	No
0.1400	0.0210	0.492	9.93	No
0.9452	0.1052	0.423	16.1	No
0.4669	0.0695	0.723	21.8	No
0.9334	0.1399	0.925	35.1	No
1.4051	0.1951	0.895	39.0	No
2.3540	0.2893	0.780	40.3	Yes
1.8622	0.2931	1.290	61.6	Yes

Table 7. Radial and shear stresses calculated using the elastic model analysis for scratches on nickel/sapphire

Normal force (Newtons)	Tangential force (Newtons)	Radial stress (GPa)	Shear stress (MPa)	Film de-adhesion
0.9376	0.1274	0.74	28.3	Yes
1.3988	0.2135	1.10	47.8	No
1.8660	0.2818	1.18	56.7	Yes
1.8653	0.2839	1.20	57.6	Yes
1.3874	0.2470	1.47	63.9	Yes
1.3840	0.2570	1.59	68.8	Yes

THE PULL TEST

In theory, the pull test is the most straightforward of the techniques discussed. In practice, however, it is not so easily used. Most of the films used in this research were more adherent to their substrates than the epoxy of the bonding studs was to the film surface or the pin head. Another problem was that the fracture often happened in a complex manner involving several of the interfaces and layers between the pin, epoxy, film, and substrate. Because it was not always known where failure occurred first, it was difficult to determine what the maximum stress reading of the pull tester was actually measuring.

The epoxy precoated on the pull test pin was examined under a microscope before curing and found to be continuous but to contain few thin spots scattered over the surface. It is hoped that the epoxy became more evenly distributed during curing. The surfaces of the pins were very rough: arithmetic average surface roughnesses were approximately 3 μm . This roughness increased the surface area to which the epoxy could bond and promoted mechanical locking. The ultimate yield strength of the epoxy was specified as 62 to 69 MPa, and this was usually achieved before the epoxy or either of its interfaces failed.

Stresses developed in the specimens during film growth and cooling can greatly affect the results of the pull test. For one set of chromium films evaporated onto glass substrates, the substrates were under sufficient compression under the film that the test pin removed a hemispherical section of glass of approximately the same diameter as the test pin rather than the film from the substrate. Test pins epoxied directly to the glass, where no film was present to put the substrate in compression, did not have this effect, even to much greater loads.

Two techniques were used to introduce reproducible flaws into the film in an attempt to lower the apparent adhesion of the film to within the range of the pull tester. In the first method, a Vickers hardness indent was made on the film surface. The cracks propagating from the corners of the pyramidal indent served as the flaws that might lead to film de-adhesion. Unfortunately, this proved not to be the case: the adhesion of the films remained beyond the range of the tester, probably because the cracks were too small. Even if this had worked, it would be very difficult

to analyze an apparent adhesion increase caused by ion beam mixing because it is not known precisely how the mixing affects the parameters involved. It is known qualitatively from other researchers that ion beam mixing increases surface hardness⁵⁴⁻⁵⁶ and inhibits crack propagation.⁵⁹ These variations between mixed and unmixed films would mean that cracks produced by a standard indent load on unmixed material could not be exactly reproduced on a mixed system and the flaw itself would become a variable in the analysis.

In the second method, a thin layer of gold was sputter deposited onto a small portion of the substrate. The test film was then deposited through a mask such that a portion of this new film overlapped the gold layer. Because the gold was nonadherent (experimentally) to the sapphire and glass substrates, it served as a release layer for the test film, and the resulting failure was treated from a fracture mechanics point of view. The mild shadowing effect of the mask used during gold deposition caused the edge of the gold layer under the test film to be tapered; thus, this was treated as a reproducible crack, and the analysis was made using the concept of fracture toughness as indicated by the stress intensity factor K . For the Mode I crack opening mode, K_I is given in ASTM Special Technical Publication 410 (ref. 60) as

$$K_I = 1.1 \sigma \sqrt{\pi a} ,$$

where a is the crack length and σ is the normal stress.

Because the point of the analysis was not to determine a material property but to find some means of comparison of the fracture strength for similar but flawed systems, it was not significant that the specimens used in this research did not meet the specimen size requirements given for fracture toughness testing. All specimens used for comparison were of almost identical shape and size.

By using K_I , which incorporates the geometry of the crack, errors in pin placement were not as critical because they were accounted for by careful measurement of the crack length.

This latter method of a gold release layer was used to investigate the adhesion of 500-nm zirconium films on sapphire substrates. The gold layer was approximately 20 nm thick. For comparison, some pull tests

were performed on areas of the test film that did not overlap the release layer. None of the pulls that were performed without a release layer resulted in any film loss. The other tests resulted in varying amounts of film loss over a wide range of applied stresses (Table 8). Note that the specimen with the largest percentage of test film removed had an intermediate value of K_I .

It was assumed that the epoxy failed first in the cases where both the film/substrate interface and one of the epoxy interfaces failed and the stresses were recalculated for the actual area supporting the load. Such calculated stresses were much higher than the tensile strength of the epoxy. This was deemed unreasonable, and, thus, it was assumed that the zirconium/sapphire interface failed first at some stress less than the final maximum reading at which stress the remaining epoxy failed. Calculation of the stresses based on this assumption gave stresses on the remaining intact system that were approximately equal to the tensile strength of the epoxy. This latter, then, was a reasonable assumption. Because the stress to cause failure of at least part of the test film occurred at a smaller stress than the maximum shown in Table 8, it can be concluded that the stress intensity factors in Table 8 represent an upper limit of those required to cause film de-adhesion.

Table 8. Pull test results for specimens with gold release layer^a

Specimen	Gold release layer	Stress at failure (MPa)	Maximum crack length (mm)	Stress intensity factor (MPa \sqrt{m})	Test film removed (%)
477 c	No	64.74	--	--	0
477 d	No	59.57	--	--	0
478 b	No	69.98	--	--	0
480 d	No	56.75	--	--	0
478 a	Yes	5.45	0.396	0.212	26
479 c	Yes	35.10	0.770	1.899	20
480 a	Yes	38.61	1.389	2.806	13
480 b	Yes	25.65	0.472	1.086	65

^aDifferent identification letters refer to separate tests on the same specimen. "Test film removed" refers to the test area not including that over the release layer.

The gold layer does have an effect on the stress intensity. Table 8 reveals the adhesive strength of the film to the substrate to be greater than 55 MPa (the strength of the epoxy) if no release layer is present. If the effect of the layer were solely to reduce the effective area supporting the applied load, thus increasing the stress on the system, recalculation of the stresses based on the area under the pin but not over the gold layer should reveal maximum stresses of about the same order of magnitude as when no release layer was used. Table 9 shows this not to be the case: the stresses recalculated for the specimens omitting the pin area over the gold material were, in general, much less than the strength of the epoxy. Failure would not have occurred at these low stresses if the release layer did not have an effect on the stress intensity.

Some reasons that the crack resulting from the gold layer did not propagate further between the test film and substrate include (1) the gold may not have been completely continuous at a thickness of 20 nm, (2) the crack tip caused by the edge of the layer may not have been sharp enough, and (3) the zirconium film may not have been continuous over the edge of the gold. Also, gold on sapphire tends to agglomerate during heating, and this may have occurred during the test film deposition or during the epoxy cure cycle. More extensive crack propagation might be obtained after the investigation of these factors.

Table 9. Stresses recalculated assuming reduced area under the pin by omitting area over the gold release layer

Specimen	Stress at failure recalculated omitting pin area over gold layer (MPa)
478 a	5.79
479 c	38.68
480 a	71.29
480 b	38.47

EFFECTS OF ION-BEAM MIXING

Adhesion to Sapphire Substrates

Scratch Adhesion. The scratch test was used to investigate the effect of ion beam mixing on film adhesion for chromium, nickel, and zirconium films on sapphire substrates.

The as-deposited thicknesses of the zirconium, chromium, and nickel films were 0.18, 0.17, and 0.20 μm , respectively. It was found from the E-DEP-1 code (ref. 58) that the average projected ranges (the depth at which most of ions come to rest) of iron ions into these materials were 0.47, 0.36, and 0.31 μm , respectively. Because the shape of the concentration of iron ions vs depth curve is generally gaussian, only a relatively few iron ions came to rest in the film. The computer code PROFILE (ref. 61), which calculates the distributions of ions implanted into surfaces, revealed that the maximum concentration of the iron ions, which occurs at the interface and diminishes quickly away from the interface, was less than 6.5 at. % for the nickel film and was even less for the other films. Thus, it was reasonable to assume that the structural and alloying effects were minimal. The cause of the "ion beam mixing" was, instead, the energy transferred and the defects created near the interface as a result of the collisions associated with the passage of the ion.

For some of the chromium/sapphire and zirconium/sapphire specimens, the scratch test data revealed critical values of the normal load, plastic shear stress, and elastic shear stress necessary to cause de-adhesion; the data for other specimens, however, was very inconsistent, and no critical values were discernible. This difference may be due to some unrecognizable difference in the specimens themselves or to some uncontrollable testing conditions, such as air humidity or stylus damage.

For those specimens exhibiting critical values for de-adhesion, ion beam mixing greatly improved the adhesion of the chromium films. Although there was a large amount of scatter in the data, normal forces as low as 0.20 N resulted in film stripping in the unmodified regions.

None of the scratches in the modified region, however, resulted in a loss of adhesion, even for normal forces as high as 3.92 N. Critical shear stresses calculated from the equations of Benjamin and Weaver that assumed fully plastic conditions showed a marked improvement of 350% for one of the specimens (Table 10). Analysis of data for the same specimen using Laugier's elastic equations also revealed an increase in the critical shear stress of over 300% (Table 11).

No increase in the adhesion of nickel films to sapphire substrates was evident among the wide scatter of the data obtained by each of the analysis methods. This scatter may be due to the extrusion of nickel films under the stylus, as previously discussed.

Table 10. Comparison of critical shear stresses calculated using the plastic model analysis for scratches on chromium/sapphire

Normal force (Newtons)	Tangential force (Newtons)	Shear stress (GPa)	Film de-adhesion	Ion-beam mixed
0.1875	0.0254	0.1949	Yes	No
0.9464	0.1016	0.4378	Yes	No
0.9464	0.1016	0.4378	Yes	No
0.9464	0.1016	0.4378	Yes	No
0.9474	0.0988	0.4380	Yes	No
2.3492	0.3034	0.6898	Yes	No
2.3554	0.2851	0.6908	Yes	No
2.3564	0.2822	0.6909	Yes	No
2.3564	0.2822	0.6909	Yes	No
2.3799	0.2133	0.6943	Yes	No
2.3799	0.2133	0.6943	Yes	No
3.7817	0.4178	0.8818	No	Yes
3.7817	0.4178	0.8818	No	Yes

Table 11. Comparison of critical shear stresses calculated using the elastic model analysis for scratches on chromium/sapphire

Normal force (Newtons)	Tangential force (Newtons)	Shear stress (MPa)	Film de-adhesion	Ion-beam mixed
0.1875	0.0254	9.60	Yes	No
2.3799	0.2133	9.85	Yes	No
2.3799	0.2133	9.85	Yes	No
0.9474	0.0988	12.7	Yes	No
0.9464	0.1016	14.2	Yes	No
0.9464	0.1016	14.2	Yes	No
0.9464	0.1016	14.2	Yes	No
2.3564	0.2822	37.5	Yes	No
2.3564	0.2822	37.5	Yes	No
2.3554	0.2851	38.6	Yes	No
2.3492	0.3034	46.0	Yes	No
3.7817	0.4178	39.7	No	Yes
3.7817	0.4178	39.7	No	Yes

Two sets of data were taken and analyzed for the zirconium/sapphire systems. For the first set, normal forces as low as 0.094 N and shear stresses calculated from the plastic model as low as 0.13 GPa resulted in film de-adhesion in the unmixed region; normal forces as high as 0.94 N and shear stresses as high as 0.44 GPa failed to cause de-adhesion in the ion-beam-mixed regions. These numbers represent an increase of 900 and 230%, respectively, because of the mixing. However, analysis assuming elastic conditions for this set showed no correlation between the radial and shear stresses and film de-adhesion. As already discussed, these films were subject to tensile failure behind the moving stylus, so the elastic theory concerning failure ahead of the stylus would not provide an adequate description.

For the second set of zirconium/sapphire data, the highest values of the normal load and the plastic model shear stress resulted in film de-adhesion, but there was no increase in these critical values with ion-beam mixing. Using the elastic analysis for either the mixed or unmixed regions, no critical stresses could be determined for this set.

Tensile Adhesion. The pull test was also used to investigate the adhesion of the zirconium films. Even in the unmixed condition, the adherence of the test films was beyond the range of the tester, so a gold release layer was used to initiate failure. Unfortunately, this was sometimes still insufficient to cause de-adhesion. Most of the failures that did occur involved several of the interfaces in the system, and, thus, the analysis was not straightforward. Another problem encountered was that ion-beam mixing also greatly increases the adhesion of gold to sapphire, so additional care was needed to ensure correct placement of the specimen masks such that no gold was mixed.

Gold was chosen for the release layer material because it does not "wet" sapphire. Because of its nonwetting characteristics and, thus, nonadherence, the gold film and the superimposed test film were often removed during sample preparation and handling. As a result, data for the ion-beam-mixed case were gathered for only one ion-beam condition. In each of the pull tests in the ion-beam-mixed region, the only part of the zirconium film removed was that directly over the gold layer: the crack caused by the presence of the gold did not propagate between the mixed film and the substrate. The crack length for the test performed on the same specimen in the unmixed region was intermediate to the crack lengths used in the mixed region (Table 12). The average maximum stress at failure and the average stress intensity factor for the mixed region were greater than the upper limits of these for the unmixed region (Table 8) by 40 and 30%, respectively. This indicated significant adhesion enhancement by ion beam mixing because both regions had similar flaws, but the mixed region withstood a greater stress and a greater stress intensity factor with no zirconium removal.

Table 12. Pull test results for ion-beam-mixed specimens^a

Specimen	Stress at failure (MPa)	Stress crack length (mm)	Test intensity factor (MPa \sqrt{m})	Film removed (%)
479 a (mixed)	37.03	0.942	2.22	0
479 b (mixed)	60.68	0.546	2.76	0
479 c	35.10	0.770	1.90	20

^aDifferent identification letters refer to separate tests on the same specimen. "Test film removed" refers to the test area not including that over the gold release layer.

Adhesion to Silicon Carbide and Silicon Nitride Substrates

The effect on thin film adhesion of ion beam mixing was also investigated for four material systems having silicon nitride or silicon carbide as substrates:

1. 30 nm aluminum on silicon nitride,
2. 30 nm aluminum on silicon carbide,
3. 30 nm zirconium on silicon carbide, and
4. 15- or 30-nm zirconium on silicon nitride.

The pull test was used to test the adhesion of these films to their substrates because the opaqueness of the substrate meant that light transmission through the film could not be used to judge de-adhesion by scratching. Optical and scanning electron microscopy, surface profilometry, and energy dispersive X-ray spectroscopy were all used to determine which interfaces and layers failed.

Scanning electron microscopy revealed the films to be porous and somewhat discontinuous because of a rough, polycrystalline substrate surface (Fig. 29). An additional layer of the original film material was evaporated onto the surface to have a more continuous surface against which to epoxy the pull test pins. This layer was evaporated after the ion beam mixing was complete because the ion energies used this experiment were insufficient to penetrate the thicker films.

In preparation for the second deposition, both of the aluminum-coated specimens were cleaned in Micro laboratory cleaning solution. The parting agent of this solution removed some of the original aluminum films from their substrates. Based on visual inspection, a very thin layer may have remained, particularly in the ion-beam-mixed regions, but this could not be quantified. As a result of this experience, the cleaning procedure was discontinued for all specimens already bearing a film. The additional aluminum layer was deposited on the substrate as planned.

YP4815

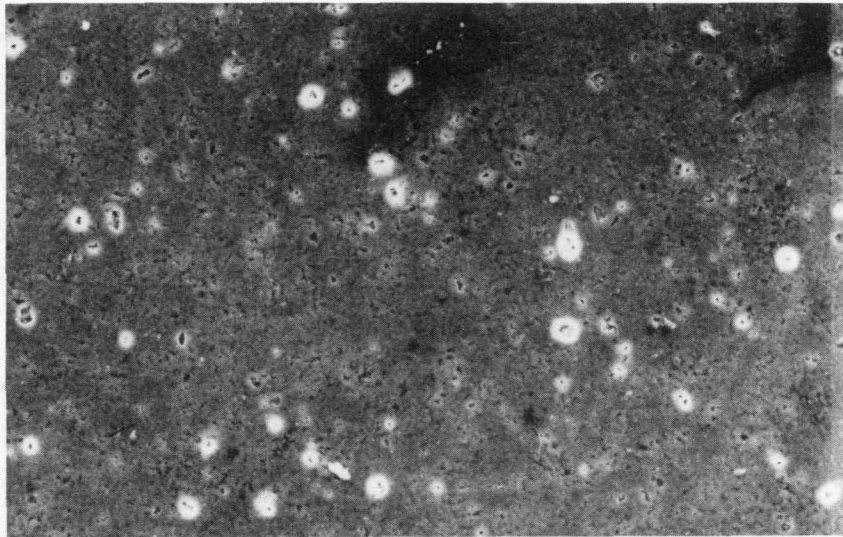


Fig. 29. Original 30-nm zirconia film on silicon carbide. The bright spots are electron discharges from the substrate, revealing the pores in the film. Scanning electron micrograph, 300X.

Aluminum Film on Silicon Nitride. The test conditions examined for the aluminum on silicon nitride were

1. 200-nm aluminum, as deposited (no underlying layer);
2. 200-nm aluminum plus an underlying layer of unknown thickness, as deposited; and
3. 200-nm aluminum plus an underlying layer of unknown thickness, ion beam mixed to a dose of 0.5×10^{16} ions/cm² at an energy of 200 keV.

In the pull test, all failures in all three of the regions occurred at zero measurable force. Surface profilometry and energy dispersive X-ray spectroscopy confirmed that the aluminum film was completely removed from the test pins. Based on these data, it was concluded that the adhesion of the aluminum to the silicon nitride was very poor and the ion beam mixing had no measurable effect.

This experiment gave insight into some aspects of the pull test. During the manual procedure of inserting the shank of the pin into the testing machine, several of the pins broke from the specimen, removing the film from the substrate. From a practical viewpoint, it is very difficult to insert the pin without touching it to some portion of the unit, and, thus exerting some unknown forces and moments. Also, the grips of the tester must be tightened onto the shank below the platen, and this, too, can exert a moment on the film as the specimen is drawn down into the platen and aligned. Although these forces may be sufficient to remove the film from the substrate, as in this case, they cannot be quantified. Thus, the pull test has a lower limit as well as the previously discussed upper limit.

Aluminum Film on Silicon Carbide. Four types of regions were examined for the aluminum film on the silicon carbide substrate:

1. 200-nm aluminum, as deposited (no underlying layer);
2. 200-nm aluminum plus an underlying layer of unknown thickness, as deposited;
3. 200-nm aluminum plus an underlying layer of unknown thickness, ion beam mixed to a dose of 0.5×10^{16} ions/cm² at an energy of 200 keV; and

4. 200-nm aluminum plus an underlying layer of unknown thickness, ion beam mixed to a dose of 2.0×10^{16} ions/cm² at an energy of 200 keV.

The pull test results are summarized in Table 13. These data reveal a significant increase in adhesion as a result of ion-beam mixing, and the strength of the bond increased with ion dose. The presence of the underlying layer made no difference for the unmixed films. Energy dispersive X-ray spectroscopy measurements showed clearly that the failure occurred at the aluminum/silicon carbide interface and not within the aluminum film itself.

Table 13. Pull test strength of aluminum film on silicon carbide substrate

Region	Dose ($\times 10^{16}$ ions/cm ²)	Average pull strength (MPa)
a	0	0
b	0	0
c	0.5	24.82
d	2.0	37.92

As already noted, the original ion-beam-mixed film may have been removed during the cleaning procedure. If so, the adhesion increase of the additional film to the substrate may be due to a change in the wettability or surface energy of the substrate as a result of the ion bombardment. This is consistent with the work of Baglin and Clark⁵³ who have reported that ion irradiation lowers the interfacial energy and, thus, enhances adhesion.

If the film was only partially removed, the portions remaining would be those with the best adhesion to the substrate. If the adhesion of the second film to the first is good, as it proved to be in this case, the adhesion increase as a result of the mixing of the first film would be reflected in the results of the pull test.

Zirconium Film on Silicon Carbide. The film adhesion was tested for four film conditions for the zirconium on silicon carbide:

1. 30 plus 500-nm zirconium, as deposited;
2. 30 plus 500-nm zirconium, ion beam mixed to a dose of 0.5×10^{16} ions/cm² at an energy of 200 keV;
3. 30 plus 500-nm zirconium, ion beam mixed to a dose of 2.0×10^{16} ions/cm² at an energy of 200 keV; and
4. 30 plus 500-nm zirconium, ion beam mixed to a dose of 2.0×10^{16} ions/cm² at an energy of 350 keV.

The data gathered from these pull tests are rather difficult to interpret because the failure was of a complex nature involving the several interfaces in the pin/epoxy/film/substrate system. Judgment of which interface failed was based on inspection of the test site--if epoxy remained on the specimen surface, it was deemed that the pin/epoxy interface failed; if the film was the topmost layer, the epoxy/film interface failed; if the substrate was exposed, failure occurred at the film/substrate interface.

Assuming that the pin/epoxy interface failed first in the tests where both the film/substrate and the pin/epoxy interfaces experienced failure, the remaining portions of the film/substrate interface then failed at the maximum measured load. Recalculation of the stress based on the measured areas of film removed resulted in stresses ranging up to 1696 MPa. This is not a likely situation because the tensile strength of the epoxy, still carrying the load from the tester to the interface, is approximately 69 MPa.

If, however, it is assumed that the film/substrate interface failed locally first at some low load, leaving an epoxy/film/substrate system intact to carry the load, the maximum stresses can be recalculated based on the area of film remaining. These maximum stresses are much closer to the specified maximum epoxy strength, and, thus, this is the more likely scenario. Very localized failure of the film/substrate interface is also supported by the observation that the areas of film removed from the substrate are generally very small spots rather than continuous

regions and the total area of these spots averages only about 15% of the total pin contact area (Fig. 30). Because the film/substrate interface is disrupted only locally and not generally, the adhesion strength can be specified as being greater than the maximum stress reported.

The results for the two zirconium/silicon carbide specimens are shown in Table 14. For the first set, ion beam mixing did not appear to have much effect; noted, however, that only the region receiving the larger dose at the higher energy exhibited a strength greater than the mean of the given values. For the second set, the larger-dosed region exhibited a marked adhesion increase.

YP4814

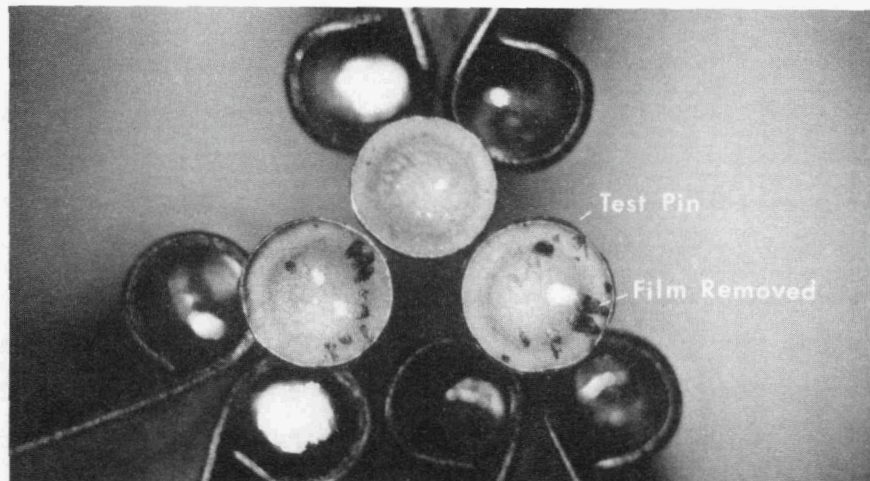


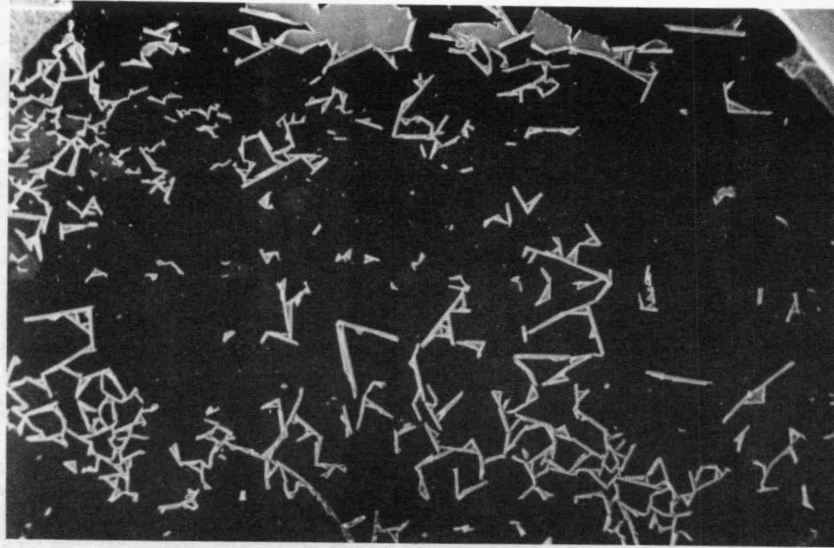
Fig. 30. Dark spots of film removed with the test pins. 8X.

Table 14. Pull test strength of zirconium film
on silicon carbide substrate

Specimen and region	Dose ($\times 10^{16}$ ions/cm ²)	Energy (keV)	Pull strength in excess of (MPa)
1 a	0	---	75.22
1 b	0.5	200	68.05
1 c	2.0	200	65.43
1 d	2.0	350	89.64
2 a	0	---	0
2 b	0.5	200	0
2 c	2.0	200	59.09

As previously mentioned in Chap. III, the specimens undergo a mild thermal cycle in the course of the second film deposition. For one of the zirconium/silicon carbide systems, this cycle, combined with the internal stresses generated in the film growth, produced sufficient thermal stress to cause film de-adhesion to occur spontaneously. This de-adhesion, however, was not uniform across the three regions of the specimen represented on this bar, and it appeared to be a function of ion dose. Figure 31 shows the specimen surface in areas that have not been ion beam mixed on either end of the mixed segment. The de-adhesion of Fig. 31 is shown at higher magnification in Fig. 32. Figures 33 and 34 show the surface in regions that have been ion-beam mixed to a dose of 0.5 and 2.0×10^{16} ions/cm², respectively. In these micrographs, the film material appears as a lighter gray than the substrate. The oval regions are areas damaged during Rutherford backscattering experiments, and the circles are the pull test sites.

YP4802



YP4803

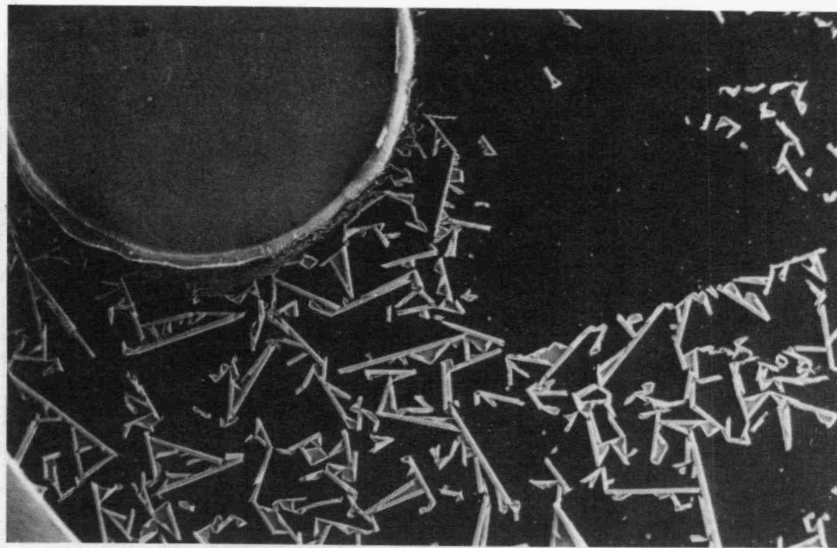


Fig. 31. De-adhesion of zirconium film from silicon carbide specimen surface in unmixed regions. Scanning electron micrograph, 20X.

YP4806

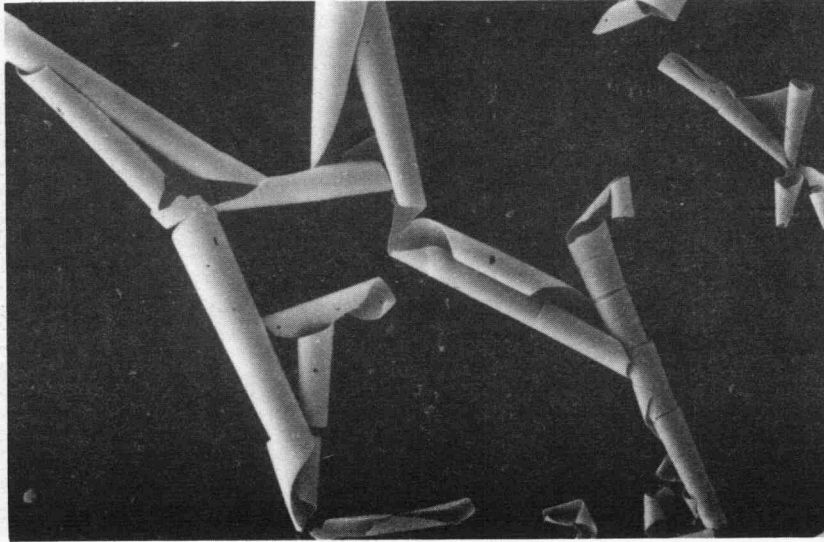


Fig. 32. De-adhesion of Fig. 31 at higher magnification. Scanning electron micrograph. 250X.

YP4808

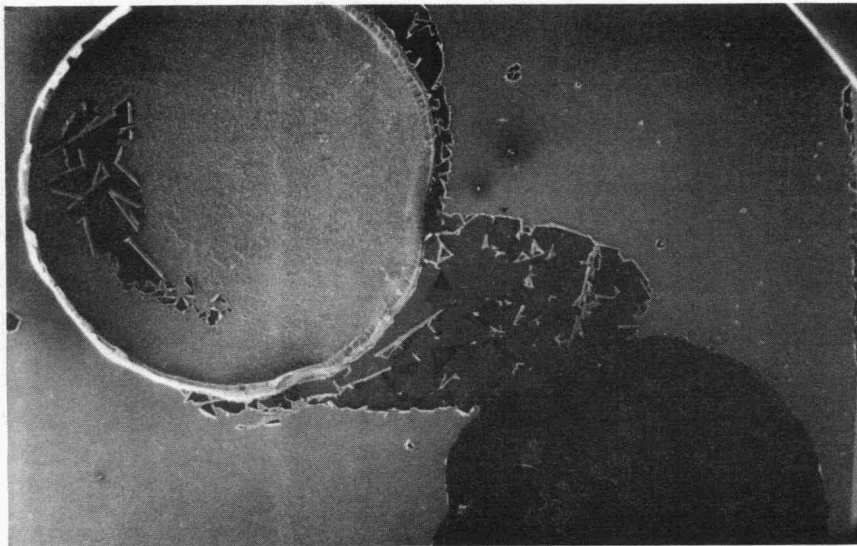


Fig. 33. Zirconium on silicon carbide specimen surface, ion-beam mixed to a dose of 0.5×10^{16} ions/cm². Scanning electron micrograph. 20X.

YP4807

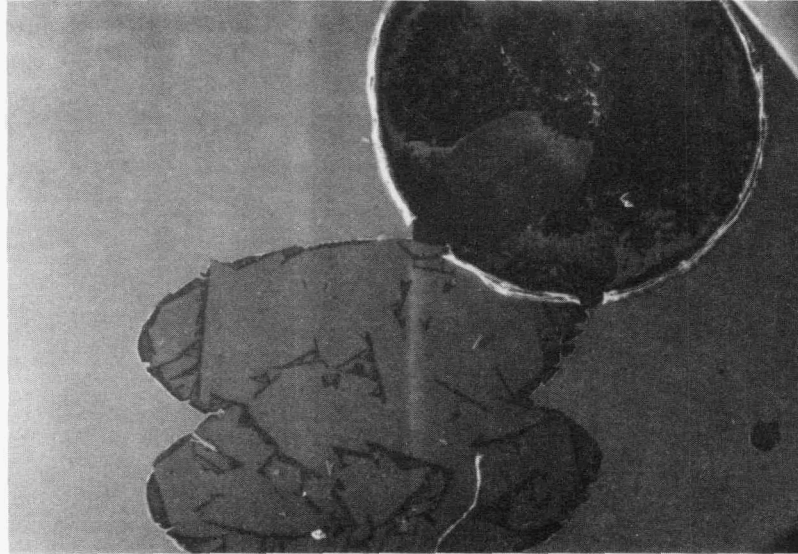


Fig. 34. Zirconium on silicon carbide specimen surface, ion-beam mixed to a dose of 2.0×10^{16} ions/cm². Scanning electron micrograph. 20X.

The interpretation of these pictures is as follows. The adhesion of the additional 500-nm zirconium to the original 30-nm zirconium was very good. However, large tensile stresses were developed in the additional layer during growth and cooling. The same stresses were present throughout the length of the specimens but had a different effect in the various regions because of differences in adhesion of the original layer. In areas that had not been ion beam mixed, the internal stresses were sufficient to cause de-adhesion of the entire 530-nm film. In regions that had been ion beam mixed, the adhesion of the original 30-nm film was generally adequate to prevent the film from de-adhering and curling up, especially at the higher doses. Only very small regions of de-adhesion are visible in the mixed films, and these are fewer in the higher-dosed region.

Zirconium Film on Silicon Nitride. The original layer of zirconium was deposited in two different thicknesses, 15 and 30 nm, on the silicon nitride substrates.

For the specimen consisting of an original 15-nm zirconium film, the test parameters were

1. 500-nm zirconium, as deposited;
2. 515-nm zirconium, as deposited; and
3. 515-nm zirconium, ion-beam mixed to a dose of 0.5×10^{16} ions/cm² at an energy of 200 keV.

During testing, only in the ion-beam-mixed region did failure occur at a nonzero applied load. Assuming, as before, that failure occurred first at the pin/epoxy interface and the remaining film supported the load (i.e., stress recalculated based on area of film removed), the strength of the film/substrate interface was 172 MPa. As noted, this is unrealistic because the tensile strength of the epoxy is only 69 MPa. Assuming the film/substrate interface failed locally first, the adhesive strength of the film to the substrate is in excess of 61.7 MPa. Compared with the zero-strength values obtained for the unmixed region, this shows a significant adhesion increase (Table 15).

Table 15. Pull test strength of 515-nm zirconium film on silicon nitride substrate

Region	Dose ($\times 10^{16}$ ions/cm ²)	Average pull strength in excess of (MPa)
b	0	0
c	0.5	61.71

This specimen also underwent some spontaneous de-adhesion as a result of the internal stresses generated in growth and cooling. The ion-beam-mixed film is significantly more continuous than the unmixed region (Figs. 35 and 36), indicating better film adhesion to the substrate as a result of the ion-beam mixing.

YP4810

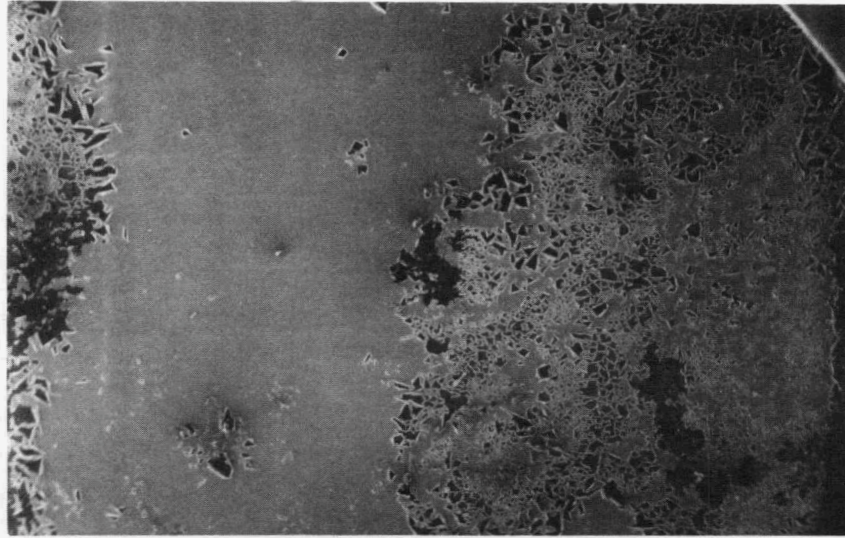


Fig. 35. Zirconium (515 nm) on silicon nitride specimen surface in unmixed region. Scanning electron micrograph. 20X.

YP4809

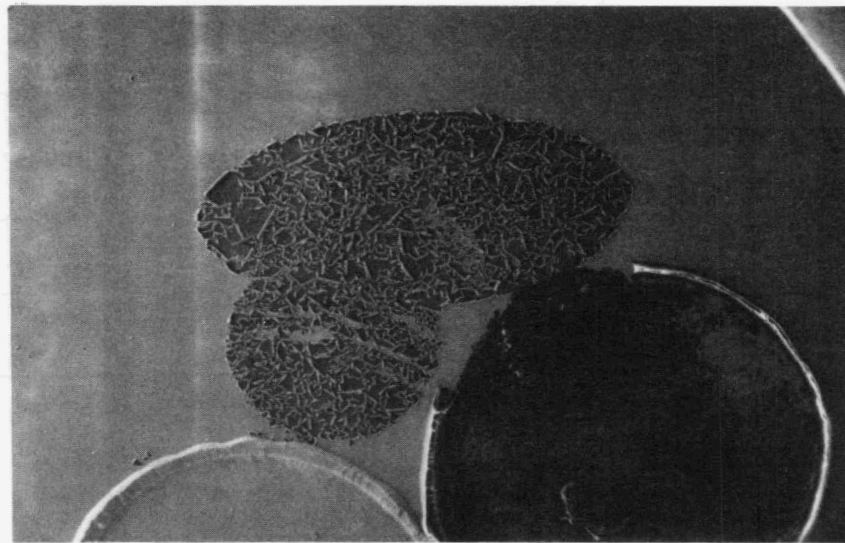


Fig. 36. Zirconium (515 nm) on silicon nitride specimen surface in mixed region. Scanning electron micrograph. 20X.

The test parameters for the specimen bearing an original 30-nm zirconium film were

1. 530-nm zirconium, as deposited;
2. 530-nm zirconium, ion beam mixed to a dose of 0.5×10^{16} ions/cm² at an energy of 200 keV;
3. 530-nm zirconium, ion beam mixed to a dose of 2.0×10^{16} ions/cm² at an energy of 200 keV; and
4. 530-nm zirconium, ion beam mixed to a dose of 2.0×10^{16} ions/cm² at an energy of 350 keV.

Based on the theory that the film/substrate interface fails locally first because the areas of film removed are small, the adhesion values for the 530-nm zirconium film on the silicon nitride substrate ranged from 6.1 to 61 MPa (Table 16). No increase in the adhesion of the film to the substrate could be detected, but the strength of the pin/epoxy interface was consistently poor, preventing the detection of more-accurate limits for the adhesion strength.

Table 16. Pull test strength of 530-nm zirconium film on silicon nitride substrate

Region	Dose ($\times 10^{16}$ ions/cm ²)	Energy (keV)	Average pull strength in excess of (MPa)
a	0	---	47.13
b	0.5	200	23.72
c	2.0	200	6.07
d	2.0	350	24.75

CHAPTER V

CONCLUSIONS

Each of the testing methods discussed can reveal information about the adhesion of a thin metallic film to a ceramic substrate. This information is different for each of the tests, however, because the loading mechanisms, the stress states induced, and the material responses measured are different. It is essential that these aspects of the tests, as well as the variables on which each depends, be understood and controlled before any significance can be given to the data.

THE SCRATCH TEST

Although each of the analyses of the scratch test was based on a great many assumptions and each failed to yield consistently a critical value of some stress that would result in film de-adhesion, these analyses gave insight into the stress state of the system and revealed some of the variables, such as hardness and modulus of elasticity, that must be examined. Both the plastic and elastic models correlated well with film de-adhesion for the chromium/sapphire systems, which showed no evidence of ductile extrusion, but neither correlated well with de-adhesion of the nickel film, which was subject to extrusion. Only the plastic model yielded critical values for the aluminum/glass and zirconium/sapphire systems. It has been shown that the zirconium films often cracked along the lines of maximum tensile stress behind the moving stylus, and because this was not a possibility in the elastic analysis, it was not unexpected that this latter model failed to describe a critical value for these systems.

While a critical normal load and critical plastic shear stress were usually identifiable for poorly adherent systems, such as aluminum to glass, the results of the scratch test on well-adherent films can be explained in terms of the relative ductilities of the film materials. For relatively brittle films, such as chromium, critical normal loads, critical plastic shear stresses, and critical elastic shear stresses existed.

For ductile materials, such as nickel, none of the analytical methods discussed revealed a critical value for film de-adhesion. Zirconium films have an intermediate ductility and sometimes exhibited the phenomena of critical normal loads and critical plastic shear stresses. Thus, the adhesion of brittle metallic films can be described in terms of critical values resulting from the scratch test; however, ductile films, the scratching of which depends more on the properties of the film than the adhesion, cannot. Table 17 shows the elongations to failure for the bulk materials,⁶²⁻⁶⁵ which may be different for the thin films but should maintain the same ranking, and summarizes these conclusions.

Table 17. Analysis methods useful in the determination of critical values for film de-adhesion for the systems investigated

System	Elongation in 5.08 cm gage length (%)	Normal load analysis	Plastic shear stress analysis	Elastic shear stress analysis
Cr/Al ₂ O ₃	0 ^a	Yes	Yes	Yes
Zr/Al ₂ O ₃	19 ^b	Yes	Yes	No
Ni/Al ₂ O ₃	50 ^c	No	No	No
Al/Glass	65 ^d	Yes	Yes	No

^a*Encyclopedia of Engineering Materials and Processes*, H. R. Clauser, ed. in chief, Reinhold Publishing Corporation, New York, 1963, p. 149.

^b*Encyclopedia of Engineering Materials and Processes*, H. R. Clauser, ed. in chief, Reinhold Publishing Corporation, New York, 1963, p. 768.

^c*Encyclopedia of Engineering Materials and Processes*, H. R. Clauser, Robert Fabian, Donald Peckner, and Malcolm W. Riley, eds., Reinhold Publishing Corporation, New York, 1963, p. 440.

^dRoss, Robert B., p. 4 in *Metallic Materials Specification Handbook*, Third Edition, E. & F. N. Spon, London, 1980.

The definition of a critical normal load or critical plastic shear stress (which is directly dependent on the normal load) was not always possible, even for brittle films. This fact implies that the correlation was not due simply to the normal load but, rather, to some other parameter or combination of factors that was also dependent on the normal load. For some sets of conditions, this latter relationship was straightforward enough that the adhesion could be measured by the critical normal load. Thus, although the scratch test can result in the description of a critical load, it is very difficult to get reliable data, and many factors must be considered.

THE PULL TEST

The pull test is a relatively straightforward technique when the tensile adhesion of the film is less than the strength of the epoxy. For some of the specimens examined in this research, where this was not the case, a release layer was used to induce at the film/substrate interface a stress intensity factor that caused de-adhesion at a load within the range of the tester. The analysis was analogous to that used in fracture toughness testing using the Mode I crack-opening mode. Comparison of film adherence was based on the calculation of the stress intensity factor necessary to cause adhesion failure. The results of this modified pull test were very promising and indicated that additional investigation to determine the optimum gold release layer parameters could increase the crack propagation and lead to even more-precise measurements. The ease of analysis, as compared with the scratch test, makes this an attractive procedure.

EFFECTS OF ION-BEAM MIXING

Scratch testing indicated a significant adhesion improvement as the result of ion beam mixing for chromium films on sapphire substrates. The analytical methods showed an increase in the critical normal force greater than 1800%, an increase in the critical plastic shear stress greater than 350%, and an increase in the critical elastic shear stress greater than 300%.

No increase in the adhesion of nickel films to sapphire substrates was detected using the scratch test because the film was subject under the stylus to ductile extrusion rather than to de-adhesion at the interface.

For zirconium/sapphire specimens, critical normal load and plastic shear stress calculations made from scratch test data showed that ion beam mixing improved the film adhesion by several hundred percent. The elastic analysis failed to reveal a critical stress because these films did not usually fail in compression ahead of the stylus, as assumed by the theory.

Tensile adhesion tests of the zirconium/sapphire systems using a gold release layer indicated significant adhesion enhancement by ion-beam mixing because both the mixed and unmixed regions had similar flaws but the mixed region withstood a greater stress (40%) and a greater stress intensity factor (30%) with no zirconium removal.

Tests exhibiting good pin/epoxy/film adhesion indicated that ion beam mixing increased the tensile adhesion of the aluminum and zirconium films to silicon nitride and silicon carbide substrates. This is supported by micrographs depicting the film response to thermal stresses in which the unmixed films de-adhere from the substrates as a result of the stresses while the mixed films have adequate adhesion to remain fixed to the substrates. Lack of sufficient pin/epoxy/film strength necessitated that the pull strength data be reported as "in excess of" the maximum value obtained in the pull test.

REFERENCES

1. Ahn, J., Mittal, K. L., and MacQueen, R. H., "Hardness and Adhesion of Filmed Structures as Determined by the Scratch Technique," p. 134 in *Adhesion Measurement of Thin Films, Thick Films, and Bulk Coatings*, K. L. Mittal, ed., ASTM, Philadelphia, PA, 1978.
2. Benjamin, P., and Weaver, C., "Measurement of Adhesion of Thin Films," *Proc. R. Soc. London A* 254 (1960) 163.
3. Butler, D. W., Stoddart, C. T. H., and Stuart, P. R., "The Stylus or Scratch Method for Thin Film Adhesion Measurement: Some Observations and Comments," *J. Phys. D: Appl. Phys.* 3(6) (1970) 877.
4. Campbell, David S., "Mechanical Properties of Thin Films," Chap. 12, p. 8 in *Handbook of Thin Film Technology*, Leon I. Maissel and Reinhart Glang, eds., McGraw-Hill Book Company, New York, 1970.
5. Weaver, Charles, "Adhesion of Thin Films," *J. Vac. Sci. Technol.* 12(1) (1975) 18.
6. Laeng, P., and Steinmann, P. A., "Adhesion Testing of Hard CVD Coatings Using the Scratch Test," p. 723 in *Proc. 8th Int. Conf. on Chemical Vapor Deposition*, John M. Blocher, Jr., Guy E. Vuillard, and Georg Wahl, eds., The Electrochemical Society, Inc., Pennington, NJ, 1981.
7. Laugier, M., "The Development of the Scratch Test Technique for the Determination of the Adhesion of Coatings," *Thin Solid Films* 76 (1981) 289.
8. Perry, A. J., "The Adhesion of Chemically Vapour-Deposited Hard Coatings to Steel--The Scratch Test," *Thin Solid Films* 78 (1981) 77.
9. Perry, A. J., Laeng, P., and Hintermann, H. E., "Adhesion Measurements on Hard Thin Well-Adhering Coatings--A Review," p. 475 in *Proc. 8th Int. Conf. on Chemical Vapor Deposition*, John M. Blocher, Jr., Guy E. Vuillard, and Georg Wahl, eds., The Electrochemical Society, Inc., Pennington, NJ, 1981.
10. Hammer, Barbara, Perry, A. J., Laeng, P., and Steinmann, P. A., "The Scratch Test Adhesion of TiC Deposited Industrially by Chemical Vapour Deposition on Steel," *Thin Solid Films* 96 (1982) 45.
11. Je, J. H., Gyarmati, E., and Naoumidis, A., "Scratch Adhesion Test of Reactively Sputtered TiN Coatings on a Soft Substrate," *Thin Solid Films* 136 (1986) 57.

12. Valli, J., Makela, U., and Matthews, A., "Assessment of Coating Adhesion," *Surface Eng.* 2(1) (1986) 49.
13. Perry, A. J., "Scratch Adhesion Testing of Hard Coatings," *Thin Solid Films* 107 (1983) 167.
14. Goldstein, I. S., and DeLong, R., "Evaluation of Microhardness and Scratch Testing for Optical Coatings," *J. Vac. Sci. Technol.* 20(3) (1982) 327.
15. Laugier, M., "Adhesion and Internal Stress in Thin Films of Aluminium," *Thin Solid Films* 79 (1981) 15.
16. Jacobson, S., Jonsson, B., and Sundqvist, B., "The Use of Fast Heavy Ions to Improve Thin Film Adhesion," *Thin Solid Films* 107 (1983) 89.
17. Weaver, C., and Parkinson, D. T., "Diffusion in Gold-Aluminium," *Philos. Mag.* 22, 8th Series (1970) 377.
18. Mehrotra, P. K., and Quinto, D. T., "Techniques for Evaluating Mechanical Properties of Hard Coatings," *J. Vac. Sci. Technol.* A3(6) (1985) 2401.
19. Kikuchi, Akira, Baba, Shigeru, and Kinbara, Akira, "Measurement of the Adhesion of Silver Films to Glass Substrates," *Thin Solid Films* 124 (1985) 343.
20. Chopra, Kasturi L., *Thin Film Phenomena*, McGraw-Hill Book Company, New York, 1969, p. 313.
21. Hamilton, G. M., and Goodman, L. E., "The Stress Field Created by a Circular Sliding Contact," *J. Appl. Mech.* 88 (1966) 371.
22. Perry, A. J., "The Adhesion of TiN on Steel," p. 737 in *Proc. 8th Int. Conf. on Chemical Vapor Deposition*, John M. Blocher, Jr., Guy E. Vuillard, and Georg Wahl, eds., The Electrochemical Society, Inc., Pennington, NJ, 1981.
23. Perry, A. J., and Pulker, H. K., "Hardness, Adhesion, and Abrasion Resistance of TiO₂ Films on Glass," *Thin Solid Films* 124 (1985) 323.
24. Hamersky, Jaroslav, "Feststellung Optimaler Parameter Bei Adhäsionsmessungen Unter Anwendung der Ritzmethode," *Thin Solid Films* 3 (1969) 263.
25. Timoshenko, S. P., and Goodier, J. N., *Theory of Elasticity*, 3rd ed., McGraw-Hill Book Company, New York, 1970, pp. 409-414.

26. Takadoum, J., Pivin, J. C., Chaumont, J., and Roque-Carmes, C., "Friction and Wear of Amorphous Ni-B, Ni-P Films Obtained by Ion Implantation into Nickel," *J. Mater. Sci.* **20** (1985) 1480.
27. Laugier, M. T., "An Energy Approach to the Adhesion of Coatings Using the Scratch Test," *Thin Solid Films* **117** (1984) 243.
28. Hintermann, H. E., "Thin Solid Films to Combat Friction, Wear, and Corrosion," *J. Vac. Sci. Technol. B* **2**(4) (1984) 816.
29. Lhermitte-Sebire, I., Colmet, R., Naslain, R., Desmaison, J., and Gladel, G., "The Adhesion Between Physically Vapour-Deposited or Chemically Vapour-Deposited Alumina and TiC-Coated Cemented Carbides as Characterized by Auger Electron Spectroscopy and Scratch Testing," *Thin Solid Films* **138** (1986) 221.
30. Swindlehurst, W., "Acoustic Emission--1: Introduction," *Non-Destructive Testing*, (June 1973) 152.
31. Pollock, A. A., "Acoustic Emission--2: Acoustic Emission Amplitudes," *Non-Destructive Testing*, (October 1973) 264.
32. Curtis, G. J., "Acoustic Emission Energy Relates to Bond Strength," *Non-Destructive Testing*, (October 1975) 249.
33. Perkins, R. A., and Meier, G. H., "Acoustic Emission Studies of High Temperature Oxidation," p. 176 in *Proc. Symposium on High Temperature Materials Chemistry--II*, Zuhair A. Munir and Daniel Cubicciotti, eds., The Electrochemical Society, Inc., Pennington, NJ, 1983.
34. Wilshaw, T. R., and Rothwell, R., "Instrumented Scratch for Measuring the Fracture Behavior of Strong Solids," *Nature: Phys. Sci.* **229** (1971) 155.
35. Room, J., and Rawlings, R. D., "Failure Mechanisms and Acoustic Emission Amplitude Distributions in Automotive Finishes," *J. Mater. Sci.* **17** (1982) 1745.
36. Bunnell, L. R., Crowe, J. C., and Hart, P. E., "Acoustic Emission Monitoring of Surface-Damaged Ceramic Materials," p. 341 in *The Science of Ceramic Machining and Surface Finishing*, National Bureau of Standards Special Publication 348, Washington, DC, 1972.
37. Chapman, B. N., "Thin Film Adhesion," *J. Vac. Sci. Technol.* **11** (1974) 106.
38. Jacobsson, Roland, "Measurement of the Adhesion of Thin Films," *Thin Solid Films* **34** (1976) 191.

39. Collins, L. E., Perkins, J. G., and Stroud, P. T., "Effect of Ion Bombardment on the Adhesion of Aluminium Films on Glass," *Thin Solid Films* 4 (1969) 41.

40. Noda, Shoji, Doi, Haruo, Yamamoto, Nobuyuki, Hioki, Tatsumi, Kawamoto, Jun'ichi, and Kamigaito, Osami, "Improvement for Adhesion of Thin Metal Films on Ceramics by Ion Bombardment and the Application to Metal-Ceramic Joining," *J. Mater. Sci. Letters* 5 (1986) 381.

41. Auner, G., Hsieh, Y. F., Padmanabhan, K. R., Chevallier, J., and Sorensen, G., "Effect of Ion Implantation on Thin Hard Coatings," *Thin Solid Films* 107 (1983) 191.

42. Varchenya, S. A., and Upit, G. P., "Adhesive Strength of the Interface Between a Metal Film and Crystalline Quartz," *Thin Solid Films* 122 (1984) 59.

43. Jacobsson, R., and Kruse, B., "Measurement of Adhesion of Thin Evaporated Films on Glass Substrates by Means of the Direct Pull Method," *Thin Solid Films* 15 (1973) 71.

44. Cannon, R. M., Fisher, R. M., and Evans, A. G., "Decohesion of Thin Films from Ceramic Substrates," p. 799 in *Thin Films--Interfaces and Phenomena*, R. J. Nemanich, P. S. Ho, and S. S. Lau, eds., Materials Research Society, Pittsburgh, PA, 1985.

45. Picraux, S. Thomas, and Peercy, Paul S., "Ion Implantation of Surfaces," *Scient. Am.* 252(3) (1985) 102.

46. Basta, Nicholas, "Ion-Beam Implantation," *High Technol.* (February 1985) 57.

47. Baglin, J. E. E., "Adhesion at Metal-Ceramic Interfaces: Ion Beam Enhancement and the Role of Contaminants," p. 3 in *Thin Films: The Relationship of Structure to Properties*, Carolyn Rubin Aita and K. S. SreeHarsha, eds., Materials Research Society, Pittsburgh, PA, 1985.

48. Hondros, E. D., "Bonding of Metal/Ceramic Interfaces," p. 121 in *Science of Hard Materials*, E. A. Almond, C. A. Brookes, and R. Warren, eds., Adam Hilger Ltd., Bristol, England, 1986.

49. Griffith, J. E., Qui, Yuanxum, and Tombrello, T. A., "Ion-Beam-Enhanced Adhesion in the Electronic Stopping Region," *Nucl. Instrum. Methods* 198 (1982) 607.

50. Appleton, B. R., Naramoto, H., White, C. W., Holland, O. W., McHargue, C. J., Farlow, G., Narayan, J., and Williams, J. M., "Ion Implantation, Ion Beam Mixing, and Annealing Studies of Metals in Al_2O_3 , SiC, and Si_3N_4 ," *Nucl. Instrum. Methods Phys. Res.* **B1** (1984) 167.
51. Tombrello, T. A., "Ion Beam Enhanced Adhesion," p. 173 in *Thin Films--Interfaces and Phenomena*, R. J. Nemanich, P. S. Ho, and S. S. Lau, eds., Materials Research Society, Pittsburgh, PA, 1984.
52. Sood, D. K., Skinner, W. M., and Williams, J. S., "Helium and Electron Beam Induced Enhancement in Adhesion of Al, Au, and Pt Films on Glass," *Nucl. Instrum. Methods Phys. Res. B* **7/8** (1985) 893.
53. Baglin, J. E. E., and Clark, G. J., "Ion Beam Bonding of Thin Films," *Nucl. Instrum. Methods Phys. Res. B* **7/8** (1985) 881.
54. Lewis, M. B., and McHargue, C. J., "Ion Beam Mixing of Ceramic Alloys--Preparation and Mechanical Properties," p. 85 in *Metastable Materials Formation by Ion Implantation*, S. T. Picraux and W. J. Choyke, eds., Elsevier Science Publishing Company, Inc., New York, 1982.
55. Burnett, P. J., and Page, T. F., "Changing the Surface Mechanical Properties of Silicon and Alpha- Al_2O_3 by Ion Implantation," *J. Mater. Sci.* **19** (1984) 3524.
56. McHargue, C. J., and Yust, C. S., "Lattice Modification in Ion-Implanted Ceramics," *J. Am. Ceram. Soc.* **67**(2) (1984) 117.
57. Hartley, N. E. W., "Mechanical Property Improvements on Ion Implanted Diamond," p. 295 in *Metastable Materials Formation by Ion Implantation*, S. T. Picraux and W. J. Choyke, eds., Elsevier Science Publishing Company, Inc., New York, 1982.
58. Davisson, C. M., and Manning, I., *New Version of the Energy-Deposition Code E-DEP-1: Better Stopping Powers*, NRL Report 8859, Naval Research Laboratory, Washington, DC, October 6, 1986.
59. Noda, S., Doi, H., Hioki, T., and Kamigaito, O., "Deformation and Cracking of Metal-Deposited Single Crystal Alumina and the Effects of Ion-Irradiation," *J. Mater. Sci. Letters* **4** (1985) 523.
60. Brown, William F., Jr., and Srawley, John E., *Plane Strain Crack Toughness Testing of High Strength Metallic Materials*, ASTM Special Technical Publication No. 410, ASTM, Philadelphia, PA, 1967, p. 12.

61. *Ion Implant Profile Code*, Surface Alloys Corporation, Danvers, MA, 1987.

62. *Encyclopedia of Engineering Materials and Processes*, H. R. Clauser, ed. in chief, Reinhold Publishing Corporation, New York, 1963, p. 149.

63. *Encyclopedia of Engineering Materials and Processes*, H. R. Clauser, ed. in chief, Reinhold Publishing Corporation, New York, 1963, p. 768.

64. *Encyclopedia of Engineering Materials and Processes*, H. R. Clauser, ed. in chief, Reinhold Publishing Corporation, New York, 1963, p. 440.

65. Ross, Robert B., *Metallic Materials Specification Handbook*, Third Edition, E. & F. N. Spon, London, 1980, p. 4.

INTERNAL DISTRIBUTION

- | | |
|------------------------------------|---------------------------------|
| 1-2. Central Research Library | 23. E. L. Long, Jr. |
| 3. Document Reference Section | 24. L. K. Mansur |
| 4-5. Laboratory Records Department | 25. R. W. McClung |
| 6. Laboratory Records, ORNL RC | 26. A. R. Olsen |
| 7. ORNL Patent Section | 27. B. Onay |
| 8. L. F. Allard | 28. N. H. Packan |
| 9. P. F. Becher | 29-33. J. E. Pawel |
| 10. T. M. Besmann | 34. M. L. Santella |
| 11. P. J. Blau | 35. A. C. Schaffhauser |
| 12. A. J. Caputo | 36. D. P. Stinton |
| 13. R. S. Carlsmith | 37. R. A. Strehlow |
| 14. R. E. Clausing | 38-40. P. T. Thornton |
| 15. C. K. DuBose | 41. R. O. Williams |
| 16. D. S. Easton | 42. C. S. Yust |
| 17. E. P. George | 43. H. D. Brody (Consultant) |
| 18. C. Hsueh | 44. G. Y. Chin (Consultant) |
| 19. R. J. Lauf | 45. F. F. Lange (Consultant) |
| 20. E. H. Lee | 46. W. D. Nix (Consultant) |
| 21. W. C. Oliver | 47. D. P. Pope (Consultant) |
| 22. D. R. Johnson | 48. E. R. Thompson (Consultant) |

EXTERNAL DISTRIBUTION

- | | |
|---|--|
| 49. Donald F. Adams
University of Wyoming
Laramie, WY 82071 | 52. Bruce J. Angle
Sundstrand Corporation
Turbomach Division
4400 Ruffin Road
PO Box 85757
San Diego, CA 82138-5757 |
| 50. J. W. Adams
Corning Glass Works
Corning, NY 14831 | |
| 51. Donald J. Adrian
High Velocity Corporation
701 Scarboro Road
Oak Ridge, TN 37830 | 53. Richard L. Allor
Ford Motor Company
20000 Rotunda Drive
PO Box 2053
Dearborn, MI 48121-2053 |

54. Richard T. Alpaugh
U.S. Department of Energy
Forrestal Building CE-151
1000 Independence Avenue
Washington, DC 20585
55. H. Arbabi
Brunel University
Uxbridge Middlesex
UNITED KINGDOM UB8 3PH
56. V. S. Avva
North Carolina Agricultural and
Technical State University
Greensboro, NC 27411
57. John M. Bailey
Caterpillar Inc.
Technical Center
Post Office Box 1875
Peoria, IL 61656-1875
58. Murray Bailey
NASA Lewis Research Center
21000 Brookpark Road
MS: 77-6
Cleveland, OH 44135
59. R. R. Baker
Ceradyne, Inc.
3169 Red Hill Avenue
Costa Mesa, CA 92626
60. J. Gary Baldoni
GTE Laboratories, Inc.
40 Sylvan Road
Waltham, MA 02254
61. A. L. Bement, Jr.
TRW, Inc.
23555 Euclid Avenue
Cleveland, OH 44117
62. M. Bentele
Xamag, Inc.
259 Melville Avenue
Fairfield, CT 06430
63. Clifton G. Bergeron
University of Illinois
105 South Goodwin Avenue
204 Ceramics Building
Urbana, IL 61801
64. William D. Bjorndahl
TRW, Inc.
One Space Park
Building 01, Room 2060
Redondo Beach, CA 90278
65. James A. Black
American Matrix, Inc.
118 Sherlake Drive
Knoxville, TN 37922
66. Dan Blake
Solar Energy Research
Institute
1617 Cole Boulevard
Golden, CO 80401
67. Keith Blandford
Boride Products, Inc.
2879 Aero Park Drive
Traverse City, MI 49684
68. John Blum
Norton Company
High Performance Ceramics
Goddard Road
Northboro, MA 01532-1545
69. Paul N. Blumberg
Integral Technologies Inc.
415 East Plaza Drive
Westmont, IL 60559
70. Wolfgang D. G. Boecker
Standard Oil Engineered
Materials Company
Post Office Box 832
Niagara Falls, NY 14302

71. Han Juergen Bossmeyer
BMW Technologies, Inc.
800 South Street
Waltham, MA 02154
72. J.A.M. Boulet
University of Tennessee
310 Perkins Hall
Knoxville, TN 37996
73. Raymond J. Bratton
Westinghouse Electric
Corporation
1310 Beulah Road
Pittsburgh, PA 15235
74. Catherine E. Brown
E. I. DuPont de Nemours &
Company
Wilmington, DE 19898
75. J. J. Brown
Virginia Polytechnic Institute
and State University
Blacksburg, VA 24061
76. W. Bryzik
U.S. Army Tank Automotive
Command
Warren, MI 48090
77. S. T. Buljan
GTE Laboratories, Inc.
40 Sylvan Road
Waltham, MA 02254
78. John M. Byrne, Jr.
PPG Industries, Inc.
One PPG Place
Pittsburgh, PA 15272
79. Donald J. Campbell
Air Force Wright Aeronautical
Laboratory
AFWAL/POX
Wright-Patterson AFB, OH 45433
80. Roger Cannon
Rutgers University
Post Office Box 909
Bowser Road
Piscataway, NJ 08855-0909
81. Harry W. Carpenter
19945 Acre Street
Northridge, CA 91324
82. David Carruthers
Allied-Signal Aerospace
Company
Garrett Engine Division
111 South 34th Street
Post Office Box 5217
Phoenix, AZ 85010
83. Jere G. Castor
Allied-Signal Aerospace
Company
Garrett Engine Company
111 South 34th Street
Post Office Box 5217
Phoenix, AZ 85010
84. Se-Tak Chang
Sundstrand Corporation
Turbomach Division
4400 Ruffin Road
San Diego, CA 92138-5757
85. R. J. Charles
General Electric Company
Post Office Box 8
Schenectady, NY 12301
86. En-sheng Chen
B&C Engineering Research
13906 Dentwood Drive
Houston, TX 77014
87. Albert A. Chesnes
U.S. Department of Energy
Forrestal Building CE-151
1000 Independence Avenue
Washington, DC 20585
88. Frank Childs
EG&G, Inc.
Post Office Box 1625
Idaho Falls, ID 83415
89. Gilbert Y. Chin
Bell Telephone Laboratories
Murray Hill, NJ 07974

91. Melvin H. Chiogioji
U.S. Department of Energy
Forrestal Building CE-15
1000 Independence Avenue, SW
Washington, DC 20585
92. William J. Chmura
The Torrington Company
59 Field Street
Torrington, CT 06790
93. Eugene V. Clark
Turbine Metal Technology, Inc.
7327 Elmo Street
Tujunga, CA 91042-2204
94. William L. Cleary
ORI, Inc.
1375 Piccard Drive
Rockville, MD 20850
95. Jack L. Clem
J. M. Huber Corporation
PO Box 2831
Borger, TX 79008-2831
96. Philip R. Compton
National Aeronautics and
Space Administration
Washington, DC 20546
97. Harry E. Cook
Chrysler Motors Corporation
1200 Chrysler Drive
Highland Park, MI 48288-1118
98. Stephen Copley
University of
Southern California
Los Angeles, CA 90089-0241
99. John A. Coppola
Standard Oil Engineered
Materials Company
Structural Ceramics Division
PO Box 1054, Bldg 91-2
Niagara Falls, NY 14302
100. Normand D. Corbin
Norton Company
High Performance Ceramics
Goddard Road
Northboro, MA 01532-1545
101. Charles H. Craig
Defense Technology Security
Administration
400 Army-Navy Drive
Suite 300
Arlington, VA 22202
102. William J. Croft
U.S. Army Materials
Technology Laboratory
Arsenal Street
Watertown, MA 02172
103. Gary M. Crosbie
Ford Motor Company
20000 Rotunda Drive
PO Box 2053, Room S-2079
Dearborn, MI 48121-2053
104. Floyd W. Crouse, Jr.
U.S. Department of Energy
PO Box 880
Morgantown, WV 26505
105. Raymond Cutler
Ceramatec, Inc.
163 West 1700 South
Salt Lake City, UT 84115
106. David A. Dalman
The Dow Chemical Company
Midland, MI 48640
107. James I. Dalton
Reynolds Metals Company
Fourth and Canal Streets
PO Box 27003
Richmond, VA 23261
108. Stephen C. Danforth
Rutgers University
Post Office Box 909
Bowser Road
Piscataway, NJ 08854

109. Stanley J. Dapkunas
National Bureau of Standards
Gaithersburg, MD 20899
110. Robert F. Davis
North Carolina State University
232 Riddick Laboratory
Box 7907
Raleigh, NC 27695
111. Evelyn M. DeLiso
Rutgers University
PO Box 909
Bowser Road
Piscataway, NJ 08854
112. Alan L. Drago
National Bureau of Standards
Gaithersburg, MD 20899
113. Keith F. Dufrane
Battelle Columbus Laboratories
505 King Avenue
Columbus, OH 43201
114. Edmund M. Dunn
GTE Laboratories Inc.
40 Sylvan Road
Waltham, MA 02254
115. Jeremy D. Dunning
Indiana Memorial Union 662
Indiana University
Bloomington, IN 47405
115. Dr. Sunil Dutta
NASA Lewis Research Center
21000 Brookpark Road
MS: 49-3
Cleveland, OH 44135
117. Paul N. Dyer
Air Products and Chemicals, Inc.
PO Box 538
Allentown, PA 18105
118. Robert J. Eagan
Sandia National Laboratories
Department 1840
PO Box 5800
Albuquerque, NM 87185
119. Christopher A. Ebel
Norton Company
High Performance Ceramics
Goddard Road
Northboro, MA 01532-1545
120. J. J. Eberhardt
U.S. Department of Energy
Forrestal Building CE-12
1000 Independence Avenue, SW
Washington, DC 20585
121. E. E. Ecklund
U.S. Department of Energy
Forrestal Building CE-151
1000 Independence Avenue
Washington, DC 20585
122. William A. Ellingson
Argonne National Laboratory
9700 South Cass Avenue
Argonne, IL 60439
123. Graydon A. Elliott
U.S. Army Research and
Technology Laboratory
(AVSCOM)
Fort Eustis, VA 23604
124. A. Erdely
26 Av. Gore des Eaux-Vives
1208 Geneva
SWITZERLAND
125. Charles D. Estes
U.S. Senate
Washington, DC 20510
126. Peggy Evanich
National Aeronautics and
Space Administration
Washington, DC 20546
127. Anthony G. Evans
University of California
Santa Barbara, CA 93106
128. Robert C. Evans
NASA Lewis Research Center
21000 Brookpark Road
MS: 77-6
Cleveland, OH 44135

129. Katherine T. Faber
Ohio State University
2041 College Road
Columbus, OH 43210
130. John W. Fairbanks
U.S. Department of Energy
Forrestal Building CE-151
1000 Independence Avenue
Washington, DC 20585
131. Larry Farrell
Babcock and Wilcox
Old Forrest Road
Lynchburg, VA 24505
132. H. W. Foglesong
Dow Corning Corporation
3901 South Saginaw Road
Midland, MI 48686
133. Thomas F. Foltz
Avco Corporation
Two Industrial Avenue
Lowell, MA 01851
134. Robert G. Frank
Technology Assessment Group
10793 Bentley Pass Lane
Cincinnati, OH 45140
135. Douglas W. Freitag
LTV Aerospace and Defense
Company
PO Box 225907
MS: TH-85
Dallas, TX 75265
136. George E. Gazza
U.S. Army Materials
Technology Laboratory
405 Arsenal Street
Watertown, MA 02172
137. Charles M. Gilmore
The George Washington
University
Washington, DC 20052
138. Paul Glance
Concept Analysis
950 Stephenson Highway
Troy, MI 48007-7013
139. Fred M. Glaser
U.S. Department of Energy
Washington, DC 20545
140. Joseph W. Glatz
Naval Air Propulsion
Test Center
Box 7176, PE 34
Trenton, NJ 08628
141. W. M. Goldberger
Superior Graphite Company
2175 East Broad Street
Columbus, OH 43209
142. Stephen T. Gonczy
Allied Signal Research Center
50 UOP Plaza
Des Plaines, IL 60016-6187
143. Robert J. Gottschall
U.S. Department of Energy
MS: G-256
Washington, DC 20545
144. Dr. Earl Graham
Cleveland State University
Uclid Ave East 24th Street
Cleveland, OH 44115
145. Kenneth Green
Coors Ceramics Company
17750 West 32nd Street
Golden, CO 80401
146. Robert E. Green, Jr.
Center for Nondestructive
Evaluation
Maryland Hall 107
The Johns Hopkins University
Baltimore, MD 21218

147. Lance E. Groseclose
General Motors Corporation
PO Box 420
Indianapolis, IN 46206-0420
148. T. D. Gulden
GA Technologies, Inc.
PO Box 81608
San Diego, CA 92138
149. P. Ulf Gummeson
Hoeganaes
River Road and Taylors Lane
Riverton, NJ 08077
150. Bimleshwar P. Gupta
Solar Heat Research Division
Solar Energy Research Institute
1617 Cole Boulevard
Golden, CO 80401
151. M. D. Gurney
NIPER
PO Box 2128
Bartlesville, OK 74005
152. John F. Gyekenyesi
NASA Lewis Research Center
21000 Brookpark Road
Cleveland, OH 44135
153. J. J. Habeeb
Esso Petroleum Canada
PO Box 3022
Sarina, Ontario
CANADA N7T 7M1
154. H. T. Hahn
Pennsylvania State University
227 Hammond Building
University Park, PA 16802
155. Nabil S. Hakim
General Motors Corporation
36880 Ecorse Road
Romulus, MI 48174
156. John W. Halloran
Ceramic Process Systems
840 Memorial Drive
Cambridge, MA 02139-3758
157. Kay Hardman-Rhyne
DARPA
1400 Wilson Boulevard
Arlington, VA 22209
158. R. A. Harmon
25 Schalren Drive
Latham, NY 12110
159. Stephen D. Hartline
Norton Company
High Performance Ceramics
Goddard Road
Northboro, MA 01532-1545
160. Willard E. Hauth
Dow Corning Corporation
3901 South Siginaw Road
Midland, MI 48640
161. Kevin L. Haynes
McDonnell Douglas
Astronautics Company
Box 516 E456/HQ/3N/MS329
Saint Louis, MO 63166
162. Norman L. Hecht
University of Dayton
Research Institute
300 College Park
Dayton, OH 45469-0001
163. S. S. Hecker
Los Alamos National
Laboratory
PO Box 1663
Los Alamos, NM 87545
164. Peter W. Heitman
General Motors Corporation
PO Box 420, W-5
Indianapolis, IN 46206-0420
165. Richard L. Helfferich
The Duriron Company,
Incorporated
PO Box 1145
Dayton, OH 45401
166. H. E. Helms
General Motors Corporation
PO Box 420
Indianapolis, IN 46206-0420

167. Thomas L. Henson
GTE Products Corporation
Hawes Street
Towanda, PA 18848-0504
168. Thomas P. Herbell
NASA Lewis Research Center
21000 Brookpark Road
MS: 49-3
Cleveland, OH 44135
169. Hendrik Heystek
Bureau of Mines
Tuscaloosa Research Center
PO Box L
University, AL 35486
170. Robert V. Hillery
General Electric Company
One Neumann Way
PO Box 156301
Cincinnati, OH 45215
171. T. Hine
University of Illinois
Department of Ceramic
Engineering
Urbana, IL 61801
172. Jonathan W. Hinton
Standard Oil Engineered
Materials Company
Structural Ceramics Division
PO Box 1054
Niagara Falls, NY 14302
173. George Hsu
Jet Propulsion Laboratory
4800 Oak Grove Drive
MS: 512-103
Pasadena, CA 91109
174. Stephen M. Hsu
National Bureau of Standards
Gaithersburg, MD 20899
175. Harold A. Huckins
Princeton Advanced
Technology, Inc.
56 Finley Road
Princeton, NJ 08540
176. Fred Huettic
Advanced Ceramic
Technology, Inc.
17 Deerfield Road
East Brunswick, NJ 08816
177. O. Richard Hughes
Celanese Research Company
86 Morris Avenue
Summit, NJ 07901
178. Joseph E. Hunter, Jr.
General Motors Corporation
12 Mile and Mound Roads
Warren, MI 48090-9055
179. Louis C. Ianniello
U.S. Department of Energy
Washington, DC 20545
180. Robert H. Insley
Champion Spark Plug Company
20000 Conner Avenue
Detroit, MI 48234
181. D. M. Jacques
Norton Company
HPC Library
Goddard Road
Northboro, MA 01532-1545
182. Curt A. Johnson
General Electric Company
PO Box 8
Schenectady, NY 12301
183. Douglas C. Johnson
Sundstrand Corporation
4400 Ruffin Road
PO Box 85757
San Diego, CA 92138-5757
184. Larry Johnson
Argonne National Laboratory
9700 South Cass Avenue
Bldg 362
Argonne, IL 60439
185. R. A. Johnson
General Motors Corporation
PO Box 420
Indianapolis, IN 46206-0420

186. L. A. Joo
Great Lakes Research
Corporation
Post Office Box 1031
Elizabethton, TN 37643
187. A. David Joseph
Sealed Power Corporation
100 Terrace Plaza
Muskegon, MI 49443
188. Roy Kamo
Adiabatics, Inc.
630 South Mapleton
Columbus, IN 47201
189. Allan Katz
Air Force Wright
Aeronautical Laboratory
Materials Laboratory,
AFWAL/MLLM
Wright-Patterson AFB, OH 45433
190. R. N. Katz
U.S. Army Materials
Technology Laboratory
405 Arsenal Street
Watertown, MA 02172
191. Mr. Kawaguchi
Tokai Carbon
375 Park Avenue
Suite 3802
New York, NY 10152
192. P. Victor Kelsey
Aluminum Company of America
Alcoa Technical Center B
Alcoa Center, PA 15061
193. Frederick L. Kennard, III
General Motors Corporation
1300 North Dort Highway
Flint, MI 48556
194. J. R. Kidwell
Allied-Signal Aerospace
Company
Garrett Engine Division
111 South 34th Street
Post Office Box 5217
Phoenix, AZ 85010
195. Max Klein
Gas Research Institute
8600 West Bryn Mawr Avenue
Chicago, IL 60631
196. C. E. Knapp
Norton Company
8001 Daly Street
Niagara Falls, Ontario
CANADA
197. A. S. Kobayashi
University of Washington
Seattle, WA 98195
198. David M. Kotchick
AiResearch Manufacturing
Company
2525 West 190th Street
Torrance, CA 90509
199. Bruce Kramer
George Washington University
Washington, DC 20052
200. Saunders B. Kramer
U.S. Department of Energy
Forrestal Building CE-151
1000 Independence Avenue
Washington, DC 20585
201. D. M. Kreiner
Allied-Signal Aerospace
Company
Garrett Engine Division
111 South 34th Street
PO Box 5217
Phoenix, AZ 85010
202. Pieter Krijgsman
Ceramic Design Int.
Hold., Ltd.
PO Box 68
8050 AB Hattem
THE NETHERLANDS
203. W. J. Lackey
Georgia Tech Research
Institute
Atlanta, GA 30332

204. Everett A. Lake
Air Force Wright
Aeronautical Laboratory
AFWAL/POOS
Wright-Patterson AFB
OH 45433
205. Hari S. Lamba
General Motors Corporation
Electro-Motive Division
LaGrange, IL 60525
206. James Lankford
Southwest Research Institute
6220 Culebra Road
PO Drawer 28510
San Antonio, TX 78284
207. John G. Lanning
Corning Glass Works
Corning, NY 14831
208. David C. Larsen
Corning Glass Works
Sullivan Park, FR-51
Corning, NY 14831
209. Dr. S. K. Lau
Standard Oil Engineered
Materials Company
Technology Division
Box 832
Niagara Falls, NY 14302
210. Harry A. Lawler
Standard Oil Engineered
Materials Company
Structural Ceramics Division
PO Box 1054, Bldg 91-2
Niagara Falls, NY 14302
211. Alan Lawley
Drexel University
Philadelphia, PA 19104
212. Daniel Lee Temescon
2850 7th Street
Berkeley, CA 94710
213. June-Gunn Lee
Korea Advanced Institute of
Science and Technology
PO Box 131
Dong Dac Mun, Seoul
KOREA
214. E. M. Lenoë
Air Force Office of Scientific
Research
APO San Francisco
CA 96503-0110
215. Stanley R. Levine
NASA Lewis Research Center
21000 Brookpark Road
Cleveland, OH 44135
216. David Lewis
Naval Research Laboratory
4555 Overlook Avenue, SW
Washington, DC 20375
217. Winston W. Liang
AMERCOM, Inc.
8948 Fullbright Avenue
Chatsworth, CA 91311
218. Bill Long
Babcock and Wilcox
PO Box 1260
Lynchburg, VA 24505
219. L. A. Lott
EG&G, Inc.
PO Box 1625
Idaho Falls, ID 83415
220. Bryan K. Luftglass
Chem Systems, Inc.
303 South Broadway
Tarrytown, NY 10591
221. Robert Lundberg
Svenska Silikatforsknings-
institutet
Swedish Institute for
Silicate Research
Box 5403
S-402 29 Gothenburg
SWEDEN

222. Michael J. Lynch
General Electric Company
PO Box 414, 7B-36
Milwaukee, WI 53201
223. James W. MacBeth
Standard Oil Engineered
Materials Company
Structural Ceramics Division
Box 1054
Niagara Falls, NY 14302
224. Vincent L. Magnotta
Air Products and Chemicals, Inc.
PO Box 538
Allentown, PA 18105
225. Tai-il Mah
Universal Energy Systems
4401 Dayton-Xenia Road
Dayton, OH 45432
226. L. Manes
Commission of the European
Communities
Ispra Establishment
1-21020 Ispra (Varese)
ITALY
227. Gerald R. Martin
Fleetguard, Inc.
Cookeville, TN 38501
228. Dr. John L. Mason
Allied-Signal Aerospace Company
AiResearch Los Angeles Division
2525 West 190th Street
Torrance, CA 90509
229. J. McCauley
U.S. Army Materials Technology
Laboratory
DRXMR-MC
Arsenal Street
Watertown, MA 02172-0001
230. William J. McDonough
Keramont
4233 South Fremont Avenue
Tucson, AZ 85714
231. Bryan J. McEntire
Norton Company
TRW Ceramics
Goddard Road
Northboro, MA 01532-1545
232. Thomas D. McGee
Iowa State University
Ames, IA 50011
233. H. Christopher McGowan
Advanced Ceramic
Technology, Inc.
17 Deerfield Road
East Brunswick, NJ 08816
234. Malcolm G. McLaren
Rutgers University
PO Box 909
Bowser Road
Piscataway, NJ 08854
235. Arthur F. McLean
6225 N Camino Almonte
Tucson, AZ 85718
236. Brian L. Mehosky
Standard Oil Engineered
Materials Company
4440 Warrensville Center Road
Cleveland, OH 44128
237. P. K. Mehrotra
Kennametal, Inc.
PO Box 639
Greensburg, PA 15601
238. Joseph J. Meindl
Reynolds International, Inc.
PO Box 27002
6603 West Broad Street
Richmond, VA 23261
239. D. Messier
U.S. Army Materials
Technology Laboratory
DRXMR-MC
Arsenal Street
Watertown, MA 02172

240. Arthur G. Metcalfe
Solar Turbines, Inc.
2200 Pacific Highway
PO Box 80966
San Diego, CA 92138
241. Thomas N. Meyer
Aluminum Company of America
Alcoa Technical Center
Alcoa Center, PA 15069
242. W. Miloscia
Standard Oil Engineered
Materials Company
4440 Warrensville Center Road
Cleveland, OH 44128
243. Bill Moehle
Ethyl Corporation
451 Florida Avenue
Ethyl Tower
Baton Rouge, LA 70801
244. Helen Moeller
Babcock and Wilcox
PO Box 11165
Lynchburg, VA 24506-1165
245. Frederick E. Moreno
Turbo Energy Systems, Inc.
350 Second Street, Suite 5
Los Altos, CA 94022
246. Peter E. D. Morgan
Rockwell International
1049 Camino Dos Rios
PO Box 1085
Thousand Oaks, CA 91360
247. Lawrence M. Murphy
Thermal Systems Research
Branch
Solar Energy Research
Institute
1617 Cole Boulevard
Golden, CO 80401
248. Solomon Musikant
General Electric Company
PO Box 8555
MS: U-1219
Philadelphia, PA 19101
249. Pero Nannelli
Pennwalt Corporation
900 First Avenue
PO Box C
King of Prussia, PA 19406-0018
250. Robert M. Neilson, Jr.
EG&G Idaho, Inc.
PO Box 1625
Idaho Falls, ID 83415
251. William D. Nix
Stanford University
Stanford, CA 94305
252. Richard D. Nixdorf
American Matrix, Inc.
118 Sherlake Drive
Knoxville, TN 37922
253. Brian M. O'Connor
The Lubrizol Corporation
29400 Lakeland Boulevard
Wickliffe, OH 44092
254. W. Richard Ott
Alfred University
Alfred, NY 14802
255. Muktesh Paliwal
GTE Products Corporation
Hawes Street
Towanda, PA 18848-0504
256. Hayne Palmour III
North Carolina State
University
2158 Burlington Engineering
Laboratories
PO Box 5995
Raleigh, NC 27607
257. Joseph N. Panzarino
Norton Company
Goddard Road
Northboro, MA 01532-1545
258. Pellegrino Papa
Corning Glass Works
Corning, NY 14831

259. James G. Paschal
Reynolds Metals Company
PO Box 76154
Atlanta, GA 30358
260. Arvid E. Pasto
GTE Laboratories, Inc.
40 Sylvan Road
Waltham, MA 02254
261. Donald O. Patten
Norton Company
High Performance Ceramics
Goddard Road
Northboro, MA 01532-1545
262. James W. Patten
Cummins Engine Company, Inc.
Box 3005, Mail Code 50183
Columbus, IN 47202-3005
263. Timothy M. Pattison
Textron Lycoming
MS: LSM1
550 Main Street
Stratford, CT 06497
264. Robert A. Penty
Eastman Kodak Company
901 Elmgrove Road
Rochester, NY 14650
265. Gary R. Peterson
U.S. Department of Energy
785 DOE Place
Idaho Falls, ID 83402
266. R. Byron Pipes
University of Delaware
2001 Spencer Laboratory
Newark, DE 19716
267. Robert C. Pohanka
Office of Naval Research
800 North Quincy St, Code 431
Arlington, VA 22217
268. Stephen C. Pred
ICD Group, Inc.
1100 Valley Brook Avenue
Lyndhurst, NJ 07071
269. Karl M. Prewo
United Technologies
Corporation
Silver Lane, MS: 24
East Hartford, CT 06108
270. Hubert B. Probst
NASA Lewis Research Center
21000 Brookpark Road
Cleveland, OH 44135
271. Carr Lane Quackenbush
Norton Company
High Performance Ceramics
Goddard Road
Northboro, MA 01532-1545
272. Brian Quigy
National Aeronautics and
Space Administration
Washington, DC 20546
273. George Quinn
U.S. Army Materials
Technology Laboratory
Arsenal Street
Watertown, MA 02172
274. Dennis T. Quinto
Kennametal, Inc.
PO Box 639
Greensburg, PA 15601
275. S. Venkat Raman
Air Products and
Chemicals, Inc.
PO Box 538
Allentown, PA 18105
276. Dennis Readey
Ohio State University
2041 College Road
Columbus, OH 43210
277. Robert R. Reeber
U.S. Army Research Office
PO Box 12211
Research Triangle Park
NC 27709

278. K. L. Reifsnider
Virginia Polytechnic Institute
and State University
Blacksburg, VA 24061
279. Paul Rempes
Williams International
2280 West Maple
MS: 6-5
Walled Lake, MI 48088
280. T. M. Resetar
U.S. Army Materials
Technology Laboratory
DAXMA-MC
Arsenal Street
Watertown, MA 02172
281. K. T. Rhee
Rutgers University
PO Box 909
Bowser Road
Piscataway, NJ 08854
282. Roy W. Rice
W. R. Grace and Company
7379 Route 32
Columbus, MD 21044
283. David W. Richerson
Ceramatec, Inc.
163 West 1700 South
Salt Lake City, UT 84115
284. Paul Rieth
Ferro Corporation
661 Willet Road
Buffalo, NY 14218-9990
285. Michael A. Rigdon
Institute for Defense Analyses
1801 Beauregard Street
Alexandria, VA 22311
286. John E. Ritter, Jr.
University of Massachusetts
Amherst, MA 01003
287. Giulio A. Rossi
Norton Company
High Performance Ceramics
Goddard Road
Northboro, MA 01532-1545
288. Barry R. Rossing
Lanxide Corporation
Tralee Industrial Park
Newark, DE 19711
289. David J. Rowcliffe
SRI International
333 Ravenswood Avenue
Menlo Park, CA 94025
290. Donald W. Roy
Coors Ceramics Company
17750 West 32nd Street
Golden, CO 80401
291. Bruce Rubinger
Gobal
50 Milk Street, 15th Floor
Boston, MA 02109
292. Robert Ruh
Air Force Wright
Aeronautical Laboratory
Materials Laboratory
AFWAL/M LLM
Wright-Patterson AFB,
OH 45433
293. Robert J. Russell, Sr.
Norton Company
High Performance Ceramics
Goddard Road
Northboro, MA 01532-1545
294. George P. Safol
Westinghouse Electric
Corporation
Pittsburgh, PA 15235
295. J. Sankar
North Carolina Agricultural
and Technical State
University
Greensboro, NC 27411

296. Maxine L. Savitz
Garrett Processing Company
Ceramic Components Division
19800 South Van Ness Avenue
Torrance, CA 90509
297. Richard Schapery
Texas A&M University
College Station, TX 77843
298. J. L. Schienle
Allied-Signal Aerospace
Company
Garrett Auxiliary Power
Division
2739 East Washington Street
PO Box 5227
Phoenix, AZ 85010
299. Liselotte J. Schioler
Aerojet Tech Systems Company
PO Box 13222
Dept. 9990, Bldg. 2019-A2
Sacramento, CA 95813
300. Richard A. Schmidt
Battelle Columbus
Laboratories
505 King Avenue
Columbus, OH, 43201-2693
301. Arnie Schneck
Deere and Company
Technical Center
PO Box 128
Wood-Ridge, NJ 07075
302. Matthew Schreiner
Gas Research Institute
8600 West Bryn Mawr Avenue
Chicago, IL 60631
303. John Schuldies
Industrial Ceramic
Technology, Inc.
37 Enterprise Drive
Ann Arbor, MI 48103
304. R. B. Schulz
U.S. Department of Energy
Forrestal Building CE-151
1000 Independence Avenue
Washington, DC 20585
305. Wesley J.C. Shuster
Thermo Electron Corporation
115 Eames Street
PO Box 340
Wilmington, MA 01887
306. Murray A. Schwartz
Bureau of Mines
2401 Eye Street, N.W.
Washington, DC 20241
307. Douglas B. Schwarz
The Dow Chemical Company
52 Building
Midland, MI 48674
308. Thomas M. Sebestyen
U.S. Army Tank
Automotive Command
AMSTA-RGRT
Warren, MI 48397-5000
309. Brian Seegmiller
Coors Ceramics Company
17750 West 32nd Street
Golden, CO 80401
310. S. G. Seshadri
Standard Oil Engineered
Materials Company
PO Box 832
Niagara Falls, NY 14302
311. Peter T. B. Shaffer
Advanced Refractory
Technologies, Inc.
699 Hertel Avenue
Buffalo, NY 14207
312. Maurice E. Shank
United Technologies
Corporation
East Hartford, CT 06108
313. Laurel M. Sheppard
Advanced Materials and
Processes
Route 87
Metals Park, OH 44073
314. Dinesh K. Shetty
The University of Utah
Salt Lake City, UT 84112

315. Jack D. Sibold
Coors Ceramics Company
17750 West 32nd Street
Golden, CO 80401
316. Neal Sigmon
U.S. House of Representatives
Rayburn Building, Room B308
Washington, DC 20515
317. Richard Silberglitt
Quest Research Corporation
1651 Old Meadow Road
McLean, VA 22102
318. Maurice J. Sinnott
University of Michigan
438 West Engineering Building
Ann Arbor, MI 48109-2136
319. S. R. Skaggs
Los Alamos National Laboratory
PO Box 1663
Los Alamos, NM 87545
320. J. Thomas Smith
GTE Laboratories, Inc.
40 Sylvan Road
Waltham, MA 02254
321. Jay R. Smyth
Allied-Signal Aerospace
Company
Garrett Auxiliary Power
Division
2739 East Washington Street
PO Box 5227
MS: 93-172/1302-2K
Phoenix, AZ 85010
322. Rafal Sobotowski
Standard Oil Engineered
Materials Company
3092 Broadway Avenue
Cleveland, OH 44115
323. Thomas M. Sopko
Lubrizol Enterprises, Inc.
29400 Lakeland Boulevard
Wickliffe, OH 44092
324. Boyd W. Sorenson
Du Pont Company
Experimental Stat, Bldg 304
Wilmington, DE 19898
325. Dr. Richard M. Spriggs
Center for Advanced
Ceramic Technology
New York State College
of Ceramics at
Alfred University
Alfred, NY 14802
326. M. Srinivasan
Standard Oil Engineered
Materials Company
PO Box 832
Niagara Falls, NY 14302
327. Gordon L. Starr
Cummins Engine Company, Inc.
Box 3005, Mail Code 50183
Columbus, IN 47202-3005
328. Harold L. Stocker
General Motors Corporation
PO Box 420, T-23
Indianapolis, IN 46206-0420
329. Paul D. Stone
The Dow Chemical Company
1801 Building
Midland, MI 48674
330. Roger Storm
Standard Oil Engineered
Materials Company
PO Box 832
Niagara Falls, NY 14302
331. E. E. Strain
Allied-Signal Aerospace
Company
Garrett Engine Division
111 South 34th Street
PO Box 5217
MS: 301-2N
Phoenix, AZ 85010

332. Thomas N. Strom
NASA Lewis Research Center
21000 Brookpark Road, 77-6
Cleveland, OH 44135
333. Jerry Strong
Albright & Wilson
PO Box 26229
Richmond, VA 23260
334. Richard Suddeth
Boeing Motor Airplane Company
PO Box 7730
MS: K-76-67
Wichita, KS 67277
335. Paul Sutor
Midwest Research Institute
425 Volker Boulevard
Kansas City, MO 64116
336. J. J. Swab
U.S. Army Materials
Technology Laboratory
405 Arsenal Street
Watertown, MA 02172
337. John W. Swain, Jr.
Kollmorgen Corporation
PCK Technology Division
15424 Garrison Lane
Southgate, MI 48915
338. Lewis Swank
Ford Motor Company
20000 Rotunda Drive
PO Box 2053
Building SRL, Room S2023
Dearborn, MI 48121-2053
339. Stephen R. Tan
ICI Advanced Materials
PO Box 11
The Heath, Runcorn
Cheshire
ENGLAND WA7 4QE
340. Anthony C. Taylor
U.S. House of Representatives
Rayburn Building, Room 2321
Washington, DC 20515
341. W. H. Thielbahr
U.S. Department of Energy
550 2nd Street
Idaho Falls, ID 83401
342. John K. Tien
Columbia University
1137 S.W. Mudd Building
New York, NY 10027
343. T. Y. Tien
University of Michigan
Dow Building
Ann Arbor, MI 48109-2136
344. Julian M. Tishkoff
Air Force Office of
Scientific Research
(AFOSR/WC) Bolling AFB
Washington, DC 20332
345. Louis E. Toth
National Science Foundation
1800 G Street, N.W.
Washington, DC 20550
346. Richard E. Tressler
Pennsylvania State University
201 Steidle Building
University Park, PA 16802
347. Donald R. Uhlmann
Massachusetts Institute
of Technology
77 Massachusetts Avenue
Cambridge, MA 02139
348. Edward C. Van Reuth
Technology Strategies, Inc.
10722 Shingle Oak Court
Burke, VA 22015
349. Thomas Vasilos
Avco Corporation
201 Towell Street
Wilmington, MA 01887
350. V. Venkateswaran
Standard Oil Engineered
Materials Company
PO Box 832
Niagara Falls, NY 14302

351. John B. Wachtman, Jr.
Rutgers University
PO Box 909
Bowser Road
Piscataway, NJ 08854
352. Richard B. Wallace
General Motors Corporation
36880 Ecorse Road
Romulus, MI 48174
353. Harlan L. Watson
U.S. House of Representatives
Rayburn Building, Suite 2321
Washington, DC 20515
354. John D. Watson
BHP Research & New Technology
Melbourne Research Laboratories
245 Wellington Road
Mulgrave, Vic. 3170
AUSTRALIA
355. Albert R. C. Westwood
Martin Marietta Laboratories
1450 South Rolling Road
Baltimore, MD 21227
356. Thomas J. Whalen
Ford Motor Company
20000 Rotunda Drive
PO Box 2053
Dearborn, MI 48121-2053
357. Sheldon M. Wiederhorn
National Bureau of Standards
Gaithersburg, MD 20899
358. James C. Williams
Carnegie-Mellon University
Schenley Park
Pittsburgh, PA 15213
359. Roger R. Wills
TRW, Inc.
Valve Division
1455 East 185th Street
Cleveland, OH 44110
360. J. M. Wimmer
Allied-Signal Aerospace
Company
Garrett Engine Division
111 South 34th Street
Post Office Box 5217
Phoenix, AZ 85010
361. David Wirth
Coors Ceramics Company
17750 West 32nd Street
Golden, CO 80401
362. Thomas J. Wissing
Eaton Corporation
26201 Northwestern Highway
Post Office Box 766
Southfield, MI 48037
363. Dale Wittmer
Southern Illinois University
at Carbondale
Department of Mechanical
Engineering and
Energy Processes
Carbondale, IL 62901
364. George W. Wolter
Howmet Turbine Components
Corporation
699 Benston Road
Whitehall, MI 49461
365. James C. Wood
NASA Lewis Research Center
21000 Brookpark Road
MS: 500-210
Cleveland, OH 44135
366. Roger P. Worthen
Eaton Corporation
26201 Northwestern Highway
PO Box 766
Southfield, MI 48076
367. Hun C. Yeh
Garrett Processing Company
Ceramic Components Division
19800 Van Ness Avenue
Torrance, CA 90509

368. Thomas M. Yonushonis
Cummins Engine Company, Inc.
Box 3005, Mail Code 50183
Columbus, IN 47202-3005
369. Don Zabierek
Air Force Wright
Aeronautical Laboratory
AFWAL/POTC
Wright-Patterson AFB
OH 45433
370. Charles Zeh
U.S. Department of Energy
PO Box 880
Morgantown, WV 26505
371. Anne Marie Zerega
U.S. Department of Energy
Forrestal Building CE-15
1000 Independence Avenue
Washington, DC 20585
372. Martin Zlotnick
Nichols Research Corporation
8618 Westwood Center Dr.
Suite 200
Vienna, VA 22180-2222
373. Klaus M. Zwilsky
National Research Council
2101 Constitution Avenue
Washington, DC 20418
374. Department of Energy
Oak Ridge Operations Office
Assistant Manager for Energy
Research and Development
PO Box 2001
Oak Ridge, TN 37831
- 375-384. Department of Energy
Office of Scientific and
Technical Information
Office of Information Services
PO Box 62
Oak Ridge, TN 37831
- For distribution by microfiche
as shown in DOE/TIC-4500,
Distribution Category UC-95.

